Title
Defining the Molecular Pathogenesis of the Neurodegenerative Disease Spinoecerebellar Ataxia Type 7

Permalink
https://escholarship.org/uc/item/8j67n5x0

Author
Stoyas, Colleen Ann

Publication Date
2017

Supplemental Material
https://escholarship.org/uc/item/8j67n5x0#supplemental

Peer reviewed|Thesis/dissertation

UNIVERSITY OF CALIFORNIA, SAN DIEGO

Defining the Molecular Pathogenesis of the Neurodegenerative Disease

Spinoecerebellar Ataxia Type 7

A dissertation submitted in partial satisfaction of the requirements for the

degree Doctor of Philosophy

in

Biomedical Sciences

by

Colleen Ann Stoyas

Committee in charge:

Professor Albert La Spada, Chair
Professor Eric Bennett
Professor Lawrence Goldstein
Professor Tariq Rana
Professor Christina Sigurdson

2017

The Dissertation of Colleen Ann Stoyas is approved, and it is acceptable in
quality and form for publication on microfilm and electronically:

_____

_____

_____

_____

_____

Chair

University of California, San Diego

2017

DEDICATION

This work is dedicated to my grandmother, Nancy E. Sullivan,

My most ardent supporter and most fiercely loving person I have ever known.

Her memory inspires me to be the best person I can be, every single day.

TABLE OF CONTENTS

LIST OF FIGURES

LIST OF SUPPLEMENTAL FILES

Supplemental Table 1 List of all differentially regulated genes in SCA7

Supplemental Table 2 Putative Transcription Factor Binding Site Analysis

ACKNOWLEDGEMENTS

I would like to thank my advisor, Dr. Al La Spada, for his guidance throughout this work and for supporting me through my many pursuits. Through him I have learned patience, persistence, and the ability to communicate effectively. I am most grateful for the opportunity to work on this amazing project, with its many nuances and layers. Having the opportunity to meet SCA7 and other ataxia patients at the National Ataxia Foundation Investigators meetings has transformed my understanding of what it means to work on rare disease, and this work is also for them. Additionally, I would like to thank Dr. Johan Auwerx at the École polytechnique fédérale de Lausanne in Switzerland for his support of this project. In addition to measurements and reagents, he has taken time to provide feedback on this project and my personal questions and musings regarding the bioenergetics side of this project. I would like to thank Dr. Christina Sigurdson, who has been a constant source of encouragement and support throughout my time at UCSD. I would also like to thank Dr. Larry Goldstein for welcoming me into his lab for a rotation early in my program, and for inspiring me through his communicative abilities and public advocacy for science. Likewise, I would like to thank Dr. Tariq Rana and Dr. Eric Bennet for their feedback throughout this project.

I would like to thank all the members of the La Spada lab, past and present. I would especially like to thank Dr. ChenChen Niu for sharing her precious and extremely difficult mouse line with me, without which I could not

have completed this project. I would also like to acknowledge that she began the RNA-seq project, and graciously allowed me to mine her data. I would also like to thank Dr. Jackie Ward, a previous student in the lab, who's collaboration and fervor for advocacy have encouraged me to continue my pursuits despite difficulties. I would also like to thank Dr. Pawel Switonski for his help with the revisions of my paper, and for being a great bay-mate. I would like to thank Dr. Bryce Sopher for his endless wisdom on many projects throughout my time in the lab. Furthermore, thank you to Edith Lopez for her work supporting my mouse colonies, and Dr. Susan Mayo for all of the impossible tasks she completed for me. I would like to thank all of the members of the lab for their friendship inside and outside of the building. I would also like to specifically thank Dr. Somashish Gosh-Dastidir, for being my enthusiastic support for the last five years. I wouldn't have made it through this training without him and his laughter.

Thank you to my collaborators outside of the lab, first and foremost being David Bushart and Dr. Vikram Shakkottai at the University of Michigan. Without them the electrophysiology aspect of this project would not have come to fruition. Thank you to Dr. Terry Gaasterland for her work analyzing the RNA-seq data, and Dr. Alex Savtchenko for his time and effort helping me with the calcium imaging experiments. Finally thank you to Dr. Karim Gariani and Dr. Johan Auwerx for the NAD^+ measurements.

I would like to thank my family and many good friends. Completing a PhD has been an achievement for all of us. Thank you for all of your love, patience,

and laughter. To my parents, thank you for unwavering support. To my siblings Nick, Kelly, and Joey, thank you for keeping me grounded in what is important, and distracted with silly things that aren't. I love you all so much. Thank you to my lifelong friends, and all of the friends I have made in San Diego. There's too many to list, but you have all helped me achieve this in your own ways.

Finally, I would like to thank my 'pack', my husband Paul and our fur-child Ringo. The two of them give me a reason to wake up and seize each day, fill me with constant joy and smiles, and for some reason accept and celebrate all of my flaws. Completing this doctorate and pursing my career is not only possible but extremely enjoyable because we are a team. Together we take on the world. And together we're better!

VITA

Education

2017   Ph.D., Biomedical Sciences
              University of California, San Diego

2011   B.Sc., Integrative Biology Honors
              University of Illinois, Urbana-Champaign

Publications

Stoyas CA, Bushart D, Ward JM, Switonski P, Niu CC, Savtchenko A, Gariani K, Gaasterland T, Auwerx J, Shakkottai VG, La Spada AR (2017). Sirt1 restores proper calcium homeostasis to achieve neuroprotection in spinocerebellar ataxia type 7. In revision.

Ward JM, **Stoyas CA**, Sopher BL, Fan W, Lazarowski ER, Muotri AR, Evans RM, La Spada AR (2017). Spinocerebellar ataxia type 7 is characterized by defects in mitochondrial and metabolic function. In revision.

Stoyas CA and La Spada AR. The CAG – polyglutamine repeat diseases: A clinical, molecular, genetic and pathophysiological nosology. Handbook of Clinical Neurology: Neurogenetics Edition. Elsevier. Release date September 1, 2017.

ABSTRACT OF THE DISSERTATION

Defining the Molecular Pathogenesis of the Neurodegenerative Disease

Spinoecerebellar Ataxia Type 7

by

Colleen Ann Stoyas

Doctor of Philosophy in Biomedical Sciences

University of California, San Diego, 2017

Professor Albert La Spada, Chair

Sirtuin 1 (Sirt1) is a NAD^+-dependent protein deacetylase with established effects in countering age-related diseases, including neurodegeneration, yet the basis for Sirt1 neuroprotection remains elusive. Spinocerebellar ataxia type 7 (SCA7) is an inherited neurodegenerative disorder in which CAG-polyglutamine (polyQ) repeat expansions in the ataxin-7 gene produce cerebellar degeneration in affected human patients. As transcription dysregulation likely contributes to SCA7 pathogenesis, we

performed transcriptome analysis on SCA7 mice, observed downregulation of genes controlling calcium flux, and documented abnormal calcium-dependent membrane excitability in both SCA7 mouse cerebellum and SCA7 patient-derived neuronal cells. Transcription factor binding site analysis of SCA7 down-regulated genes revealed sites for peroxisome proliferator-activated receptors, which are known Sirt1 targets, and we detected marked cerebellar changes in NAD^+ metabolism that are known to reduce Sirt1 function. We then crossed Sirt1 transgenic mice with two different SCA7 mouse models, and observed amelioration of cerebellar neurodegeneration, calcium flux defects, and membrane excitability in Sirt1-SCA7 bigenic mice. Finally we detected a direct functional interaction between Sirt1 and Atxn7 protein, which persisted in the presence of polyQ-expanded Atxn7 and correlated with increased turnover of Sirt1. These findings indicate that Sirt1 achieves neuroprotection by promoting proper calcium regulation, reinforce an emerging view that cerebellar ataxias exhibit altered calcium homeostasis due to metabolic dysregulation, and suggest a normal role for a Sirt1-Atxn7 interaction that is perturbed in SCA7.

Chapter 1:

Introduction

Clinical description of SCA7

Spinocerebellar ataxia type 7 (SCA7) is an autosomal dominant, often rapidly progressive cerebellar ataxia accompanied by visual impairment. SCA7 has a wide global distribution, occurring in all major racial groups at a prevalence of ~1 in 500,000[1-7]. SCA7 is caused by a CAG/polyglutamine (polyQ) repeat expansion at the 5' end of the coding region of the ataxin-7 (*atxn7*) gene[8,9], and is therefore one of the nine polyQ diseases. SCA7 is also a member of the larger family of proteinopathies, a family of neurodegenerative disorders characterized by toxic misfolded proteins that includes more common degenerative diseases such as Alzheimer's disease (AD), Parkinson's disease (PD), and amyotrophic lateral sclerosis (ALS). SCA7 patients display prominent dysarthria and can develop increased tendon reflexes, decreased vibration sense, and visual impairment due to a cone-rod dystrophy form of retinal degeneration, ultimately resulting in blindness[10,11]. Neurodegeneration and reactive gliosis occur in the cerebellar cortex, dentate nucleus, inferior olive, pontine nuclei, and occasionally the basal ganglia. Cerebellar tissue from SCA7 patients demonstrates extensive loss of cerebellar Purkinje cells[12-14]. Interestingly, volume loss may develop in the pons prior to cerebellar atrophy, indicating disease onset in the brainstem, rather than the cerebellar folia[15]. As with other proteinopathies, nuclear inclusions are common in vulnerable cell populations and include ubiquitin proteasome system (UPS) components[16,17].

Polyglutamine Diseases

The polyQ family includes nine different neurodegenerative diseases: Huntington's disease (HD), spinal and bulbar muscular atrophy (SBMA), dentatorubral pallidoluysian atrophy (DRPLA), and six spinocerebellar ataxias (SCA 1, 2, 3, 6, 7 & 17).   These diseases typically strike in midlife with progressive neuronal dysfunction and neuron loss, taking place years after symptom onset. Interestingly, each of these diseases strikes a particular subset of neurons, despite widespread expression of the different polyQ-expanded proteins throughout the brain and non-neural tissues[18].   Except for SBMA, which is X-linked (and displays sex-limited inheritance), all other CAG-polyQ diseases are dominantly inherited. Healthy individuals possess *ATXN7* alleles ranging in size from 7 – 35 CAGs, with patients possessing 37 to >300 repeats[9]. SCA7 is among the most unstable and polymorphic of all coding repeat expansions, displaying both somatic and germline instability. Successive generations of families affected with SCA7 and other polyQ-expansion diseases thus exhibit anticipation, with larger alleles corresponding to an earlier age of onset and increasing disease severity manifested as more rapid disease progression[5,10,19].   Larger repeat expansions occur in male germlines, and anticipation is so prononuced in SCA7 that paternal transmission is accociated with increased spontaneous miscarriage rates in affected kindreds[19,20].

Infantile-onset SCA7

SCA7 patients display a significant correlation between repeat length and type of clinical presentation, with repeat expansions <59 CAG triplets commonly

yielding initial cerebellar symptoms, and repeat expansions ≥59 CAG triplets resulting in visual impairment as the initial complaint in affected SCA7 patients[5,20]. Expansions ranging from 180-460 repeats generate infantile-onset SCA7 and display a wider specturm of clinical phenotypes including muscle wasting, hypotonia, and congestive heart failure (reviewed in Whitney et al.[21]). Ultimatley these patients succumb to multiorgan failure prior to exiting infancy[21-23].

Ataxin-7 function

The ataxin-7 (Atxn7) protein was identified as a novel polypeptide of unknown function. While studies in the yeast *Saccharomyces cerevisiae* revealed that the yeast orthologue of Atxn7, Sgf73, is a core component of the SAGA (Spt7-Ada1-Gcn5 Acetyltransferase) transcription co-activator complex[24], independent studies concomitantly identified ATXN7 as a core component of the mammalian STAGA (Spt3-Taf9-Ada-Gcn5-Acetyltransferase) transcription co-activator complex and closely related TATA-binding protein-free TAF containing complex (TFTC)[25,26]. Transcription co-activator complexes are large protein complexes that mediate interactions between RNA polymerase II and transcription activators, and are recruited to perform a variety of functions, including chromatin remodeling[27,28]. The STAGA complex possesses both histone acetyltransferase and histone deubiquitinase activity, and is composed of four sub-complexes with distinct functions: the SPT module implicated in pre-initiation complex assembly, the TAF module responsible for co-activator

architecture, the Gcn5 histone acetyltransferase (HAT) module, and the Usp22 deubiquitination module (DUBm)[29]. The HAT and DUB activity of SAGA facilitate transcription by disassembling nucleosomes at the promoter region[30,31], an activity that is conserved in human STAGA[32-36]. While the exact function of Atxn7 is unknown, polyQ-Atxn7 integrates into the STAGA complex, and can alter HAT activity of STAGA in retinal photoreceptor cells and even of SAGA in yeast[26,37]. Atxn7 directly interacts with the cone-rod homeobox protein (CRX), a member of the otd/Otx homeodomain transcription factor family uniquely expressed in retinal photoreceptor cells[38,39]. Indeed, it was the identification of this interaction between Atxn7 and CRX and the demonstration that polyQ-Atxn7 interferes with CRX transcription activation, which led to the initial realization that Atxn7 might be a transcription factor[39,40].

Mouse SCA7 models

Multiple mouse models have been generated to further understand SCA7 and give insight into the pathogenesis of this disease. Our lab has generated several models where human 92Q ataxin-7 is expressed throughout the CNS, as well as specifically targeted to different types of cerebellar neurons and glia[41,42]. For this study we have chosen to utilize our previously generated mPrP-fxSCA7 92Q-BAC mouse model[42] (hereto referenced as fxSCA7 92Q). These animals express the *atxn7* gene with 92 polyglutamine (polyQ) repeats in a bacterial artificial chromosome with expression driven by the murine prion protein promoter (mPrP) and display progressive cerebellar degeneration with

symptom onset at 20 weeks of age[42]. We selected the fxSCA7 92Q mice because they display widespread modest expression of Ataxin-7-92Q protein throughout the CNS, exhibit gradually progressive cerebellar degeneration with symptom onset and 20 weeks of age, and presents key aspects of SCA7 neurodegeneration[42,43].

Additional mouse models of SCA7 recapitulate the juvenile onset form of the disease, such as the SCA7$^{266Q/5Q}$ knock-in mouse (hereto referred as SCA7 266Q)[44]. These SCA7 266Q animals display a severe manifestation of SCA7 that resembles the infantile onset form with symptom onset at 5 weeks of age, dramatically shortened lifespan, and an intense disease phenotype that includes shrinking of Purkinje cell soma[44]. Our group obtained this unyielding disease model and utilized it in coordination with the fxSCA7 92Q animals to verify hypotheses were relevant in multiple disease models of SCA7.

Induced pluripotent stem cells and neurodegenerative disease modeling

While rodent models have produced important insight into the pathology of neurodegenerative diseases, they are inherently not human and do not naturally suffer from long term diseases of aging. The discovery that adult somatic cells could be reprogrammed to a pluripotent state by introduction of four defined transcription factors in 2007[45] and reprogrammed from human fibroblasts to possesses a similar differentiation potential as embryonic stem cells[46] thus provided a novel model to study human disease where affected tissue sample is prohibitive to sample. These induced pluripotent stem cells

(iPSCs) provide a method to study human samples directly by differentiating them into the cell type of interest. Differentiation protocols have been developed for a variety of specific neural cell types[47], including neural progenitor cells (NPCs). These cells exhibit gene expression patterns functionally similar to cells in the early stage of fetal development[48], but have been shown to recapitulate disease-specific phenotypes associated with a number of adult-onset neurodegenerative diseases[49-51]. To determine if our mouse models recapitulate phenotypes consistent with human disease, we verified our mouse studies in NPCs differentiated from SCA7 patient-derived iPSCs and those of unaffected family members (Ward *et al*, 2017; In revision).

Calcium handling and ataxia

Purkinje cells are a class of specialized neurons in the cerebellum, and are among the most metabolically active of all neurons[52], as they receive an enormous amount of synaptic input from various brainstem and cerebellar neurons, which they integrate to provide the only efferent output from the cerebellum for precise control of voluntary movement. Given the extent of synaptic activity occurring in Purkinje cells and the neural circuitry for which they form the central hub, regulation of calcium influx is crucial for proper Purkinje cell function[53]. Calcium flux and signaling rely upon transmembrane ion channels and endoplasmic reticulum (ER) calcium channels, as well as calcium responsive signal transduction enzymes, such as kinases and lipases. Degeneration of Purkinje cells is a common feature of inherited ataxia in

humans and mice, and one predominant theme is that mutations in genes encoding calcium regulatory proteins account for numerous ataxias in humans and mice[54]. Interestingly, many of these ataxia disease genes converge upon the inositol (1,4,5) triphosphate receptor (ITPR) signaling pathway, which modulates calcium release from the ER to regulate Purkinje cell function[55].

Sirt1 and neurodegeneration

The sirtuin family of proteins are NAD^+-dependent deacetylases first identified in yeast. After the discovery that over-expression of Sir2 promotes lifespan extension in yeast[56] attention turned to Sirtuin-1 (Sirt1), its mammalian orthologue, and five closely related proteins (Sirt2 – Sirt6) that comprise this family of highly conserved proteins. Once controversal[57,58], it is now widely accepted sirtuins play a critical role in aging and lovetiy control in diverse model organisms, including mice[59-62]. Additionally caloric restriction in mouse models of neurodegeneration yields amelioration of disease symptoms and pathology[63-66], and Sirt1 can elicit neuroprotection in a wide range of neurodegenerative disorders, such as Huntington's disease HD[67,68]. Furthermore, a number of Sirt1 targets promote neuroprotective pathways in the CNS[69], but the basis for Sirt1 neuroprotection remains uncertain.

Questions and goals of the thesis

The hypothesis that led to the work herein is that altered transcriptional activity is a key feature of SCA7 pathogenesis. As Atxn7 is a member of the

transcription co-activator complex STAGA and polyQ-expanded Atxn7 incorporates and alters complex activity, I felt that unbiased transcriptome analysis would reveal general pathways involved in SCA7 disease progression and perhaps explain cerebellar specificity of this disease. In Chapter 2 I describe interrogation of differentially expressed genomic transcripts from cerebellar RNA derived from our fxSCA7 92Q mouse model. We identified reduced expression of genes involved in calcium homeostasis and phosphatidyl-inositol signaling, and verified that these gene expression changes correlated with changes in neuronal firing in SCA7 mice and patient-derived cells. With the goal of identifying possible therapeutic targets in SCA7, my next line of investigation utilized putative transcription factor binding site analysis to identify two targets of Sirt1 in the promoters of these differentially expressed genes. We described altered metabolism of NAD^+, the necessary Sirt1 cofactor, and demonstrated Sirt1 overexpression ameliorates disease phenotypes of two SCA7 mouse models. Importantly, Sirt1 overexpression rescues expression of the genes identified in Chapter 2. We hypothesized that the addition of NAD^+ would also rescue neuronal firing phenotypes observed in neuronal cells differentiated from SCA7 patient iPSCs, and achieved this by administration of the NAD^+ precursor nicotinamide riboside (NR). The identification of Sirt1 targets from our altered gene expression dataset, NAD^+ metabolism, Sirt1 overexpression, and NAD^+ supplementation experiments are described in detail in Chapter 3. Based on data in yeast, I hypothesized and verified a functional interaction between Sirt1 and Atxn7 that may also contribute to SCA7 pathogenesis, and describe this

work in Chapter 4. The implications of this interaction in SCA7, however, will ultimately be the goal of follow up studies. With this work, I establish for the first time dysfunction in calcium handling in SCA7, and describe a novel mechanism for Sirt1 neuroprotection by promoting proper calcium regulation. These studies have identified multiple potential therapeutic targets for SCA7 and other diseases of cerebellar dysfunction, and implicate a normal role in metabolism for Atxn7 via its direct interaction with Sirt1.

Chapter 2:

Perturbation of Calcium Flux and Homeostasis Contribute to SCA7 Pathogenesis

Abstract

In order to impartially identify changes in gene expression in spinocerebellar ataxia type 7 (SCA7), we performed RNA-sequencing analysis on cerebellar tissue from our fxSCA7 92Q mice. Pathway analysis revealed reduction of transcripts known to influence calcium homeostasis and phosphatidyl-inositol signaling, pathways implicated in other forms of ataxia. We observed that expression of these genes varies with respect to disease progression, resulting in dramatic reduction in advanced SCA7. We describe neuronal dysfunction in the Purkinje cells and cerebellar granule neurons of our SCA7 mouse model, and in neuronal precursor cells differentiated from SCA7 patient iPSCs. These data demonstrate that alterations in cerebellar calcium flux at the gene and functional level are a novel feature associated with SCA7 pathogenesis.

2.1 Introduction

Spinocerebellar ataxia type 7 (SCA7) is an inherited neurological disorder characterized by cerebellar ataxia, dysarthia, opthalmoplegia, and retinal degeneration[9,70,71]. SCA7 is caused by a CAG/polyglutamine (polyQ) repeat expansion in the *ataxin-7* gene that is dominantly inherited and displays anticipation across generations[10,19,72]. While *ataxin-7* is ubiquitously expressed, SCA7 disease pathology is largely confined to the retina, cerebellum, and brainstem. Neurodegenerative changes are most apparent in the Purkinje cell and molecular layers of the cerebellum, and are characterized by atrophy and nuclear inclusions[71].

SCA7 is one of nine polyQ degenerative disorders, a disease family that also includes spinalbulbar muscular atrophy (SBMA), Huntington disease (HD), dentatorubropallidolusyian atrophy (DRPLA), and five other forms of inherited ataxias (SCA1, 2, 3, 6, and 17)[73]. An important hypothesis in the polyQ disease field, proposed at the discovery of the first polyQ disease, is that polyQ expansions produce disease by disrupting transcription[74]. The various polyglutamine disease proteins have little in common in terms of structural domains, other than the polyQ expansion tract, and the fact that they are all directly involved in transcription regulation, either as a transcription factor or co-regulator[75]. While the exact function of ataxin-7 protein (Atxn7) is unknown, its involvement in retinal degeneration is explained by physical interaction with CRX, a photoreceptor-specific transcription factor, and reduction of CRX target gene expression in the presence of the polyQ expansion[38,39]. Independent of the CRX interaction, Atxn7 is a highly conserved member of the transcription co-activator complex STAGA (Spt3-Taf9-Ada-Gcn5-Acetyltransferase)[25]. This complex promotes transcription in part by remodeling promoter regions through intrinsic Gcn5 histone acetlytransferase (HAT) and Usp22 histone deubiquitinase (DUB) activities [29]. Integration of polyQ-expanded Atxn7 into the STAGA complex alters both HAT and DUB activity[26,76,77], suggesting that epigenetic dysregulation is a central feature of SCA7 disease pathogenesis. Yet it remains unclear how these changes may confer the cerebellar specifity observed in SCA7.

The autsomoal dominant cerebellar ataxias, referred to as the spinocerebellar ataxias (SCAs), are clinically heterogenous and casued by

mutations in at least 24 identified genes[78-80]. While these mutations are expressed widely throughout the body, degeneration of the Purkinje cells of the cerebellum is a prevelant feature of inherited ataxia in humans and mice. A common aspect of several of these genes is downstream siganling pathway convergence on the inositol (1,4,5) triphosphate receptor type 1 (IP3R1), which modulates calcium release from the endoplasmic reticulum to regulate Purkinje cell function[53,55,80]. Autonomous pacemaking of Purkinje is highly dependent on the regulation of calcium entry and intracellular calcium concentration of Purkinje cells[81], and proper spiking relies on regulation of calcium influx[53].

In order to understand the changes in transcription underlying SCA7, we completed an unbiased transcriptome analysis on cerebellar tissue from our mPrP-fxSCA7 92Q-BAC mouse model[42] (hereto referenced as fxSCA7 92Q). Network analysis identified enrichment of gene expression alterations in the phosphatidyl-inositol signaling and calcium homeostasis pathways in the SCA7 cerebellum. We then validated that these gene expression changes translated to physiological differences by documenting altered calcium handling in Purkinje cells firing and cerebellar granule neurons derived from fxSCA7 92Q mice. Finally we validated these findings are relevant to human disease by describing susceptibility to calcium stress and irregular calcium flux in response to depolarizing stimuli in neuronal precursor cells (NPCs) differentiated from induced pluripotent stem cells (iPSCs) derived from human SCA7 patients. This is the first time alterations in calcium signaling and electrophysiology have been reported for SCA7.

2.2 Results

SCA7 transcriptome analysis reveals altered expression of genes regulating calcium flux

To determine the molecular basis for SCA7 cerebellar degeneration, we performed unbiased transcriptome analysis on cerebellar RNAs from presymtomatic (12 week old) and visibly symptomatic (29 week old) fxSCA7 92Q transgenic mice. High throughput RNA-sequencing (RNA-seq) analysis of SCA7 cerebellar RNAs in comparison to matched littermate controls yielded a list of 100 genes with significantly altered expression levels in the cerebellum of both presymptomatic and symptomatic fxSCA7 92Q mice (**Supplemental Table 1** and **Figure 2.1a**). These differentially regulated genes were subjected to pathway analysis via DAVID Bioinformatics Database version 6.7 (https://david.ncifcrf.gov/)[82,83] and literature review. Overrepresentation of gene ontology (GO) categories and Kyoto Encyclopedia of Genes and Genomes (KEGG) pathways were examined (Bonferroni-corrected $P<0.05$ was considered significant). Notably, genes involved in the phosphatidyl-inositol signaling (P=3.2E-4) and the calcium signaling pathway (P=5.0E-3) were coordinately down regulated in the cerebellum of fxSCA7 92Q mice (**Figure 2.1b**). Importantly, many of the identified genes involved in calcium handling are mutated in other forms of ataxia or when deleted produce ataxic phenotypes in mice[80,84] and **Figure 2.2**), underscoring their importance for normal cerebellar function. To validate these findings we performed RT-qPCR analysis on RNAs isolated from the cerebella of

an independent cohort of fxSCA7 92Q animals, and confirmed significant expression reductions in all tested genes (**Figure 2.1c**).

To interrogate the temporal nature of changes in calcium handling gene expression, we examined the expression of identified genes at pre-, early-, and post-symptomatic time points in our fxSCA7 92Q mice. Reduction of most interrogated calcium handling genes is present at the pre-symptomatic time point, with the exception of the large over expression of the ATP2A3 gene (**Figure 2.3a**). This gene encodes one of the sarco/endoplasmic reticulum Ca^{2+}-ATPases (SERCA), which couple ATP hydrolysis with translocation of calcium from the cytosol into the lumen of the sarcoplasmic reticulum[85]. By the age of symptom onset, this upregulation was mitigated and the remaining identified genes are either reduced or no different from wild-type littermates (**Figure 2.3b**). Consistent with our unbiased transcriptome study and another independent cohort (Figure 2.1), expression of all interrogated calcium handling genes is reduced at an advanced symptomatic time point (**Figure 2.3c**).

Calcium flux defects are apparent in multiple cell types of SCA7 cerebellum

When modeling spinocerebellar ataxia in mice neuronal dysfunction typically precedes overt neuron loss[86,87], and many of the identified down-regulated calcium homeostasis genes play an important role in Purkinje neuron spiking[87-91]. Purkinje cells integrate information from brainstem and cerebellar neurons to provide the only efferent output to the movement control regions of the CNS to insure proper coordination of voluntary fine motor tasks. As fxSCA7 92Q

mice exhibit gradually progressive cerebellar degeneration without frank loss of Purkinje cell neurons[42], we chose to directly evaluate cerebellar Purkinje cell electrophysiology in early symptomatic (25 week old) animals by patch-clamp analysis of acute cerebellar slices. Representative traces of Purkinje cell firing in cerebellar slices illustrate irregular firing in the fxSCA7 92Q animals (**Figure 2.4a**). While the average firing frequency is unchanged (**Figure 2.4b**), the variation of Purkinje cell spike frequency is increased in fxSCA7 92Q mice (**Figure 2.4c**). As illustrated previously, irregular spiking, as represented by the spiking coefficient of variation (CV), is correlated with impaired calcium handling in Purkinje neurons[92]. Additionally we found that the threshold to dendritic calcium spiking was lower in the fxSCA7 92Q animals (**Figure 2.4d-e**), indicating these neurons are hyper-excitable. Taken together, this detection of altered Purkinje cell firing patterns in SCA7 mice is consistent with aberrant calcium handling[87], and provides physiological validation of the calcium regulatory gene expression alterations revealed by the unbiased transcriptome analysis (Figure 2.1).

To determine if aberrant electrophysiological function is restricted to just Purkinje cells or a general feature of SCA7 cerebellar degeneration, we generated primary cerebellar granule neurons (CGNs) from fxSCA7 92Q animals and wild-type littermates and monitored changes in intracellular calcium. Cells were made permeable to the calcium-chelator Fluo-4 NW flourophore and intensity of calcium release, measured by florescence intensity, from each cell was measured as CGN cultures were subjected to a potassium chloride stimulus and recorded for 20 seconds. Consistent with the high coefficient of variation in Purkinje neuron firing

observed (Figure 2.3c), CGNs have an increased variance in cytosolic calcium after stimulation (**Figure 2.5a**), however do not reproduce the hyper-excitability phenotype observed in the cerebellar slices (**Figure 2.5b**). These data indicate that decreased expression of calcium handling genes alters electrophysiology in multiple cell types of the cerebellum in fxSCA7 92Q animals.

Calcium handling is disrupted in SCA7 patient-derived NPCs

Our results indicate that altered calcium flux is a central feature of SCA7 neurodegeneration, but as our findings are limited to mouse model experimentation, we sought to address the role of calcium flux dysregulation in human SCA7 patients. To do so, we derived induced pluripotent stem cells (iPSCs) from fibroblasts of different SCA7 patients and related, unaffected controls, and after confirming retention of CAG repeat expansions in iPSCs derived from SCA7 patients, we generated neuronal progenitor cells (NPCs) (Ward et al 2017, in revision). Based on the calcium handling deficiencies described in the SCA7 mouse models and the variance of gene expression observed temporally (Figure 2.3) we hypothesized these cells would be susceptible to thapsigargin, a non-competitive inhibitor of the SERCA Ca^{2+}-ATPases that raises intracellular calcium concentration[85]. Upon thapsigargin treatment we observed a marked increase in cell death in SCA7 NPCs (**Figure 2.6a**), indicating a deficit of calcium mobilization in the cells. To examine calcium flux regulation, we repeated the intracellular calcium labeling experiments described for the cerebellar granule neurons and measured response to a potassium chloride stimulus. We noted a marked increase

in calcium concentration variability in SCA7 patient-derived NPCs (**Figure 2.6b**), and a nearly 50% increase in the percentage of SCA7 NPCs responding to this stimulus (**Figure 2.6c**). These studies recapitulate the findings in fxSCA7 Purkinje neurons (Figure 2.4) and the flux phenotype in fxSCA7 CGNs, supporting a role for altered regulation of calcium homeostasis in SCA7 patients.

2.3 Discussion

Spinocerebellar ataxias (SCAs) share a subset of clinical and pathological features that have increasingly been linked to gene mutations that converge on ion channels and transmembrane transporters[93], and network analysis identifies calcium homeostasis and signaling pathways as playing a central role in pathogenesis[80]. While never previously described in SCA7, alterations in calcium signaling and/or electrophysiology have been described in at least eight other SCAs (SCA1, SCA2, SCA3, SCA5, SCA6, SCA14, SCA15/16) (reviewed in [84]). In an unbiased fashion, we identified decreased expression of calcium handling genes in the presence of polyQ-expanded Atxn7, and identified altered calcium handling in multiple cerebellar cell types involved in SCA7 disease and in neuronal precursor cells derived from SCA7 patient iPSCs.

Central to the role of calcium disruption in SCAs is convergence of the phosphatidyl-inositol signaling pathway on the inositol triphosphate receptor type 1 (ITPR1)[55,80], a pathway abudnantly represented this study. While the polyglutamine expanded SCAs are the most common source, mutations in over 40 genes cause ataxia. A persistent mystery surrounding this class of diseases is why

mutations in such a large number of genes, most of which are widely expressed throughout the brain and even the entire body, primarily cause ataxia and not, for instance, dementia or epilepsy[55]. The answer may lie in cerebellar-specific methods of coincidence detection, or the process by which neurons encode information detecting the occurrence of temporally close but spatially distributed input signals. Purkinje cells are the sole output of the cerebellar cortex, and their firing rate is modulated by the parallel and climbing fibers of the cerebellum[94,95]. The interaction between these two pathways drives an unusual form of heterosynaptic plasticity in Purkinje cells that is reliant on release of calcium from the endoplasmic reticulum (ER) by ITPR1[55].

In classical hippocampol synaptic plasticity, it is N-methyl-D-aspartate (NMDA) receptors that serve as coincidence detectors, modulating calcium release from the ER via ryanodine receptors[55]. Interestingly in the cerebellum NMDA receptors appear to play a smaller role, as Purkinje cells have dense concentrations of ITPR1 on their post-synapic ER stores[96] and express a different splice variant of ITPR1 than other central nervous system regions[97]. Additional evidence has shown ultimately it is the interaction between calcium and inositol triphosphate on ITPR1 that underlies coincidence detection in Purkinje cells[55]. As this study detected decreased expression of multiple genes involved in inositol triphosphate signalling in SCA7, the unique importance of ITPR1-dependent signaling to cerebellar function may describe why a mutation in *ataxin-7* leads to degeneration of this specific brain region.

Abnormal calcium levels in Purkinje cells are thought to uncouple plstasticity to activate toxic cascades[84], and we identify for the first time this process in SCA7 by describing changes in Purkinje and granule cell firing in a mouse model of SCA7, as well as in neural precursor cells derived from SCA7 patients. ITPR1 expression, among other calcium signaling genes identified in this study, is downregulated in transgenic SCA1 mice[98], indicating a distruption to the phosphatidyl-inositol signaling pathway may be a common mechanism among the heritable ataxias. Intruigingly polyglutamine expanded Ataxin-2 and Ataxin-3, but not their wild type conterparts, interact with ITRP1 and sensitize its inositol triphosphate-induced calcium release to disrupt calcium signaling in mutant neurons[99,100]. While we have not validated this specific mechanism, the electrophysiological phenotypes we observed in SCA7 are consistent with these prior observations.

One appealing treatment target for ataxia in general is neuronal calcium signaling. As the regular tonic firing of cerebellar Purkinje cells is mediated by calcium-activated potassium channels (SK and BK)[101], positive modulators of these channels can be employed to rectify Purkinje cell firing abnormalities. Indeed, riluzole, which in addition to inhibiting glutamate release also activates SK channels, has been evaluated in patients with ataxia in two different clinical trials and has yielded encouraging results[102,103]. Of the three SK channel subtypes expressed in neurons, the SK2 subtype is most highly expressed in Purkinje cells; hence, potent small molecules that selectively activate SK2 channels could be effective treatments for SCA7 and related ataxias.

With these results, we have taken the first step in characterzing Purkinje cell dysfunction in SCA7, as well as provided reasoning for the cerebellar specificity of this disease. As single mutations in genes involved in inositol triphosphate signalling pathway lead to a variety of ataxias[55,80,84], the widespread down-regulation suggests mutant Atxn7 somehow influences this pathway. In the next chapter I will describe our efforts to establish the mechanism of Atxn7 in regulating inositol triphosphate signaling and interrogate methods of rescuing expression of calcium handling genes in SCA7.

2.4 Experimental procedures

Mouse studies

All animal experimentation adhered to NIH guidelines and was approved by, and performed, in accordance with the University of California, San Diego Institutional Animal Care and Use Committee (IACUC) and the University of Michigan Committee on the Use and Care of Animals.

High throughput RNA sequencing (RNA-seq)

Total RNA from the cerebellum of fxSCA7 92Q mice and wild-type littermates aged 12 and 29 weeks (n=3 per group) was isolated using TRIzol (Life Technologies). Samples were then sent to BGI Americas for deep sequencing on the Illumina HiSeqTM 2000 system (50SE). Analysis of genome-wide expression data was performed by aligning raw reads of biologically independent samples to

the reference mouse genome (mm10) using TopHat[104]. Cufflinks software package[105] was used to assemble individual transcripts from the mapped reads. Cuffdiff, a part of the Cufflinks package, was used to calculate gene expression levels and test for the statistical significance of differences in gene expression. Reads per kilobase per million mapped reads (RPKM) were calculated for each gene and used as an estimate of expression levels. Heatmaps and hierarchical clustering were generated using Genesis software[106].

Real-time quantitative PCR (RT-qPCR)

Mice were euthanized under isoflurane anesthesia, and cerebella were rapidly removed and flash-frozen in liquid nitrogen. Tissue was stored at -80°C until processing. RNA was isolated from the whole cerebellum of animals using TRIzol (Life Technologies), and treated with DNAse I in the form of TURBO-DNAse (Life Technologies) to remove traces of genomic DNA. Reverse transcription was performed with SuperScript Reverse Transcriptase (Life Technologies). Quantitative PCR was carried out using TaqMan probes (Life Technolgies) and TaqMan Universal PCR Mix (Life Technologies) on a CFX384 Touch system (Bio-Rad), with a 10minute gradient to 95$^{\circ C}$ followed by 40 cycles of 95$^{\circ C}$ for 15 seconds and 60$^{\circ C}$ for 1 minute. Gene expression was normalized to GAPDH levels. Delta CT values were calculated as $C_t^{target} - C_t^{GAPDH}$. All experiments were performed with three technical replicates. Relative fold changes in gene expression were calculated using the $2^{-\Delta\Delta Ct}$ method[107]. Data are presented as the average of the

biological replicates + standard error of the mean (S.E.M.). Select genes were validated via RT-qPCR as described above.

Patch-clamp electrophysiology solutions

Artificial cerebrospinal fluid (aCSF) contained the following (in mM): 125 NaCl, 2.5 KCl, 26 NaHCO$_3$, 1.25 NaH$_2$PO$_4$, 2 CaCl$_2$, and 10 glucose. For all recordings other than dendritic capacitance measurements, pipettes were filled with internal recording solution containing the following (in mM): 119 K-Gluconate, 2 Na-Gluconate, 6 NaCl, 2 MgCl$_2$, 0.9 EGTA, 10 HEPES, 14 Tris-phosphocreatine, 4 MgATP, 0.2 Tris-GTP, at pH 7.3 and osmolarity 290 mOsm. For dendritic capacitance measurements, internal recording solution contained (in mM): 140 CsCl, 2 MgCl$_2$, 1 CaCl$_2$, 10 EGTA, 10 HEPES, 4 Na$_2$ATP, at pH 7.3 and osmolarity 287 mOsm.

Preparation of brain slices for acute electrophysiological recordings

Mice were anesthetized by isoflurane inhalation and decapitated. The brain was removed and submerged in pre-warmed (33°C) aCSF. Acute parasagittal slices were prepared in aCSF held at 32.5-34°C on a VT1200 vibratome (Leica) to a thickness of 300 μm. Once slices were obtained, they were incubated in carbogen-bubbled (95% O$_2$, 5% CO$_2$) aCSF at 33°C for 45 minutes. Slices were then stored in carbogen-bubbled aCSF at room temperature until use. During recording, slices were placed in a recording chamber and continuously perfused with carbogen-bubbled aCSF at 33°C at a flow rate of 2.5 mL/min.

Patch-clamp electrophysiology recordings

Purkinje neurons were visually identified for patch-clamp recordings using a 40x water immersion objective and a Nikon Eclipse FN1 upright microscope with infrared differential interference contrast (IR-DIC) optics. Identified cells were visualized using NIS Elements image analysis software. Borosilicate glass patch pipettes were pulled to resistances of 3-4 MΩ for all recordings. Recordings were performed 1-5 hours after slice preparation. Data were acquired using an Axopatch 200B amplifier, Digidata 1440A interface (MDS Analytical Technologies), and pClamp-10 software (Molecular Devices). All data were digitized at 100 kHz. Whole-cell recordings were rejected if the series resistances changed by >20% during the course of recording, or if the whole-cell series resistance rose above 15 MΩ. All voltages are corrected for the liquid gap junction potential, which was calculated to be 10 mV[87].

Analysis of firing properties from patch-clamp recordings

Electrophysiology data were analyzed offline using Clampfit 10.2 software (Molecular Devices). Firing frequency and coefficient of variation (CV) calculations were performed in the cell-attached configuration on spikes in a 150 second time interval obtained ~5 minutes after formation of a stable seal. The CV was calculated as follows:

$$CV = \frac{Standard\ Deviation\ of\ Interspike\ Interval}{Mean\ Interspike\ Interval}$$

The firing frequency distribution was obtained by identifying the percentage of cells in each incrementing 10 spike/second bin. The CV distribution was similarly obtained by sorting CV values into incrementing 0.02 bins. A moving average trendline was added to the CV distribution histogram to outline the shape of the distribution.

To determine whether the distribution of CV values was significantly different between genotypes, a Fisher's exact test was performed between the populations of regular firing and irregular firing cells for each genotype. Regular spiking was defined as cells with a CV cutoff value within 3 standard errors of the mean wild-type CV (to represent a 99% confidence interval of the wild-type mean). All cells at or under this cutoff value were considered to be regular firing cells, while all cells above this cutoff value were considered to be irregular firing cells.

Threshold to dendritic calcium spikes in patch-clamp recordings

Threshold to elicit dendritic calcium spikes was performed at 25 weeks of age as described previously[108]. Briefly, cells were held at -80 mV in whole-cell current clamp mode and injected with current in +50 pA increments in the presence of tetrodotoxin to block somatic sodium spikes. The amount of injected current to elicit calcium spikes was recorded. Input resistance for each cell was calculated by generating an input-output curve for injected current vs. membrane potential, with only membrane potential values of under -75 mV in an effort to minimize active conductances during measurements[108].

Primary neuron culture

Primary cerebellar granule neurons (CGNs) were derived from 7-day old fxSCA7 92Q pups and wild-type littermates as previously described[109] with minor modifications. Briefly, cerebella from 7-day old fxSCA7 92Q pups and wild-type littermates were digested with 0.25% Trypsin (Life Technologies). After neutralization with 10% serum, cells were tritirated and centrifuged for 5min at 800 x *g*. The pellet was resuspended in Neurobasal-A Media (Thermo Fisher Scientific), 10% B27 serum-free supplement (Thermo Fisher Scientific), 25mM KCl and added to polystyrene flat-bottomed 96-well plates (Grenier) coated with poly-L-ornithine/laminin at a concentration of 28,000 cells per well, six wells per animal. Neurons were aged seven days prior to performing Fluo-4 NW calcium imaging experiments.

NPC differentiation

All work done with fibroblasts and resulting iPSC-derived NPCs obtained informed consent from SCA7 patients and unaffected family members and approved by the Institutional Review Boards in accordance with the requirements of the Code of Federal Regulations on the Protection of Human Subjects (45 CFR 46 and 21 CFR 50 and 56), including its relevant Subparts, and the UCSD Embryonic Stem Cell Research Oversight (ESCRO) Committee (Project #130337ZF). NPCs were generated with STEMdiff Neural Induction Medium (NIM) (StemCell Technologies) according to manufacturer's monolayer culture protocol instructions. Briefly, iPSCs were gently dissociated with Accutase

(StemPro, ThermoFisher), pelleted, and resuspended in NIM at 1-2 x 106 cells/mL, then plated on Matrigel coated dishes. Cells were passaged one more time in NIM and plated in dishes coated with poly-L-ornithine (15 ug/mL) and laminin (10 ug/mL) (Sigma-Aldrich). Cells tested negative for mycoplasma, and were thereafter passaged and expanded in STEMdiff Neural Progenitor Medium (NPM) (StemCell Technologies) on poly-L-ornithine/laminin-coated dishes at a density of 0.5-210 x 105 cells/well for cell death assay, and 25,000-50,000 cells per well for Fluo-4 NW imaging calcium experiments.

NPC cell death assay

24 hours after plating 0.5-210 x 105 NPCs, cells were given fresh media containing 1:1000 DMSO or 1uM thapsigargin and incubated for 24 hours. NPCs were then treated with trypsin in excess and collected by centrifugation. The cell pellet was suspended in 300uL of staining solution containing 8uM propidum iodide (8uM centration), which stains only dead nuclei, and Calcein-AM (4uM concentration), which stains only live nuclei, in PBS. Cells were incubated in the dark at room temperature for 15 minutes and intermediately mixed. 20uL of cell suspension was pipetted onto a glass slide and cells were immediately imaged using the inverted fluorescence scope (Nikon Eclipse 80i). For each condition, pictures of 8 random fields were taken, each field represented by green and red channel. Images were analyzed in order to determine the number of dead cells presented as a fraction of all cells in the field. (dead index = dead cells / (dead cells + live cells)). To determine the number of green (live) cells and red (dead) cells, a

short script was written in Python and was executed using Fiji distribution of ImageJ. In short, the script allowed automation of steps that are necessary to count cells in ImageJ. These steps include threshold adjusting, particle separation, particle analysis, and particle counting. Adequate threshold and size limits were implemented to exclude background signal fluctuations from being counted as cells. As a result, in one experiment 8 dead indexes per treatment per cell line were obtained and averaged. Experiments were completed three times and the mean graphed as a bar with the S.E.M.

Fluo-4 NW CGN calcium Imaging Experiments

For real-time recordings of intracellular calcium dynamics in our cell lines, cells were plated in 96-well plates at the densities described above. Prior to measurements, cells were loaded with Fluo-4 NW Calcium Assay Kit (Life Technologies, Carlsbad, CA). We have added 200 ng/ml (650 nM) Hoechst 33342 (Life Technologies, Carlsbad, CA). Plates were incubated with the dye at 37°C for 30 minutes, then at room temperature for an additional 15 minutes. After extensive wash, cells were incubated in neuronal media for 10 min. To perform optical recordings, we utilized ImageXpress® Micro XLS System (Molecular Devices) equipped with a Spectra X light engine (Lumencor) and standard filter sets. Raw movies were acquired at 50 fps, and pre-processed using MetaExpress Imaging software (Molecular Devices).

The image analysis and physiological parameter calculation was conducted using ImageJ analysis program. The analysis was performed in a similar manner

on fluorescence traces generated from each neuron. Parameter tables were analyzed using Microsoft Excel 2013 and OriginPro software (OriginLab, CA). Variance analysis of the individual neurons has been performed for each calcium signal for minimum of 4 individual neurons per well. Mathematical variance ($\sigma2$) is defined as the sum of the squared distances of each term (χ) in the distribution of the mean (μ) divided by the number of samples (N) and calculated as follows:

$$\sigma^2 = \frac{\Sigma\,(\chi - \mu)^2}{N}$$

Resulting variance data were plotted as mean with S.E.M. Single cell traces were gated to remove non-responding and low responding cells by selecting only those cells with a $(Ca^{2+})_i$ value at the peak of the transient that was included in the top 80% range of cells measured in the well. The setting was maintained for all the group of analysis. At least five wells were recorded for each test condition.

Statistical Analysis

Statistic tests are described in the figure legends for all data. Statistical analysis was done using Microsoft Excel, Prism 6.0 (GraphPad), SigmaPlot (Systat Software), and Origin (Origin Labs). Statistical significance was defined at $P<0.05$. For one-way and two-way analysis of variance (ANOVA), if statistical significance ($P<0.05$) was achieved, then we performed post hoc analysis corresponding to the experiment, as specified by the figure legend, to account for multiple comparisons. All t-tests are two-tailed Student's t-tests unless otherwise indicated, and level of significance (alpha) was always set to 0.05.

Acknowledgements

Figures

Figure 2.1 Genes central to calcium homeostasis are down regulated in SCA7
A) RNA-seq reveals 100 differentially regulated gene transcripts in mPrP-fxSCA7 92Q-BAC mouse model at age 29 weeks. RNA was isolated from cerebellar tissue of animals aged 12 and 29 weeks, fxSCA7 92Q and wild-type littermate controls (n=3 per group). Relative levels of gene expression are compared to wild-type age 12 weeks. Black = no change, green = down regulated, red = up regulated. **B)** There is down regulation of mRNA expression of genes important to calcium homeostasis and inositol triphosphate metabolism in cerebellar tissue of mPrP-fxSCA7 92Q-BAC animals. **C)** RT-qPCR of independent cohort verifies RNA-seq results. RNA was isolated from cerebellar tissue obtained from fxSCA7 92Q animals and wild-type littermate controls at age 30 weeks. Biological replicates WT: n=7, fxSCA7 92Q: n=8, are the average of three technical replicates. Mean of biological replicates plus S.E.M shown, two-tailed *t*-test *$P<0.05$, ** $P<0.01$.
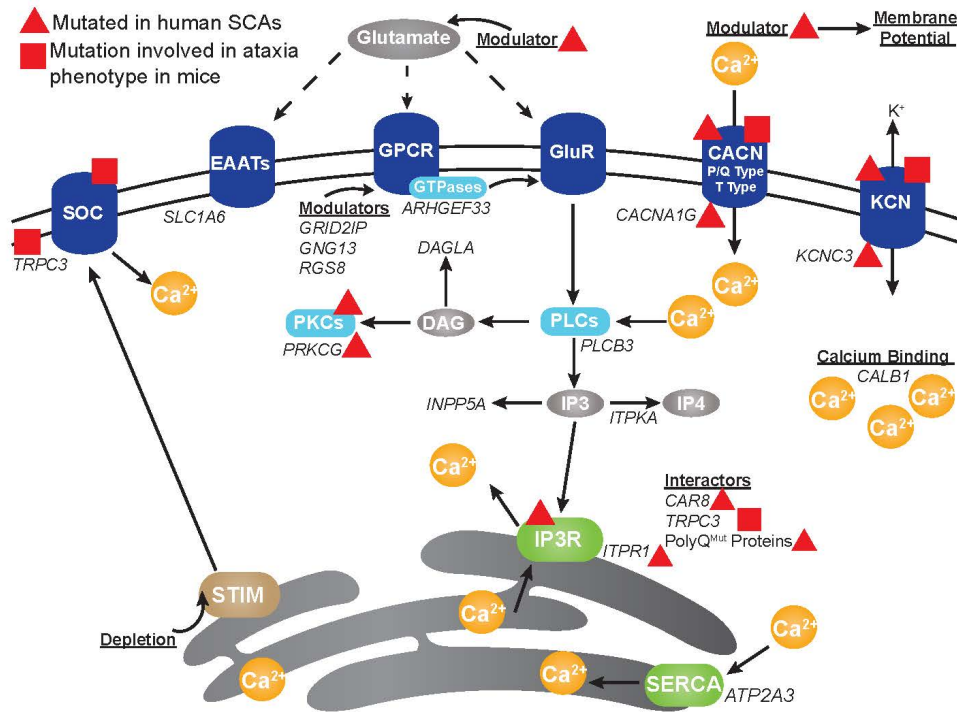
Figure 2.2 Calcium handling genes are implicated in spinocerebellar ataxia
Here we see a diagram of the cell membrane, membrane-based cell signaling pathways, and the ER, indicating genes and proteins involved in regulating calcium homeostasis and flux. Genes identified in this SCA7 study are also altered in mouse models and human spinocerebellar ataxias (SCAs). Black italics indicate genes down-regulated in RNA-seq analysis of cerebellar tissue from mPrP-fxSCA7 92Q-BAC mouse model. Red triangle indicates genes (black italics) or proteins (cylindrical shapes) that are mutated in human SCAs. Red square indicates genes or proteins that when mutated generate an ataxic phenotype in mice.
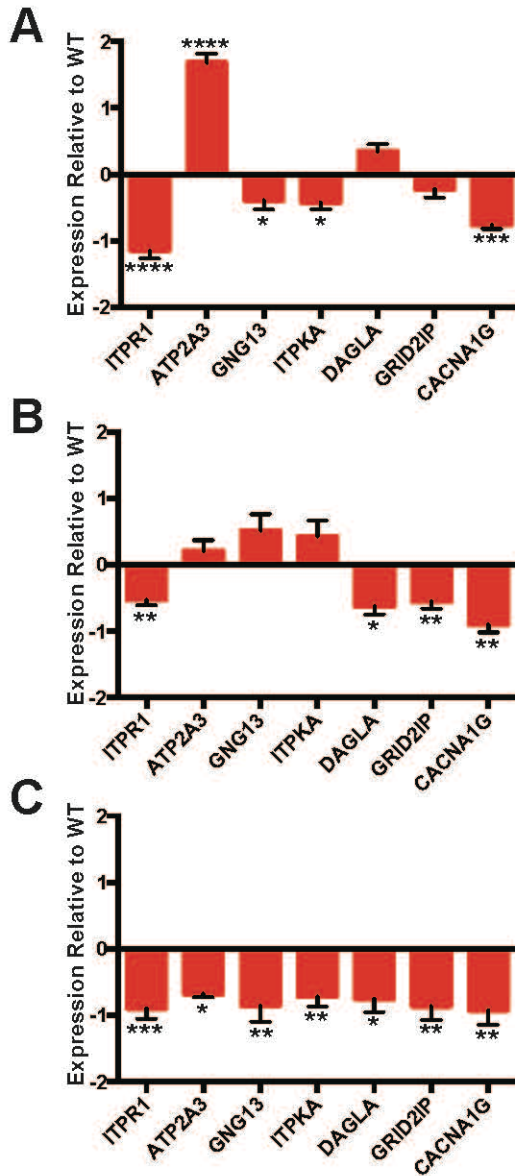
Figure 2.3 Calcium homeostasis gene expression changes with age
RNA was isolated from the cerebellum of fxSCA7 92Q animals and wild-type littermates at presymptomatic, early symptomatic, late symptomatic time points. Expression of genes relevant to calcium signaling were measured using RT-PCR analysis. All values are on a $\log_2$ scale. **A)** At 12 weeks of age presymtomatic fxSCA7 92Q animals have widely varied, both increased and decreased, gene expression when compared to wild-type littermates. **B)** At the early symptomatic age of 20 weeks, expression of some calcium homeostasis genes are down-regulated. **C)** By the advanced symtptomatic age of 36 weeks, expression of all tested calcium homeostasis genes is significantly reduced in fxSCA7 92Q animals compared to wild-type litter mates. For all groups at all time points: n=6. Two-tailed t-test; $*P<0.05$, $**P<0.01$, $***P<0.0005$, $****P<0.0001$ Error bars = S.E.M.
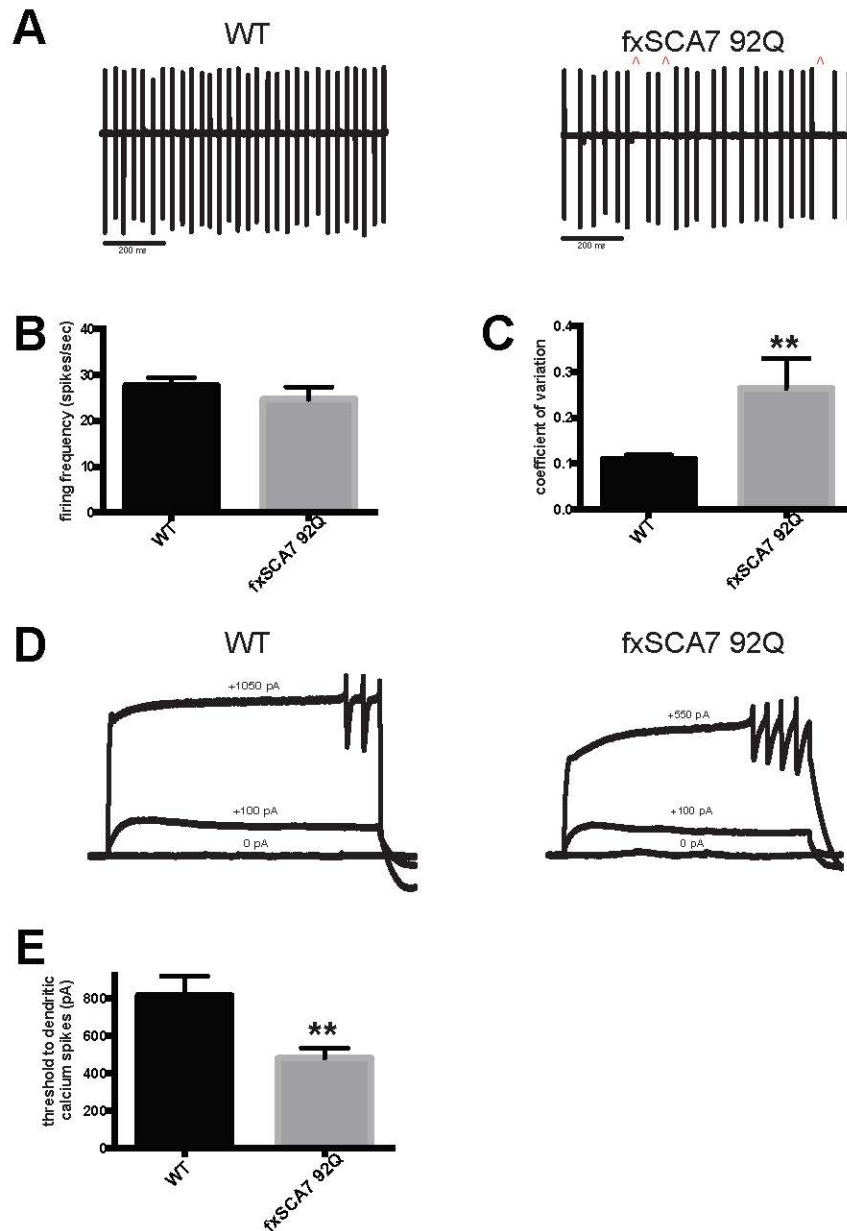
Figure 2.4 Cerebellar Purkinje cells have altered electrophysiology in SCA7
A) Representative traces of Purkinje cell firing obtained via patch-clamp recordings in the cell-attached configuration from mPrP-fxSCA7 92Q-BAC and wild-type littermate controls at age 25 weeks. ^denotes irregularity in spiking. **B)** Purkinje neurons from the posterior cerebellum of fxSCA7 92Q mice show no change in spike frequency, **C)** but have increased spike irregularity (measured by coefficient of variation of the spike frequency). WT n=32, fxSCA7 92Q n=24, two-tailed t-test **$P<0.01$. **D)** Representative traces of Purkinje cell spiking recordings obtained in the whole-cell current clamp configuration from fxSCA7 92Q mice and wild-type littermate controls at 25 weeks. In the presence of tetrodotoxin to block sodium spikes, cells were held at -80 mV and injected with steps of current in +50 pA increments. The amount of current at which dendritic calcium spikes first appear was recorded as the threshold to dendritic calcium spikes [110]. **E)** The threshold to dendritic calcium spikes was significantly lower in fxSCA7 92Q Purkinje neurons, indicating hyperexcitiability. WT n=9, fxSCA7 92Q n=11, mean with S.E.M. shown, two-tailed *t*-test **$P<0.01$
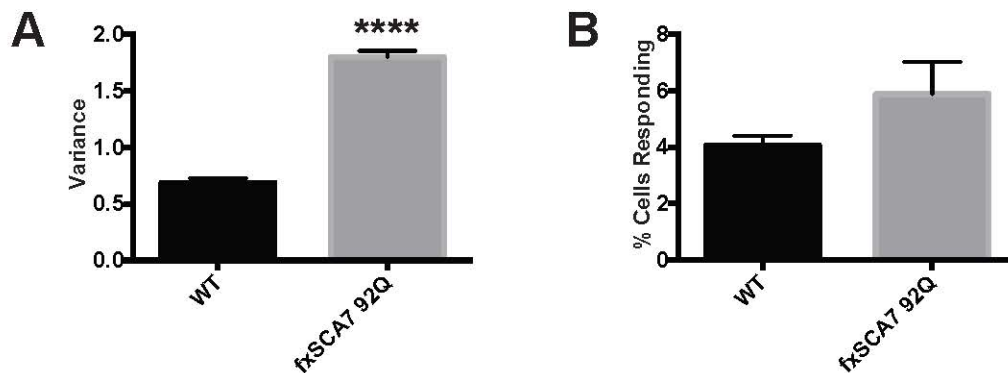
Figure 2.5 Cerebellar granule neurons have altered firing in SCA7
Primary cerebellar granule neurons (CGNs) derived from mPrP-fxSCA7 92Q-BAC were dyed with Fluo-4 NW, subjected to a 40mM KCl stimulus, and imaged live for 20 seconds. As Fluo4 NW is a calcium chelator, changes in signal intensity identify cytosolic calcium changes due to firing. Cells were classified as "responding" when Fluo-4 NW intensity was altered from basal levels and calcium response could be traced over entire recording period. The variance of the resulting Ca^{2+} amplitude curve was calculated to determine regularity of firing in CGNs. **A)** CGNs from fxSCA7 92Q animals had increased variation in calcium traces, **B)** but no difference in responsivity to stimulus. Neurons were harvested per individual animal, and plated in triplicate. Technical replicates of n=3 per animal per condition were utilized, and averaged. The mean with S.E.M. of biological replicates of WT n=6, fxSCA7 92Q n=7 animals is shown. Two-tailed *t*-test, ****$P<0.0001$.
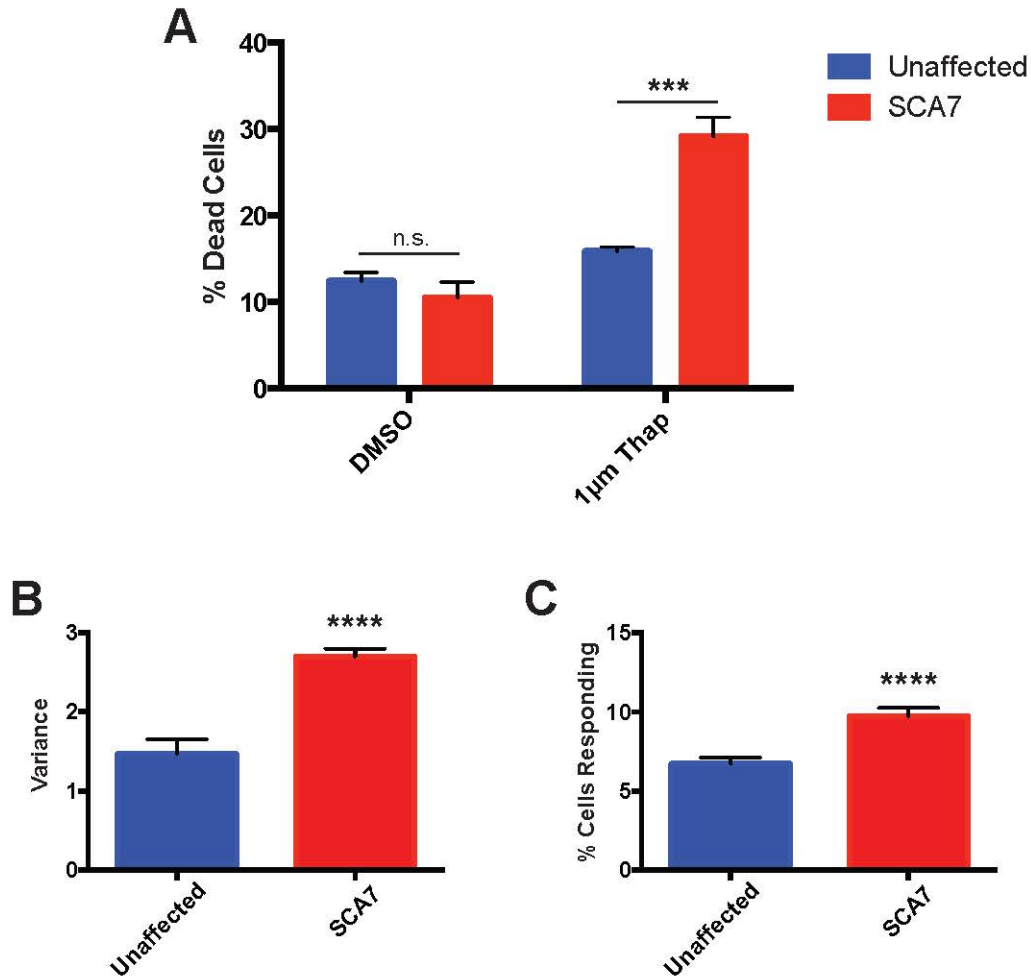
Figure 2.6 SCA7 patient-derived NPCs display altered calcium homeostasis
A) Neural precursor cells (NPCs) were derived from two SCA7 patients (65Q and 70Q) and unaffected family members (10Q). NPCs were treated with 1uM thapsigargin for 24 hours, then stained with propidium iodide to identify dead nuclei and Calcein-AM to identify live nuclei. Death index was quantified by (dead cells/(dead cells +live cells))*100. Experiments were completed on three clones per condition, and the experiment repeated 3 times. The mean of each separate experiment was utilized for statistical analysis. Mean for n=3 is shown with S.E.M. Two-way ANOVA with post-hoc comparison of all values ***P<0.001. **B)** Neural precursor cells (NPCs) were derived from an SCA7 patient (70Q) and an unaffected family member (10Q). NPCs were stained with Fluo4 NW and subjected to live cell imaging after stimulation with 100mM KCl. As Fluo4 NW is a calcium chelator, changes in signal intensity identify cytosolic calcium changes due to firing. Under normal (Non-Treated) conditions, SCA7 patient NPCs have an increased response to stimulation than unaffected NPCs. Cells were considered "responding" when they produced a significant change in the amplitude of Ca^{2+} (Fluo4 NW intensity). **C)** The variance of the resulting Ca^{2+} amplitude curve was calculated to determine regularity of firing in NPCs. Variance was increased in SCA7 patient derived NPCs in response to stimulation. Replicates per condition include measurements from two clones derived from each patient. Recordings we repeated on two days, error bares = S.E.M. Unaffected Non-Treated n=21, SCA7 Non-Treated n=29, Unaffected treated with 1mM NR n=19, SCA7 treated with 1mM NR n=27. Two-tailed t-test, ****P<0.0001.

Chapter 3:

SCA7 Transcriptome Abnormalities in Calcium Homeostasis Derive from Sirt1 Dysfunction

Abstract

To determine upstream regulators of pathways altered in SCA7 disease, we examined the differentially expressed genes defined in Chapter 2 for common transcription factor binding motifs in their promoters. We identified sites regulated by the transcription factors PGC-1α and HIF-1α, two targets of the NAD^+-dependent deacetylase Sirt1. We then assessed NAD^+ metabolism in the cerebellum, and found profound defects in NAD^+, known to decrease Sirt1 function. Genetic over-expression of Sirt1 in two different SCA7 models resulted in amelioration of cerebellar neurodegeneration, calcium flux defects, and membrane excitability in Sirt1-SCA7 bigenic mice. We also rescued disease phenotypes in SCA7 patient-derived neuronal cells with exogenous NAD^+ precursor molecules. These findings indicate that Sirt1 achieves neuroprotection by promoting proper calcium regulation.

3.1 Introduction

After the discovery that over-expression of the NAD^+-dependent deacetylase silent information regulator 2 (Sir2) promotes lifespan extension in yeast[56] attention turned to Sirtuin-1 (Sirt1), its mammalian orthologue, and five closely related proteins. It has since been demonstrated that the sirtuin family of proteins coordinate metabolic responses to changes in nutritional availability to maintain homeostasis in mammals through their NAD^+-dependent deacetylase enzymatic activity[111,112]. While the role of Sirt1 in aging and longevity has been perviously debated[57,58], it is now well established that brain-

specific Sirt1 over-expression in mice delays the aging process and extends lifespan[61]. These same mice also display enhanced neural activity in the hypothalamus and amplified neruobehavioral responses to diet-restricting conditions[113].

Activation of Sirt1 has neuroprotective effects in Alzheimer's disease[114-118], Parkinson's disease[119,120], Huntington's disease[67,68,121-123], and amyotrophic lateral sclerosis[116,124], making this protein an obvious target for neurodegeneration research[69]. Mechanisms of Sirt1 neuroprotection identified in these diseases include activation of the Foxo3a, PGC-1-α, TORC1 and CREB transcriptional pathways and resulting downstream gene expression[125-128]; activation of heat shock factor 1 (HSF1) and thus transcription of molecular chaperones[129-131]; inhibition of NF-κB signalling and reduction of microglial inflammation[132]; and others (reviwed in [62,133,134]). No proposed mechanism of Sirt1 neuroprotection, however, has addressed regional specificity of these diseases in confined areas of the central nervous system (CNS), and the basis for Sirt1 neuroprotection remains uncertain.

As described in Chapter 2, our unbiased transcriptome analysis of SCA7 transgenic mice identified an enrichment of gene expression alterations in the phosphatidyl-inositol signaling and calcium homeostasis pathways in the SCA7 cerebellum. Further *in silico* analysis identified a novel role for Sirt1 in modulating these pathways. Upon *in vivo* investigation we discovered marked changes in NAD+ metabolism, creating an environment favoring altered Sirt1 deacetylation activity in the cerebellum of SCA7 mice. Based upon these

findings, we pursued a genetic rescue in two different SCA7 mouse models by crossing Sirt1 over-expressing mice with PrP-floxed-SCA7 92Q BAC ("fxSCA7 92Q") transgenic mice[42], and with SCA7$^{5Q/266Q}$ (SCA7 266Q) knock-in mice[44]. We observed marked amelioration of cerebellar neurodegeneration and rescue of altered Purkinje cell membrane excitability in Sirt1-SCA7 bigenic mice. We also interrogated SCA7 patient stem cell models, and documented abrogation of calcium handling defects in SCA7 patient-derived neuronal cells upon treatment with a NAD$^+$ precursor molecule. These provocative findings thus indicate that Sirt1 neuroprotection in SCA7 involves regulation of calcium homeostasis, and provide a novel druggable pathway for SCA7 therapy.

3.2 Results

Sirt1 dysfunction accounts for altered expression of calcium regulatory genes in SCA7

To determine the mechanism for the transcription dysregulation observed in fxSCA7 92Q mice (the subject of Chapter 2), we compiled a list of coordinately down-regulated genes detected in the transcriptome analysis, and performed bioinformatics analysis to identify enriched transcription factor binding sites (TFBSs) in promoter regions using oPOSSUM v3.0 (http://opossum.cisreg.ca/oPOSSUM3/)[135-137]. Cutoffs were a z score of ≥10 and a Fisher exact test score of ≥7 (consistent with[80]). Among the top TFBSs hits were PPARG::RXRA (Peroxisome Proliferator Response Element [PPRE])

and HIF1::ARNT (Hypoxia Response Element [HRE]) (**Supplemental Table 2**), which are respectively regulated by PGC-1α[138] and HIF-1α. Both PGC-1α[139] and HIF-1α[140] are Sirt1 substrates, which upon Sirt1 deacetylation are stabilized and activated. Of the calcium homeostasis and signaling genes found to be altered in SCA7, 10 contain putative PPREs, including the *Itpr1* gene which codes for the inositol (1,4,5) triphosphate receptor type 1 (IP3R1) (**Figure 3.1**). We then determined that while there is approximately a 50% reduction of *Sirt1* gene expression measured by RNA isolated from the cerebellum of fxSCA7 92Q mice at the pre-symptomatic age of 12 weeks (**Figure 3.2a**), this difference is ameleorated by the early and late symptomatic ages of 20 and 36 weeks (**Figure 3.2b,c**). We then measured expression of the nicotinamide-nucleotide adenyltransferases (NMNATs), a key enzyme for synthesis of the necessary Sirt1 cofactor, nicotinamide adenine dinucleotide (NAD^+)[141]. In mammals three different NMNAT isoforms (NMNAT1-3) have been described, each with different tissue and subcellular localizations[142]. We observed that expression of *NMNAT1*, the nuclear nicotinamide-nucleotide adenyltransferase[143], is decreased in the cerebellum of fxSCA7 92Q animals (**Figure 3.2d**). Expression of *NMNAT2* and *NMNAT3*, which are both present in various cytolosolic compartments[141], remains unchanged (**Figure 3.2e,f**). We also obtained normalized microarray data from the cerebellum of SCA7 266Q mice[138], which recapitulate a severe, juvenile-onset-like version of SCA7[44], through the National Center for Biotechnology Information (NCBI) Gene Expression Omnibus (GEO) (no. GSE9914)[138]. These data show *NMNAT1* is the single

most differentially downregulated gene at an early symptomatic time point, providing independent validation of our findings in the fxSCA7 92Q mice.

Given this decrease in NMNAT1 expression in two SCA7 models, we hypothesized the activity of many NAD$^+$-dependent enzymes may be relevant to SCA7 pathogenesis. We explored a role for poly(ADP-ribose) polymerase-1 (PARP1)-mediated, as PARP1 can consume large amounts of nicotinamide adenine dinucleotide (NAD$^+$), the necessary co-factor for Sirt1 activity[144]. Indeed, previous studies have shown that decreased PARP1 activity, due to genetic reduction or chemical inhibition, yielded a marked increase in NAD$^+$ levels accompanied by enhanced Sirt1 activity[145,146], indicating that PARP1 and Sirt1 may compete for NAD$^+$ in the nucleus. To test this hypothesis, we performed immunoblot analysis of PARP1 protein expression in the cerebellum of SCA7 266Q mice, and documented a significant increase in PARP1 levels in SCA7 cerebellar protein lysates (**Figure 3.3a**, quantified in **Figure 3.3b**). We then pursued accurate determination of NAD$^+$ levels in the CNS of the SCA7 266Q mice by mass spectrometry. We documented a significant reduction in NAD$^+$ in the cerebellum, with no change in NAD$^+$ levels in the cortex or liver (**Figure 3.3c**). These results, in combination with the Sirt1 and NMNAT1 expression changes in the fxSCA7 92Q mice, indicate that Sirt1 dysfunction likely underlies the transcription abnormalities observed in SCA7 cerebellar degeneration.

Sirt1 transgenic overexpression rescues disease phenotype, neurodegeneration, and membrane excitability in SCA7 mice

To determine if enhanced Sirt1 function can ameliorate SCA7 disease phenotype and neurodegeneration we pursued a genetic rescue in two different SCA7 mouse models, our fxSCA7 92Q mice[42] and in SCA7 266Q mice[44]. To achieve Sirt1 over-expression, we obtained a Sirt1 targeted transgenic over-expression model, where the Sirt1 cDNA is regulated by a strong ubiquitous promoter-enhancer system (CAGGS) with a floxed STOP cassette, and is targeted to the Collagen A1 locus[147]; we crossed these mice with CMV-*Cre* driver mice to derive mice that ubiquitously over-express Sirt1 (the "Sirt1 OX" line); and we quantified Sirt1 expression at ~3-fold endogenous mouse Sirt1 in the CNS by immunoblot analysis (**Figure 3.4a-c**). We then crossed the resultant Sirt1 OX mice with the fxSCA7 92Q mice, or with SCA7 266Q knock-in mice, and we compared motor function, neuropathology, and survival in cohorts of Sirt1 OX-SCA7 bigenic mice and littermate SCA7 transgenic / knock-in mice. We also determined that a few of the calcium homeostasis target genes with altered expression in SCA7 were significantly increased in the singly transgenic Sirt1 OX mice when compared to wild-type littermates at what would be pre-symptomatic (**Figure 3.5a**) and early symptomatic (**Figure 3.5b**) timepoints in the fxSCA7 92Q model. This observation was not maintained in the older Sirt1 OX animals (**Figure 3.5c**), but does support a direct role for Sirt1 in regulating expression of the calcium homeostasis gene set we identified as altered in SCA7.

In crosses with the SCA7 266Q mice, we documented a marked amelioration of cerebellar degeneration in Sirt1 OX–SCA7 266Q bigenic mice, as cerebellar immunostaining analysis revealed increased Purkinje cell calbindin immunoreactivity and reduced gliosis (**Figure 3.6a**). This improvement in cerebellar histology in the Sirt1 OX–SCA7 266Q mice was accompanied by a rescue of Purkinje cell body size (**Figure 3.6b**). A Kaplan-Meier plot revealed that Sirt1 OX–SCA7 266Q mice display improved survival compared to SCA7 266Q mice (**Figure 3.6c**), which was corroborated by comparing average lifespan between littermate matched cohorts of Sirt1 OX-SCA7 266Q bigenic mice and SCA7 266Q mice (**Figure 3.6d**).

Using the fxSCA7 92Q model, we then assessed the effect of genetic Sirt1 over-expression on motor function in SCA7 utilizing a neurological battery[148]. Individuals were evaluated at age 20 weeks (early symptomatic[42]), 28 weeks, and 36 weeks. Animals were assessed on a scale of 0-3 for ledge test to evaluate coordination and balance; clasping behavior to monitor loss of muscle function and tone; gait test to assess coordination and muscle function in addition monitor tremor, limp, and hindlimb involvement; and kyphosis, a dorsal curvature of the spine that is a common manifestation of motor disease in mouse models caused by a loss in muscle tone in spinal muscles secondary to neurodegeneration. A score of 0 was considered healthy, and a score of 3 severe manifestation. Each animal received a summed score out of 12 for each time point in the study. SCA7 mice show a progressive increase in this motor scoring over time[148] and (**Figure 3.7a**). We detected similar onset of motor

phenotypes in fxSCA7 92Q and Sirt1 OX-fxSCA7 92Q animals, yet observed marked improvements in motor function of bigenic animals as all groups continued to age (**Figure 3.7a**), indicating delayed disease progression in the Sirt1 OX-fxSCA7 92Q animals. To ensure animals were genotype correlated with phenotype, we validated Sirt1 overexpression at the gene expression level for each time point (**Figure 3.7b**).

As Sirt1 over-expression slows disease progression, we assessed cerebellar electrophysiological function in Sirt1 OX-fxSCA7 92Q mice by patch-clamp analysis of acute cerebellar slices from bigenic mice and singly transgenic fxSCA7 92Q controls. When we recorded Purkinje cell firing at a symptomatic time point, we documented a significant improvement in overall firing frequency in cerebellar slices from Sirt1 OX–fxSCA7 92Q mice in comparison to fxSCA7 92Q littermates (**Figure 3.8a-b**). This was also accompanied by an obvious improvement in the irregularity of Purkinje cell firing in Sirt1 OX- fxSCA7 92Q cerebellar slices (**Figure 3.8c**).

To delineate the effect of Sirt1 over-expression on the transcriptional abnormalities documented in the cerebellum of fxSCA7 92Q mice, we surveyed RNA expression levels of down-regulated calcium homeostasis and signaling pathway genes. We detected significant increases or strong increase trends in all tested genes in the cerebellum of Sirt1 OX-fxSCA7 92Q mice in comparison to singly transgenic fxSCA7-92Q mice (**Figure 3.9**). Collectively these results indicate that enhanced Sirt1 function is sufficient to rescue neurological disease phenotypes and molecular genetic abnormalities in two SCA7 mouse models.

Sirt1 chemical activation rescues calcium flux defects in SCA7 patient-derived neuronal precursor cells

As neuronal precursor cells (NPCs) derived from SCA7 patient iPSCs display calcium flux defects (described in Chapter 2), we hypothesized Sirt1 activation would restore proper neuronal activity as it did in the Sirt1 OX- fxSCA7 92Q animals. To activate Sirt1 we treated SCA7 patient-derived and unaffected family member NPCs with nicotinamide riboside (NR). An NAD^+ precursor, NR has been previously shown to increase NAD^+ levels and activate Sirt1[149]. Upon treatment with NR there was rescue of SCA7 patient NPC hyper-responsivity (**Figure 3.10a**) and calcium flux variation (**Figure 3.10b**) that are observed in non-treated SCA7 NPCs. Collectively these studies indicate Sirt1 activation and modulation of NAD^+ synthesis as a possible avenue for therapeutic intervention in SCA7.

3.3 Discussion

As was discussed in Chapter 2, we identified decreased expression of calcium regulatory genes in the cerebellum of SCA7 mice using unbiased transcriptome analysis, and documented altered calcium handling in SCA7 neurons. When we interrogated the promoters of the differentially expressed calcium regulatory genes for shared transcription factor binding sites (TFBSs), we noted a highly significant enrichment of the PPAR response element (PPRE) and the hypoxia-inducible factor response element (HRE). These results led us

to consider a role for Sirt1 in SCA7, as PGC-1α-PPARλ and HIF-1α bind these regulatory elements and are all major substrates of Sirt1. We hypothesized a role for the PPRE coactivator PGC-1α, because PGC-1α is highly expressed in the cerebellum[150], PGC-1α knock-out mice exhibit severe motor incoordination phenotypes around the time of weaning[151], and all the PPRE-containing genes down-regulated in SCA7 cerebellum, except for one, are significantly decreased in their expression in SCA1 cerebellum in model mice[152]. We interrogated changes in NAD+ metabolism to infer changes in Sirt1 deacetylation activity, as reduced NAD$^+$ is known to decrease Sirt1 function[141]. The profound defects we observed in NAD+ metabolism led us to pursue a genetic rescue of SCA7 disease phenotypes in two different SCA7 mouse models. When crossed with Sirt1 over-expressing transgenic mice, we documented marked improvements in motor function, cerebellar neurodegeneration, survival, transcription dysregulation, and Purkinje cell calcium handling and electrophysiological function in SCA7 bigenic mice. Importantly, addition of an exogenous NAD+ precursor to neuronal cells differentiated from SCA7 patient iPSCs also rescued electrophysiological function, confirming that Sirt1 dysfunction contributes to SCA7 pathogenesis.

Sirt1, the closest mammalian orthologue of yeast Sir2, remains one of the most important nutrient-sensing regulators of metabolism, cellular function, and longevity. Sirt1 over-expression in transgenic mice can confer many of the benefits of caloric restriction, including improved metabolic function, decreased lipid levels, and enhanced glucose homeostasis. Of particular interest for

neurotherapeutics, independent studies have reported that increased expression of Sirt1 can ameliorate neurodegenerative phenotypes in mouse models of Huntington's disease[125,126]. Sirt1 neuroprotection is thought to occur via its enzymatic regulation of key targets, with prior studies implicating RARβ, tau, FOXO3a, and mTORC1 as the likely downstream mediators of Sirt1 neuroprotection[69]. Our current results, however, indicate that Sirt1 neuroprotection also involves promotion of calcium homeostasis by transactivation of calcium regulatory genes. Sirt1 regulation of calcium homeostasis appears especially relevant for neurodegenerative disorders involving brain regions with onerous metabolic demands and rapid, ongoing neurotransmission, where the challenges of calcium flux regulation are particularly acute. The cerebellum and the Purkinje cell neurons resident therein certainly fulfill these criteria, as Purkinje cells are among the most metabolically active of all neurons and selectively express very high levels of calcium-binding proteins, such as calbindin. Of the various cerebellar ataxias, a role for calcium dysregulation in SCA7 is supported by abnormal calcium dynamics and electrophysiology both in SCA7 model mice and in neuronal cells derived from SCA7 patient stem cells.

What accounts for impaired Sirt1 function in SCA7? To address this question, we considered the necessity of the enzymatic co-factor NAD^+ in assuring maximal Sirt1 function, and evaluated gene expression of NMNAT1, a major regulating enzyme in the nuclear NAD^+ salvage pathway. We found a dramatic decrease in *NMNAT1* levels in the cerebellum of our fxSCA7 92Q

animals, and corroborated this finding in a model of juvenile onset SCA7 (SCA7 226Q) through publicly available genomic datasets. Additionally we evaluated the status of PARP1, a major consumer of nuclear NAD$^+$. We found that PARP1 levels were markedly increased in the cerebellum of SCA7 mice, and using mass spectrometry, we documented a significant reduction of NAD+ in SCA7 cerebellum. Depletion of NAD$^+$ is emerging as a likely explanation for decreased Sirt1 activity in neurodegeneration. Indeed, NAD$^+$, because of its role in promoting cellular homeostasis, is increasingly recognized as a putative regulator of aging and degenerative diseases associated with aging, as NAD+ levels significantly decline with age[153], and NAD$^+$ replenishment can promote lifespan extension and counter age-related impairments in stem cell maintenance and physiological function[153,154]. Rescue of SCA7 disease phenotypes by Sirt1 over-expression suggests that while overall NAD$^+$ levels are reduced, a substantial increase in nuclear Sirt1 may result in more rapid utilization of the nuclear NAD$^+$ pool, leading to shuttling of NAD$^+$ from cytosol to nucleus to support increased Sirt1 activity and thus neuroprotection.

In this study, we have uncovered a series of related defects that represent viable targets for rationale therapy development for SCA7 and related neurodegenerative disorders. An attractive therapeutic strategy is to boost the function of Sirt1, and while efforts are underway to identify Sirt1 activators, the existence of a promising lead small molecule is currently lacking. As our results indicate that NAD$^+$ depletion may account for impaired Sirt1 function in SCA7, one promising and highly feasible approach would be to increase NAD$^+$ levels.

A variety of choices for NAD_+ repletion are now available, including supplementation with vitamin B3 (nicotinamide), supplementation with NMN, a precursor of NAD^+ in the salvage pathway, and supplementation with nicotinamide riboside (NR), which enters the salvage pathway as NMN after being phosphorylated by NR kinases, which are highly abundant in cytosol[144,155]. Indeed, recent work indicates that NAD^+ repletion may have therapeutic application in neuromuscular disorders and neurodegenerative diseases, such as Alzheimer's disease and glaucoma[154-157]. Yet another potential neurotherapeutic target is PARP1, for which pharmacological inhibitors, some in clinical trials for cancer, are available[158]. While all of these therapeutic strategies deserve consideration as treatments for SCA7, recent findings in the neurodegenerative disease field underscore the intriguing possibility that these pathways are dysregulated in related disorders[159], highlighting the potential for therapies targeting shared pathogenic processes with broad applicability to degenerative CNS disease.

3.4 Experimental procedures

Mouse studies

All animal experimentation adhered to NIH guidelines and was approved by, and performed, in accordance with the University of California, San Diego Institutional Animal Care and Use Committee (IACUC) and the University of Michigan Committee on the Use and Care of Animals.

Real-time quantitative PCR (RT-qPCR)

Mice were euthanized under isoflurane anesthesia, and cerebella were rapidly removed and flash-frozen in liquid nitrogen. Tissue was stored at $-80^{\circ}C$ until processing. RNA was isolated from the whole cerebellum of animals using TRIzol (Life Technologies), and treated with DNAse I in the form of TURBO-DNAse (Life Technologies) to remove traces of genomic DNA. Reverse transcription was performed with SuperScript Reverse Transcriptase (Life Technologies). Quantitative PCR was carried out using TaqMan probes (Life Technolgies) and TaqMan Universal PCR Mix (Life Technologies) on a CFX384 Touch system (Bio-Rad), with a 10minute gradient to $95^{\circ C}$ followed by 40 cycles of $95^{\circ C}$ for 15 seconds and $60^{\circ C}$ for 1 minute. Gene expression was normalized to GAPDH levels. Delta CT values were calculated as $C_t^{target} - C_t^{GAPDH}$. All experiments were performed with three technical replicates. Relative fold changes in gene expression were calculated using the $2^{-\Delta\Delta Ct}$ method[107]. Data are presented as the average of the biological replicates + standard error of the mean (S.E.M.). Select genes were validated via RT-qPCR as described above.

Immunoblot analysis

For Western blot analysis, mouse cerebella were lysed in RIPA buffer (Life Technologies) and homogenized by tritiration. Immunoblotting was performed with antibodies for PARP1 (9542, Cell Signaling; 1:1000) and Sirt1

(07-131, Millipore; 1:1000). Densitometry was performed in ImageJ [160] and values normalized to β-actin (ab8226, Abcam; 1:10000).

NAD+ Quantification

NAD$^+$ was extracted using acidic then alkaline extraction methods and analyzed with mass spectrometry. Frozen tissues taken from the −80°C freezer were immediately extracted in 1 M perchloric acid and neutralized in 3 M K2CO3 on ice. After centrifugation, the supernatant was mixed with buffer A [H2O + 20 mM ammonium acetate (pH 9.4)] and loaded onto a column (150 × 2.1 mm; Kinetex EVO C18, 100 Å). HPLC was run for 2 min at a flow rate of 300 μl/min with 100% buffer A. Then, a linear gradient to 100% buffer B [methanol + 5 mM ammonium acetate (pH 8.5)] was performed (at 2 to 11 min). Buffer B (100%) was maintained for 4 min (at 11 to 15 min), and then a linear gradient back to 100% buffer A (at 15 to 17 min) began. Buffer A was then maintained at 100% until the end (at 17 to 25 min). NAD$^+$ eluted as a sharp peak at 3.3 min and was quantified on the basis of the peak area compared to a standard curve and normalized to tissue weight of frozen tissues [154,161,162].

Tissue immunohistochemistry for Soma Size

For neuropathology experiments, deeply anesthetized mice were transcardially perfused with PBS followed by 4% paraformaldehyde (PFA) in 0.1M phosphate buffer, pH 7.4. Brains were removed and postfixed with 4.0% PFA in in O.1M PB overnight, then moved to 15% followed by 30% sucrose

solutions. Free-floating 30µm sagittal brain sections were cut on a vibratome and incubated with antibodies to calbindin (C9848, Sigma; 1:500) and glial fibrilary acidic protein (GFAP) (G9269, Sigma; 1:1000), and imaged with a Zeiss LSM 780 inverted microscope. Purkinje cell soma size was quantified using area function in ImageJ [160,163]. Values shown are the average of biological replicates from separate litters. Error bars = standard error of the mean (S.E.M.).

Behavioral studies

For motor studies, mice were visually inspected by a blinded examiner for obvious neurological signs and examined using a composite neurological evaluation tool (ledge test, clasping, kyphosis and gait were scored on a scale of 0 (normal) to 3 (severely impaired)), as described previously [148]. Females and males were used, and studies performed by a blinded examiner. Changes in score were data are presented as average of biological replicates ± standard error of the mean (S.E.M.). For survival studies, animals were monitored daily and pronounced dead when reparation or heartbeat was no longer present. Cohort sizes were designated based upon power analysis for threshold effects of at least 25% difference. Ages of animals used in this study are described in figure legends.

Patch-clamp electrophysiology solutions

Artificial cerebrospinal fluid (aCSF) contained the following (in mM): 125 NaCl, 2.5 KCl, 26 $NaHCO_3$, 1.25 NaH_2PO_4, 2 $CaCl_2$, and 10 glucose. For all recordings

other than dendritic capacitance measurements, pipettes were filled with internal recording solution containing the following (in mM): 119 K-Gluconate, 2 Na-Gluconate, 6 NaCl, 2 $MgCl_2$, 0.9 EGTA, 10 HEPES, 14 Tris-phosphocreatine, 4 MgATP, 0.2 Tris-GTP, at pH 7.3 and osmolarity 290 mOsm. For dendritic capacitance measurements, internal recording solution contained (in mM): 140 CsCl, 2 $MgCl_2$, 1 $CaCl_2$, 10 EGTA, 10 HEPES, 4 Na_2ATP, at pH 7.3 and osmolarity 287 mOsm.

Preparation of brain slices for acute electrophysiological recordings

Mice were anesthetized by isoflurane inhalation and decapitated. The brain was removed and submerged in pre-warmed ($33^{o}C$) aCSF. Acute parasagittal slices were prepared in aCSF held at $32.5\text{-}34^{o}C$ on a VT1200 vibratome (Leica) to a thickness of 300 μm. Once slices were obtained, they were incubated in carbogen-bubbled (95% O_2, 5% CO_2) aCSF at $33^{o}C$ for 45 minutes. Slices were then stored in carbogen-bubbled aCSF at room temperature until use. During recording, slices were placed in a recording chamber and continuously perfused with carbogen-bubbled aCSF at $33^{o}C$ at a flow rate of 2.5 mL/min.

Patch-clamp electrophysiology recordings

Purkinje neurons were visually identified for patch-clamp recordings using a 40x water immersion objective and a Nikon Eclipse FN1 upright microscope with infrared differential interference contrast (IR-DIC) optics.

Identified cells were visualized using NIS Elements image analysis software. Borosilicate glass patch pipettes were pulled to resistances of 3-4 MΩ for all recordings. Recordings were performed 1-5 hours after slice preparation. Data were acquired using an Axopatch 200B amplifier, Digidata 1440A interface (MDS Analytical Technologies), and pClamp-10 software (Molecular Devices). All data were digitized at 100 kHz. Whole-cell recordings were rejected if the series resistances changed by >20% during the course of recording, or if the whole-cell series resistance rose above 15 MΩ. All voltages are corrected for the liquid gap junction potential, which was calculated to be 10 mV [87].

Analysis of firing properties from patch-clamp recordings

Electrophysiology data were analyzed offline using Clampfit 10.2 software (Molecular Devices). Firing frequency and coefficient of variation (CV) calculations were performed in the cell-attached configuration on spikes in a 150 second time interval obtained ~5 minutes after formation of a stable seal. The CV was calculated as follows:

$$CV = \frac{Standard\ Deviation\ of\ Interspike\ Interval}{Mean\ Interspike\ Interval}$$

The firing frequency distribution was obtained by identifying the percentage of cells in each incrementing 10 spike/second bin. The CV distribution was similarly obtained by sorting CV values into incrementing 0.02 bins. A moving average trendline was added to the CV distribution histogram to outline the shape of the distribution.

To determine whether the distribution of CV values was significantly different between genotypes, a Fisher's exact test was performed between the populations of regular firing and irregular firing cells for each genotype. Regular spiking was defined as cells with a CV cutoff value within 3 standard errors of the mean wild-type CV (to represent a 99% confidence interval of the wild-type mean). All cells at or under this cutoff value were considered to be regular firing cells, while all cells above this cutoff value were considered to be irregular firing cells.

NPC differentiation

All work done with fibroblasts and resulting iPSC-derived NPCs obtained informed consent from SCA7 patients and unaffected family members and approved by the Institutional Review Boards in accordance with the requirements of the Code of Federal Regulations on the Protection of Human Subjects (45 CFR 46 and 21 CFR 50 and 56), including its relevant Subparts, and the UCSD Embryonic Stem Cell Research Oversight (ESCRO) Committee (Project #130337ZF). NPCs were generated with STEMdiff Neural Induction Medium (NIM) (StemCell Technologies) according to manufacturer's monolayer culture protocol instructions. Briefly, iPSCs were gently dissociated with Accutase (StemPro, ThermoFisher), pelleted, and resuspended in NIM at $1\text{-}2 \times 10^6$ cells/mL, then plated on Matrigel coated dishes. Cells were passaged one more time in NIM and plated in dishes coated with poly-L-ornithine (15 ug/mL) and laminin (10 ug/mL) (Sigma-Aldrich). Cells tested negative for mycoplasma,

and were thereafter passaged and expanded in STEMdiff Neural Progenitor Medium (NPM) (StemCell Technologies) on poly-L-ornithine/laminin-coated dishes at a density of 0.5-210 x 105 cells/well for cell death assay, and 25,000-50,000 cells per well for Fluo-4 NW imaging calcium experiments.

Fluo-4 NW CGN calcium Imaging Experiments

For real-time recordings of intracellular calcium dynamics in our cell lines, cells were plated in 96-well plates at the densities described above. Prior to measurements, cells were loaded with Fluo-4 NW Calcium Assay Kit (Life Technologies, Carlsbad, CA). We have added 200 ng/ml (650 nM) Hoechst 33342 (Life Technologies, Carlsbad, CA). Plates were incubated with the dye at 37°C for 30 minutes, then at room temperature for an additional 15 minutes. After extensive wash, cells were incubated in neuronal media for 10 min. To perform optical recordings, we utilized ImageXpress® Micro XLS System (Molecular Devices) equipped with a Spectra X light engine (Lumencor) and standard filter sets. Raw movies were acquired at 50 fps, and pre-processed using MetaExpress Imaging software (Molecular Devices).

The image analysis and physiological parameter calculation was conducted using ImageJ analysis program. The analysis was performed in a similar manner on fluorescence traces generated from each neuron. Parameter tables were analyzed using Microsoft Excel 2013 and OriginPro software (OriginLab, CA). Variance analysis of the individual neurons has been performed for each calcium signal for minimum of 4 individual neurons per well.

Mathematical variance (σ^2) is defined as the sum of the squared distances of each term (χ) in the distribution of the mean (μ) divided by the number of samples (N) and calculated as follows:

$$\sigma^2 = \frac{\Sigma\,(\chi - \mu)^2}{N}$$

Resulting variance data were plotted as mean with S.E.M. Single cell traces were gated to remove non-responding and low responding cells by selecting only those cells with a $(Ca^{2+})_i$ value at the peak of the transient that was included in the top 80% range of cells measured in the well. The setting was maintained for all the group of analysis. At least five wells were recorded for each test condition.

Statistical Analysis

Statistic tests are described in the figure legends for all data. Statistical analysis was done using Microsoft Excel, Prism 6.0 (GraphPad), SigmaPlot (Systat Software), and Origin (Origin Labs). Statistical significance was defined at $P<0.05$. For one-way and two-way analysis of variance (ANOVA), if statistical significance ($P<0.05$) was achieved, then we performed post hoc analysis corresponding to the experiment, as specified by the figure legend, to account for multiple comparisons. All t-tests are two-tailed Student's t-tests unless otherwise indicated, and level of significance (alpha) was always set to 0.05.

Acknowledgements

Portions of Chapter 3 are part of a manuscript submitted for publication. Stoyas CA, Bushart D, Ward JM, Switonski PM, Niu CC, Savchenko A, Gariani K, Awuerx J, Shakkottai VG, and La Spada AR. The dissertation author is the principal author of this work.

Figures
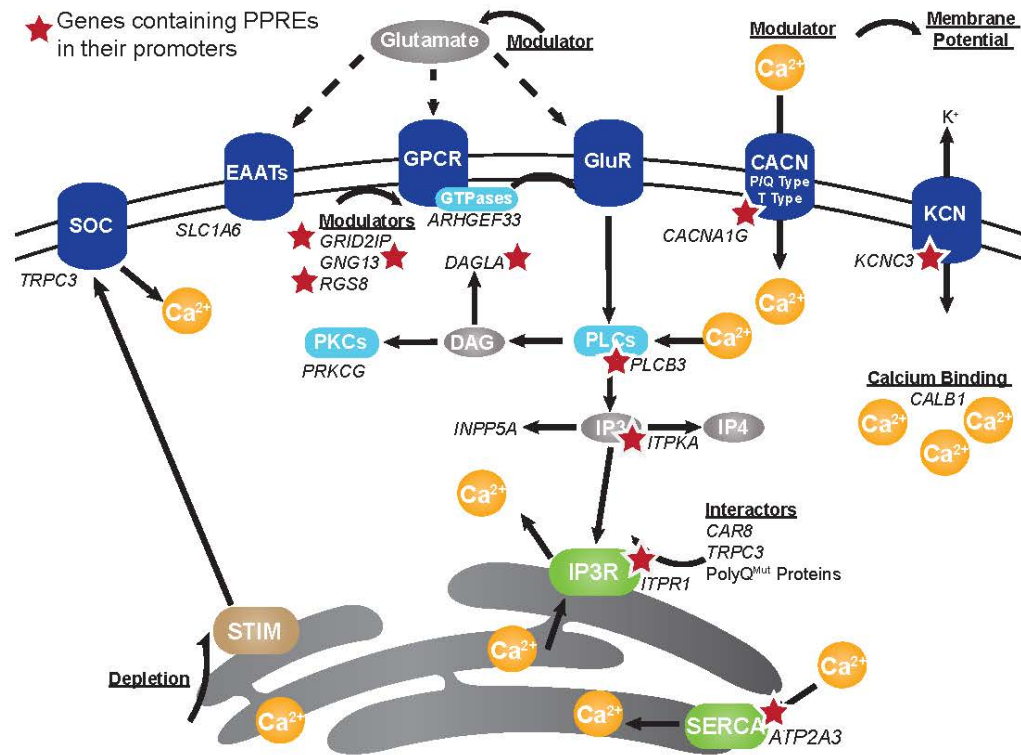
Figure 3.1 Genes central to calcium homeostasis have PPREs in their promoters
Here we see a diagram of the cell membrane, membrane-based cell signaling pathways, and the ER, indicating proteins involved in regulating calcium homeostasis and flux. Black italics indicate genes that are differentially down-regulated in SCA7 cerebellum as determined by RNA-seq analysis. Red stars demarcate the ten calcium regulatory genes identified to contain a PPAR response element (PPRE) in their promoters based on oPOSSUM 3.0 analysis (Z-score= 13.599, Fisher score= 12.631).

Figure 3.2 Sirt1 and NMNAT1 expression are altered in SCA7
We isolated RNA from the cerebellum of fxSCA7 mice aged 12, 20, and 36 weeks then performed RT-qPCR utilizing a Sirt1 probe. **A)** At age 12 weeks (presymptomat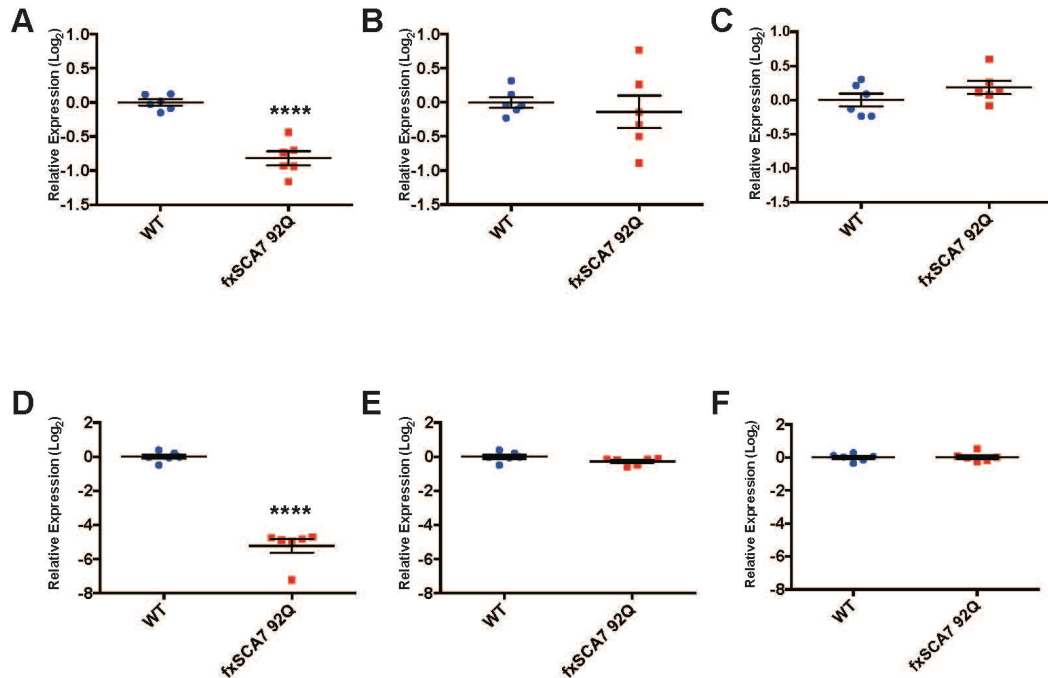ic), there is approximately a 50% reduction in Sirt1 gene expression in fxSCA7 animals. WT: n=6, fxSCA7: n=6, two-tailed t-test, ****P<0.0001. Error bars = S.E.M. **B)** At age 20 weeks (early symptomatic), there is no change in Sirt1 gene expression in SCA7. WT: n=6, fxSCA7: n=6, two-tailed t-test. Error bars = S.E.M. **C)** At age 36 weeks (progressed symptomatic), there is no change in Sirt1 gene expression in SCA7. In the 36 week old animals, we also looked at expression of the nicotinamide mononucleotide adentyltransferase (NMNAT). **D)** Expression of nuclear NMNAT1 is dramatically reduced fxSCA7 92Q animals while cytosolic **E)** NMNAT2 and **F)** NMNAT3 expression are unchanged. WT: n=6, fxSCA7: n=5, two-tailed t-test, ****P<0.0001. Error bars = S.E.M.
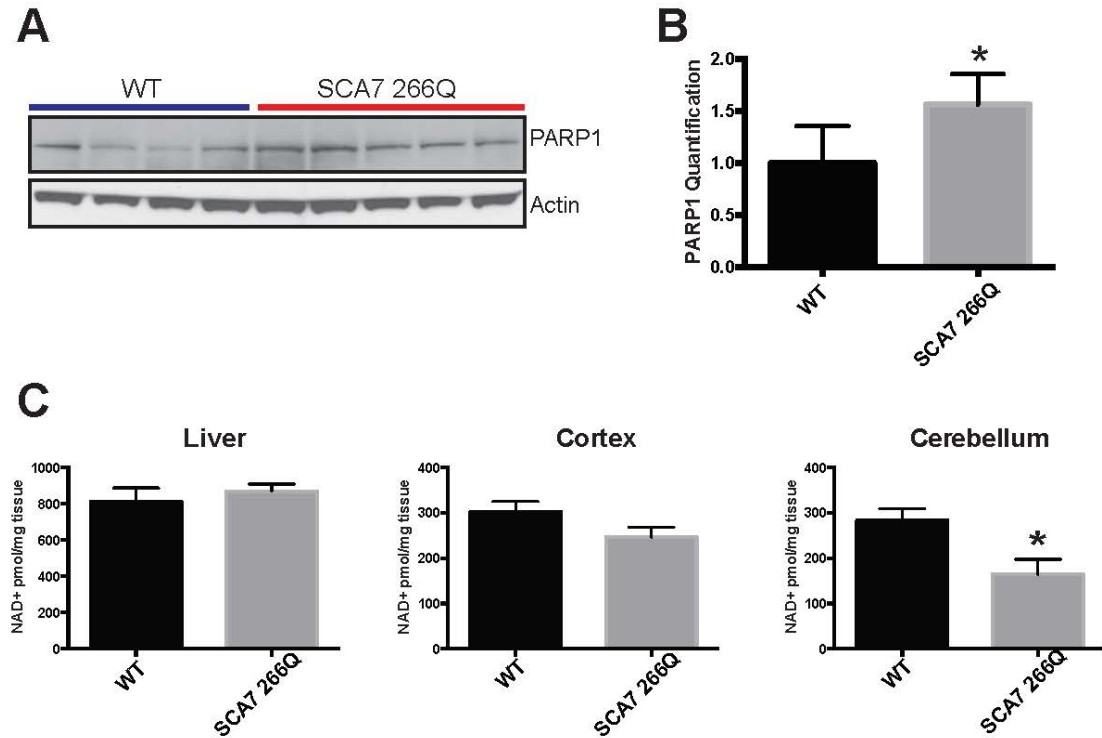
Figure 3.3 NAD$^+$ metabolism is altered in juvenile onset model of SCA7
A) We prepared cerebellar protein lysates from 8.5 week-old SCA7 266Q mice and WT controls, and then performed immunoblot analysis of PARP1. **B)** We quantified these results by densitometry analysis of PARP1 and b-actin (loading control) WT: n=4, SCA7 266Q: n=5; two-tailed *t*-test, *P <0.05. Error bars = S.E.M.. **C)** We isolated liver, cerebellum, and cortex from 8.5 week-old SCA7 266Q mice and WT controls, and then performed mass spectrometry measurement of NAD+ levels. WT: n=5, SCA7266Q: n=5; two-tailed *t*-test, *P <0.05. Error bars = S.E.M.
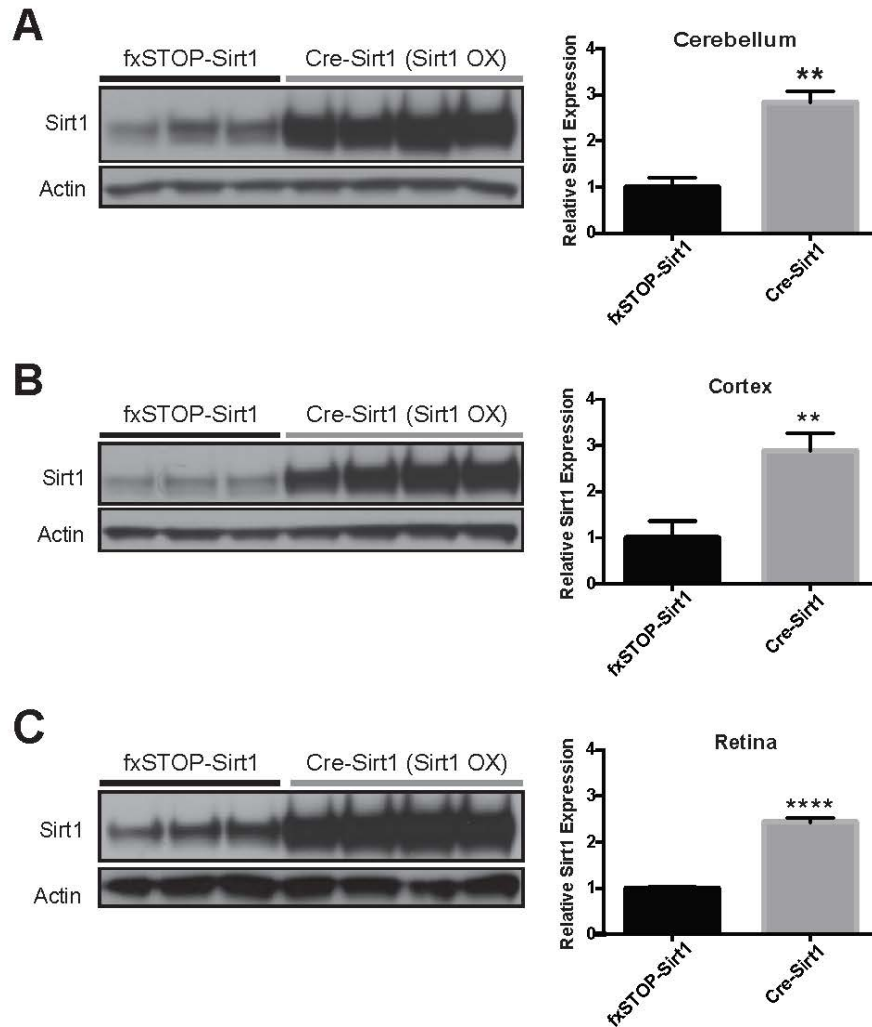
Figure 3.4 Sirt1 ubiquitous over-expressing transgenic mice exhibit increased expression of Sirt1 in central nervous system tissues
To derive transgenic mice that ubiquitously over-express Sirt1, we crossed a line of floxed STOP– Sirt1 transgenic mice (fxSTOP-Sirt1) with CMV-Cre driver mice to yield bigenic mice with excision of the floxed STOP cassette in all tissues, including the CNS and the germ line. Immunoblotting analysis of the resultant bigenic mice (Sirt1 OX) and parental fxSTOP-Sirt1 mice for Sirt1 was performed as shown, and the expression of Sirt1, relative to b-actin, quantified. **A)** We documented a ~3-fold increase in Sirt1 expression in the cerebellar and **B)** cortical tissues of the brain, and **C)** ~2.5 fold increase in Sirt1 expression in the retina. fxSTOP-Sirt1: n = 3, Sirt1 OX: n = 4; two-tailed t-test, **$*P$ <0.01, ****P <0.0001. Error bars = S.E.M.
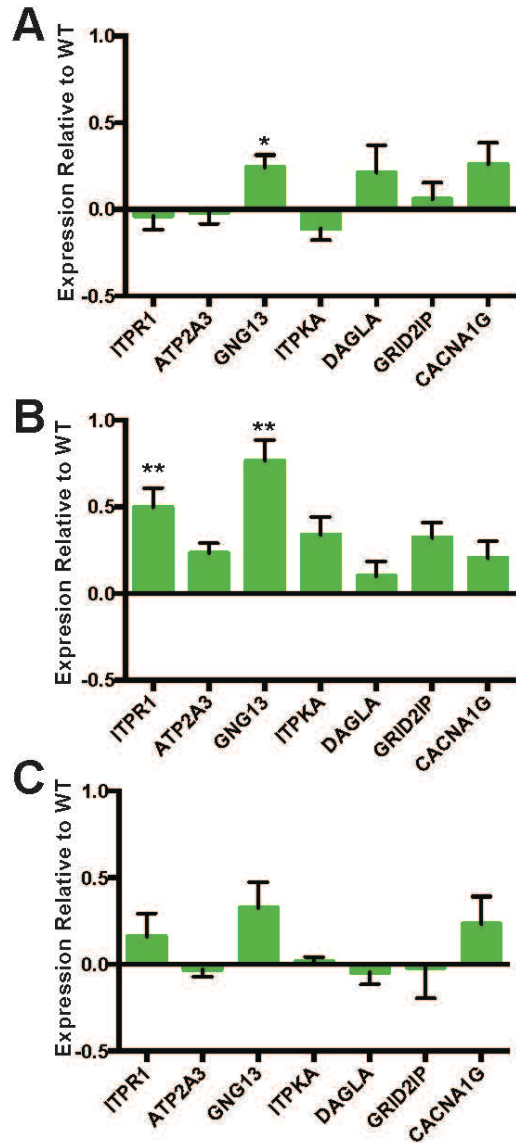
Figure 3.5 Sirt1 OX increases expression of some calcium homeostasis target genes in otherwise healthy animals

RNA was isolated from the cerebellum of Sirt1 OX animals and wild-type littermates at age 12, 20, and 36 weeks; correlating with pre-,early-, and advanced age of onset in fxSCA7 92Q animals. Expression of genes relevant to calcium signaling were measured using RT-PCR analysis, values shown in $\log_2$ scale. **A)** At 12 weeks of age one calcium homeostasis gene is upregulated in otherwise healthy Sirt1 OX animals when compared to wild-type littermates. **B)** At 20 weeks of age, expression of two calcium homeostasis genes are up-regulated in healthy Sirt1 OX animals when compared to non-transgenic littermates. **C)** By the age of 36 weeks, expression of all tested calcium homeostasis genes is not statistically different in Sirt1 OX animals when compared to wild-type littermates. For all groups at all time points: n=6. Two-tailed t-test; *P<0.05, **P<0.01. Error bars = S.E.M.
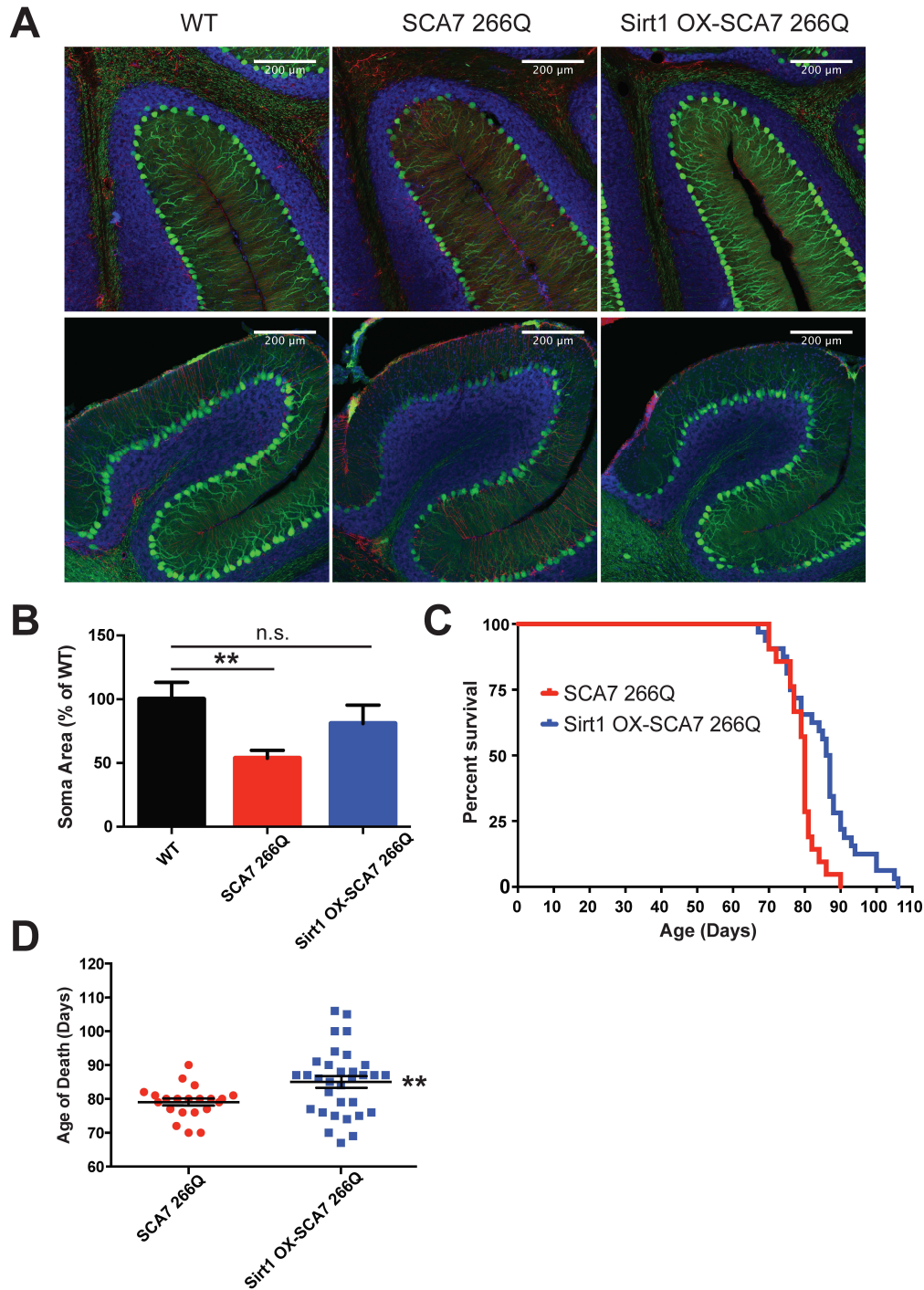
Figure 3.6 Sirt1 over-expression rescues SCA7 disease phenotype in SCA7 266Q model
A) Sirt1 OX-SCA7 266Q mice display increased calbindin immunoreactivity and decreased gliosis. Green = calbindin; Red = Glial Fibrillary Acid Protein (GFAP); Blue = DAPI. Scale bar = 200μm. **B)** Quantification of Purkinje cell soma area, based on 'A'. n= 3 mice per group, one-way ANOVA with Dunnett's post-hoc test, *$P<0.05$. C) Kaplan-Meier plot shows that Sirt1 overexpression significantly extends survival of SCA7 266Q mice. SCA7: n=21, Sirt1 OX-SCA7 266Q n=32; Log-rank (Mantel-Cox) test χ^2=10.17, df=1, **$P<0.01$. **D)** Scatter plot indicating average age of death from animals in 'C' is increased. Two-tailed *t*-test, **$P<0.01$.
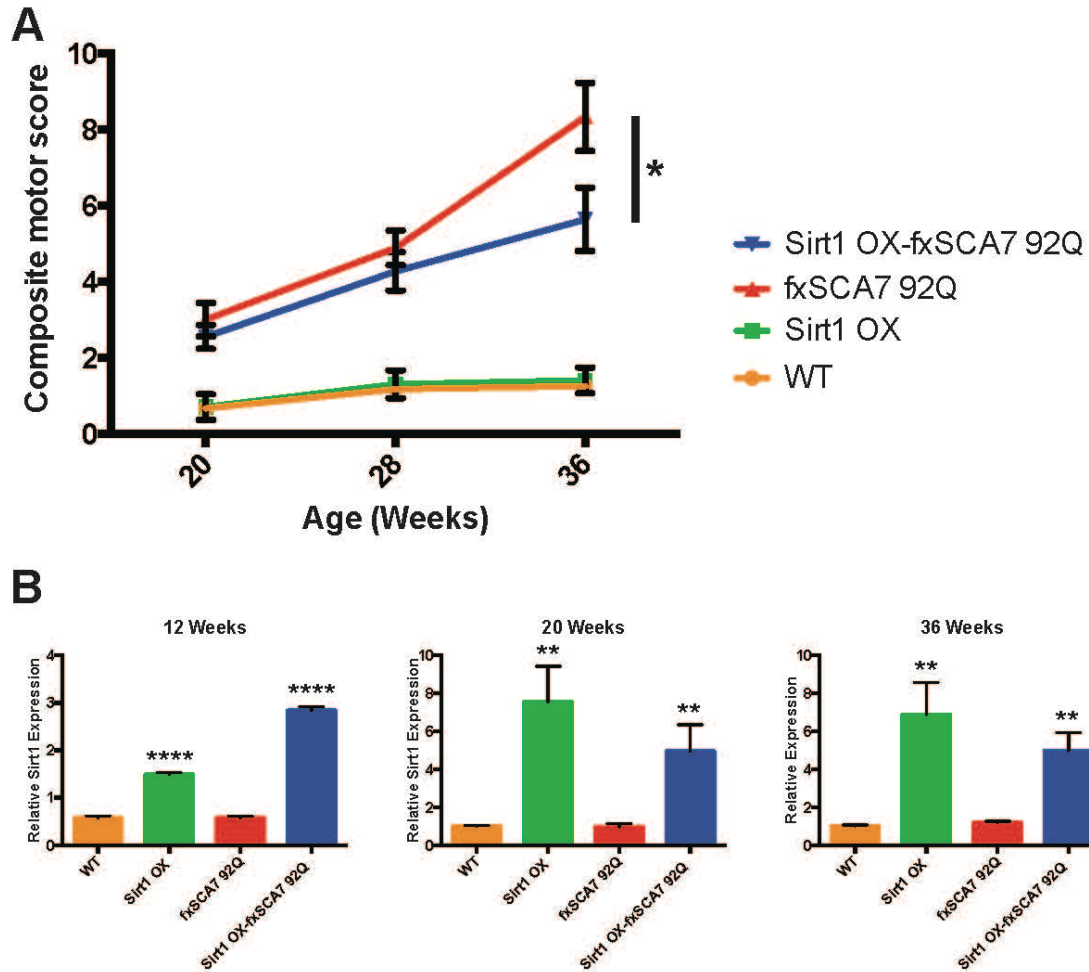
Figure 3.7 Sirt1 over-expression slows progression of motor phenotype in SCA7 92Q animals

A) We performed a neurological screening battery on cohorts of mice (n = 8 – 12 / group), of the indicated genotypes and at the indicated ages. Kyphosis, clasping, ledge test, and gait were scored on a scale of 0-3 generating a motor score out of 12 per animal. A score of zero is considered healthy, a score of 12 severely impaired. Sirt1 OX–fxSCA7 92Q mice exhibited an amelioration of motor dysfunction over time in comparison to singly transgenic fxSCA7 92Q mice. WT: n=12, Sirt1: OX n=10, fxSCA7 92Q: n=9, Sirt1 OX-fxSCA7 92Q: n=11. One-way ANOVA with Tukey's post-hoc test, *$P<0.05$. Error bars = S.E.M. **B)** Sirt1 overexpression in the cerebellum was confirmed by RT-qPCR in pre-symptomatic (12 weeks), early symptomatic (20 weeks), and post-symptomatic (36 weeks) animals. n= 6 for all groups, one-way ANOVA with Dunnet's post-hoc test, **$P<0.01$, ****$P<0.0001$. Error bars = S.E.M.
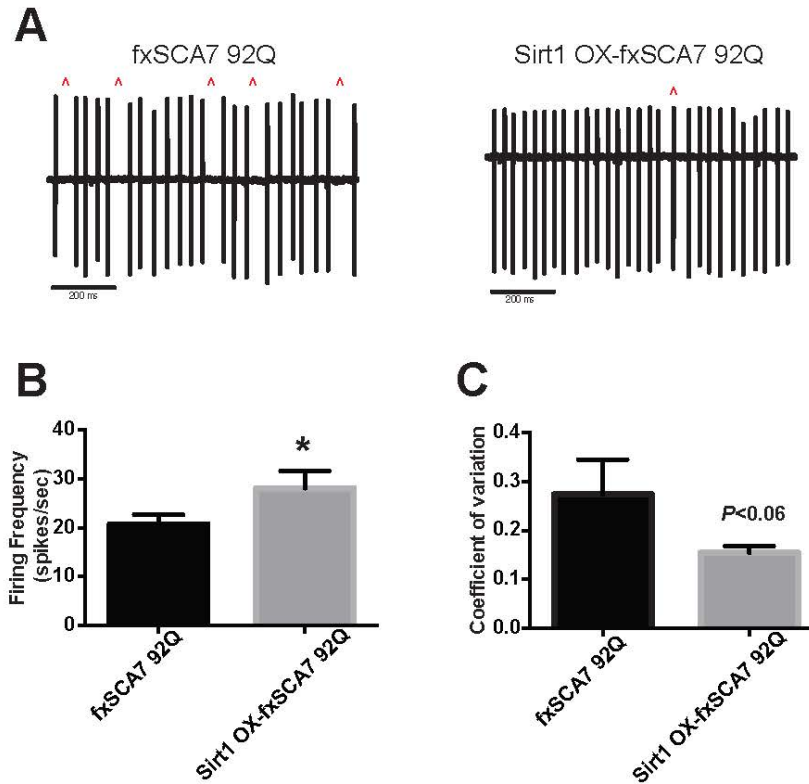
Figure 3.8 Sirt1 over-expression rescues Purkinje cell firing irregularities SCA7
A) Representative traces of cell-attached patch-clamp recordings of Purkinje cells from 28 week old fxSCA7 92Q and Sirt1 OX – fxSCA7 92Q mice illustrating irregular spiking in fxSCA7 92Q Purkinje cells that is improved in Sirt1 OX – fxSCA7 92Q Purkinje cells. **B)** Cell-attached recordings of Purkinje cell firing frequency for 28 week-old fxSCA7 92Q mice in comparison to Sirt1 uOE – fxSCA7 92Q mice (n = 4 / group). fx SCA792Q slices: n=28, Sirt1-SCA7 slices: n=27; two-tailed t-test, *P <0.05. Error bars = S.E.M. **C)** Cell-attached patch-clamp recordings of the coefficient of variation of Purkinje cell firing in 28 week-old fxSCA7 92Q and Sirt1 OX– fxSCA7 92Q mice (n = 4 / group). fxSCA7 92Q slices: n=28, Sirt1-SCA7 slices: n=27; two-tailed t-test, *P* = 0.0549.
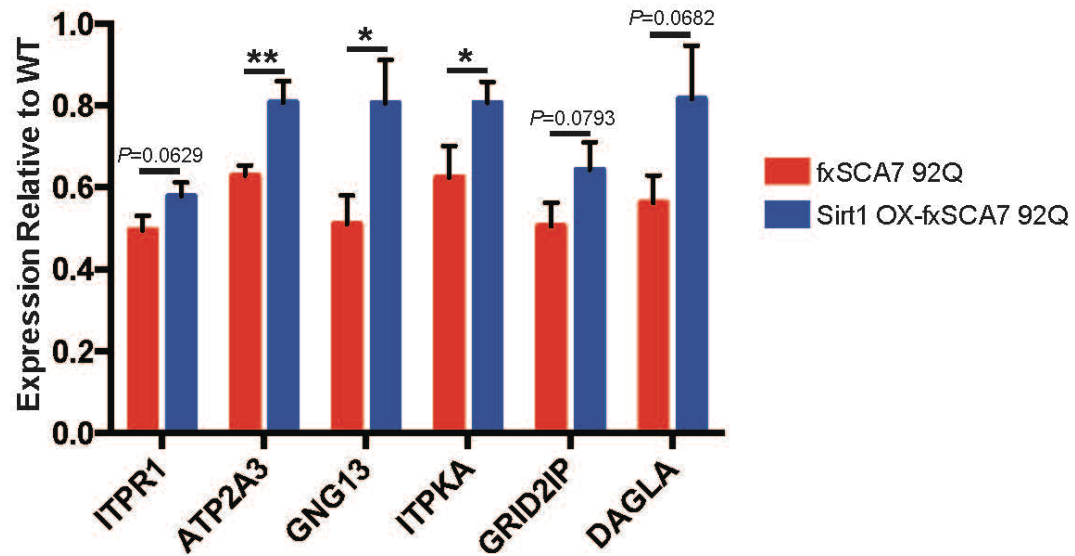
Figure 3.9 Reduced expression of calcium homeostasis genes is rescued upon Sirt1 over-expression
RNA was isolated from the cerebellar tissue of fxSCA7 92Q, Sirt1 OX-fxSCA7 92Q, and WT control mice aged 36 weeks, and subjected to qRT PCR analysis. n = 5 mice per group; three technical replicates; one-tailed *t*-test, *P <0.05, ** P <0.01. For comparisons not achieving significance, there was a strong trend (P<0.08). Error bars = S.E.M.
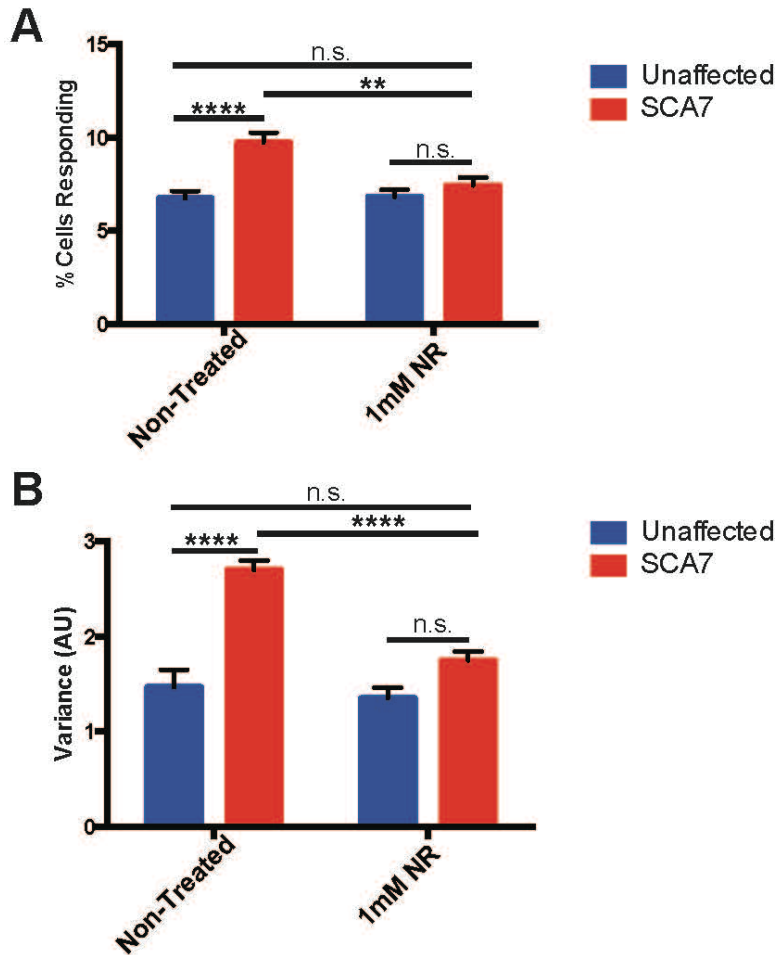
Figure 3.10   NR supplementation ameliorates disease phenotypes in SCA7 patient-derived NPCs

Neural precursor cells (NPCs) were derived from an SCA7 patient (70Q) and an unaffected family member (10Q). NPCs were treated with nicotinamide riboside for 24 hours then stained with Fluo4 NW and subjected to live cell imaging after stimulation with 100mM KCl. As Fluo4 NW is a calcium chelator, changes in signal intensity identify cytosolic calcium changes due to firing. **A)** NR treatment rescues hyper-responsive phenotype of NPCs from SCA7 patients. Cells were considered "responding" when they produced a significant change in the amplitude of Ca^{2+} (Fluo4 NW intensity). **B)** The increased variance in SCA7 patient-derived NPCs was ameliorated upon treatment with NR. Replicates per condition include measurements from two clones derived from each patient. Recordings we repeated on two days. Unaffected Non-Treated: n=21, SCA7 Non-Treated: n=29, Unaffected treated with 1mM NR: n=19, SCA7 treated with 1mM NR: n=27. Two-way ANOVA with post-hoc comparison of all groups, **$P<0.01$, ****$P<0.0001$. Error bars = S.E.M.

Chapter 4:

Defining a Physical Interaction Between

Sirt1 and Ataxin-7

Abstract

We have shown in both mouse and human models that Sirt1 dysfunction is a key feature of SCA7 pathogenesis. Given that recent work defines a direct interaction between yeast orthologues of Sirt1 and Atxn7, we wanted to determine if this interaction is maintained in mammalian cells and contributes to SCA7 pathogenesis. Utilizing in vitro translation followed by co-immunoprecipitation studies we describe for the first time a direct interaction between Atxn7 and Sirt1 that persists in the presence of polyglutamine expanded Atxn7. We also demonstrate that over-expression of Usp22, the deubiquitinase enzyme linked to STAGA by Atxn7, increases the stability of Sirt1 protein. We hypothesized that Usp22-mediated deubuiquitination of Sirt1 may be altered in the presence of polyQ-expanded Atxn7 and present supporting evidence that Sirt1 stability is altered in SCA7.

4.1 Introduction

In Chapters 1 and 2 we described a decrease in the expression of calcium homeostasis genes in SCA7, which we determined was due to altered Sirt1 deacetylase activity upstream of this pathway. While this explains a general role for Sirt1 in neurodegenerative disease, the direct relationship between Sirt1 and the polyglutamine-expansion disease SCA7 remains unclear. Although it is known ataxin-7 (Atxn7) is a core component of the mammalian STAGA transcription co-activator complex[25,26], the biological role of Atxn7 is largely uncertain. Studies in the yeast *Saccharomyces cerevisiae* revealed that

the yeast orthologue of Atxn7, Sgf73, comprises the SAGA deubiquitination module (DUBm) in addition to the deubiquinase enzyme Ubp8 and the proteins Sgf11 and Sus1[164,165]. Sgf73 plays an important functional role by tethering the DUBm to the remainder of SAGA complex via the N-terminus of the protein[166-168], an interaction that is maintained in *Drosophila* and in mammalian cells[164,165]. In yeast, the deubiquitinase protein Ubp8 is inactive without the other DUBm complex members and incorporation into SAGA[169], and histone H2B deubiquitination is reduced to the same extent in *sgf73* null yeast as it is in *ubp8* null strains[170]; however, regulation of DUBm activity is not well understood in higher organisms.

Importantly, yeast lacking Sgf73 are extremely long lived due to loss of DUBm activity, and the loss of this protein increased activity of silent information regulator 2 (Sir2). It was determinded that the two proteins have both a genetic and physical interaction[171]. While the mammalian homoglogs of Sgf73 and Sir2, Atxn7 and Sirt1, have not been shown to directly interact in mammals, Sirt1 indeed interacts with Usp22, the mammalian ortholog to the SAGA deubiquitinase enzyme Ubp8[172,173]. The exact role this intearction plays remains unclear, as Usp22 has been implicated as both recuiting Sirt1 to STAGA to modulate deacetylation of proteins in the other complex modules[173] and as deubiquinating and stabilizing Sirt1[172].

After validating the interaction between Usp22 and Sirt1, we highlight for the first time a physical interaction between Sirt1 and Atxn7. We determined these two proteins directly interact, an activity that is maintained and perhaps

enhanced by polyglutimine expansion of Atxn7. While the implications of this interaction in the presence of polyQ-expanded Atxn7 are not fully understood, we describe increased degradation of Sirt1 in this condition. These studies raise provocative questions as to the normal role of Atxn7 and STAGA function in nutrient sensing and metabolic regulation of transcriptional pathways important for ageing and neural function, and how these processes may be altered in SCA7 neurodegeneration.

4.2 Results

Mammalian Sirt1 and Usp22 physically interact

An interaction between Usp22 and Sirt1 has been previously described by mass spectrometry studies[173,174]. As we have described a role for Sirt1 in SCA7 pathogenesis, we decided to further explore and characterize the relationship between Sirt1 and the STAGA DUBm proteins. We first sought to reproduce the interaction between Sirt1 and Usp22. Upon over-expression of epitope-tagged Sirt1 and Usp22 in HEK 293T cells, we were able to co-immunoprecipitate these two proteins (**Figure 4.1a**). One study describes a role for USP22 stabilizing Sirt1 by removing polyubiquitin chains on the protein, an activity that results in supression of p53-driven cell death[172]. To test if Sirt1 is indeed post-translationally regulated by Usp22, we simply over-expressed Usp22 in HEK 293T cells and interrogated protein levels of endogenous Sirt1. We noted a marked increase in levels of enodogenous Sirt1 protein upon over-

expression of Usp22 (**Figure 4.1b**), suggesting Usp22 indeed deubiquitinates and stabilizes Sirt1 protein.

Mammalian Sirt1 interacts directly with normal and polyQ-expanded ATXN7

After validating Sirt1 interacts with Usp22 and based on previous work from our lab that Sir2 and Sgf73, the yeast orthologs to Sirt1 and ATXN7, physically interact[171], we investigated if this behavior is maintained in mammals. We were able to co-immunoprecipitate Sirt1 and normal length (10Q) Atxn7 upon over-expression of epitope-tagged Sirt1 and ATXN7 in HEK293T cells (**Figure 4.2a**). Importantly, this interaction was maintained and perhaps even enhanced in the presence of polyQ-expanded (92Q) Atxn7 (**Figure 4.2a**). As we described Sirt1 interacts with other proteins of the DUB module it is possible that the interaction we observed between this protein Atxn7 was not direct, instead mediated by the interaction between Sirt1 and Usp22. In order to test this we performed an *in vitro* translation (IVT) experiment followed my co-immunoprecipitation. Sirt1 protein generated by IVT was mixed with either normal length (10Q) or polyQ-expanded (92Q) Atxn7 generated through the same process. We then immunoprecipitated Atxn7 and discovered Sirt1 interacts with both the normal and polyQ-expanded protein directly (**Figure 4.2b**). As in Figure 4.1a, it appears there may be a stronger interaction between Sirt1 and polyQ-expanded Atxn7, however we need to further quantify this interaction.

Sirt1 protein turnover is increased in SCA7

As we know integration of polyQ-expanded Atxn7 into the STAGA complex alters Usp22 deubiquitinase activity in SCA7[26,76,77] and our work supports indepdendently published conclusions that Usp22 deubiquitinates Sirt1[172], we sought to determine if Sirt1 protein stability is altered in SCA7. To test this we turned to primary cerebellar granule neurons (CGNs) from fxSCA7 92Q animals. We treated the CGNs with cycholhexamide, a chemical that inhibits protein synthesis[175]. Sirt1 degradation over time can thus be tracked as no new protein is being synthesied (**Figure 4.3a**). We observed that after six hours of cyclohexamide treatment, there is significantly less Sirt1 protein in CGNs derived from fxSCA7 92Q animals than their wild-type littermates (**Figure 4.3b**), indicating an increased rate of degradation that persists with time. Taken together, these studies suggest a direct interaction between Sirt1 and Atxn7 that may alter Usp22-mediated DUB of Sirt1 in the presence of polyQ expansion in Atxn7.

4.3 Discussion

SAGA activity has been previously linked to the coordination of different metabolic phases of yeast growth in culture[176], yet how this translates to mammalian STAGA activity is not well understood. Recent work shows the yeast orthologue of Atxn7, Sgf73, regualtes lifespan through modulation of SAGA-mediated acetylation and Sir2-dependent deacetylation of an important

transcription coactivator for ribosomal protein genes[171,177]. These studies provacatively place Sgf73 at the center of both SAGA- and Sir2-dependent activities, perhaps modulating transcription via several pathways in response to environmental factors. Given that SAGA is a stress induced transcription coavticator complex[178] and implicated in modulating genome-wide transcription[179], the role of Sgf73 directly linking these activities to NAD$^+$ metabolism and longevity could make this protein an important sensor and modulator of transcriptional activity.

It has been observed that Sirt1, the mammalian orthologue of Sir2, is recruited to STAGA by an acetylation site on Usp22 and deacetylates other members of the STAGA complex to modulate its activity[173]. Additionally, the work described in this chapter and by others[172] support a role for Usp22 deubiquinating and stabilizing Sirt1. In light of the newly defined role placing Sgf73 at the axis of SAGA and Sir2 activities in yeast, prior work in mammalian cell lines describing the nature of the Usp22-Sirt1 interaction, and our results indicating direct interaction between Atxn7 and Sirt1, it can be hypothesized the Sirt1-Atxn7 relationship is important to modulation of transcription and maintenance of homeostasis in mammalian cells. Given that this interaction is maintained and perhaps even enhanced in the presence of polyQ-expanded Atxn7, more work will need to be done to determine the effects of the Sirt1-Atxn7 interaction on SCA7 pathogenesis. Indeed, given that histone H2B deubiquitination is decreased in SCA7 and we observed increased turnover of Sirt1 in SCA7 primary cerebellar granule neurons, we can hypothesize polyQ-

expanded Atxn7 may interfere with Usp22-mediated deubiquitination of Sirt1 in SCA7. While additional experiments must be completed to fully characterize the importance of this relationship, given the importance of Sirt1 dysfunction to SCA7 disease highlighted in Chapter 3 we can hypothesize altering the Sirt1-Atxn7 interaction in SCA7 may have pathological implications.

4.4 Experimental procedures

Cell Culture

HEK293T cells were cultured in Dulbecco's Modified Eagle's medium (DMEM) with high glucose and L-glutamine (11965118, ThermoFisher) supplemented with 10% fetal bovine serum (FBS) (16000044, ThermoFisher) and 0.1% penicillin-streptomycin (15140122, ThermoFisher). Trasnfections were completed using Lipofectamine 2000 (11668019, ThermoFisher) according to the manufactures protocol. Briefly, 1ug of plasmid DNA was incubated at room temperature with 2uL Lipofectamine 2000 in Opti-MEM reduced serum media (31985062, ThermoFisher) for 20 minutes, and added directly to cells. Cells were lysed in RIPA lysis buffer 24-48 hours post-transfection, and homogenized by tritiration.

Immunoprecipitation and immunoblot analysis

Immunoprecipitation occurred with 500ug protein in all reactions, concentrations were determined by BCA. A 50:50 mixture of Dynabeads Protein

A (10001, ThermoFisher) and Protein G (10003, ThermoFisher) was used for pre-clearning of lysates for 1hour at 4°C and incubation with antibodies for Myc (2276, Cell Signaling; 1:500) or Flag (F27425, Sigma-Aldrich; 1:50) overnight at 4°C. Beads were washed three times with PBS and protein was eluted by boiling at 90°C for 10minutes. Samples were then prepped for immunoblot analysis.

For Western blot analysis, membranes were immunoblotted with antibodies for Flag (F27425, Sigma-Aldrich; 1:1000), Myc (2276, Cell Signaling; 1:1000), HA (sc-805, Santa Cruz; 1:1000), or Sirt1 (07-131, Millipore; 1:1000). Densitometry was performed in ImageJ[160] and values normalized to β-actin (ab8226, Abcam; 1:10000).

In vitro translation (IVT)

In vitro translation (IVT) was achieved utilizing the 1-Step Human Coupled IVT Kit (88881, ThermoFisher) per the manufacturers protocol with human Myc-Atxn7 10Q, Myc-Atxn7 92Q, and HA-Sirt1 expression vectors in a pT7CFE1 expression vector. Upon completion of the reaction, Sirt1 protein reaction was dividied in half, added to either the Myc-Atxn7 10Q reaction or Myc-Atxn7 92Q reaction, and followed by immunoprecipitation with an antibody for the Myc epitope tag, as described above.

Mouse studies

All animal experimentation adhered to NIH guidelines and was approved by, and performed, in accordance with the University of California, San Diego

Institutional Animal Care and Use Committee (IACUC) and the University of Michigan Committee on the Use and Care of Animals.

Primary neuron culture

Primary cerebellar granule neurons (CGNs) were derived from 7-day old fxSCA7 92Q pups and wild-type littermates as previously described[109] with minor modifications. Briefly, cerebella from 7-day old fxSCA7 92Q pups and wild-type littermates were digested with 0.25% Trypsin (Life Technologies). After neutralization with 10% serum, cells were tritirated and centrifuged for 5min at 800 x *g*. The pellet was resuspended in Neurobasal-A Media (Thermo Fisher Scientific), 10% B27 serum-free supplement (Thermo Fisher Scientific), 25mM KCl and added to polystyrene flat-bottomed 12-well plates (Grenier) coated with poly-D-lysine at a concentration of ~200,000 cells per well, six wells per animal. Neurons were aged seven days prior to performing cyclohexamide pulse-chase experiments.

Cyclohexamide Pulse-Chase

Primary cerebellar granule neurons (CGNs) aged 7 days were treated with 5mM cyclohexamide for 0, 2, 4, 6, and 8 hours at $37^{\circ C}$. CGNs were lysed in RIPA buffer and homogenized via triteration. Protein concentrations were determined by BCA and 25ug per time point was loaded into a gel. All Western blot analysis contained all time points for a single fxSCA7 92Q animal and a wild-type littermate.

Statistical Analysis

Statistic tests are described in the figure legends for all data. Statistical analysis was done using Microsoft Excel and Prism 6.0 (GraphPad). Statistical significance was defined at $P<0.05$. All t-tests are two-tailed Student's t-tests unless otherwise indicated, and level of significance (alpha) was always set to 0.05.

Acknowledgements

This work has not been submitted for publication and is the sole product of the dissertation author.

Figures

A

B
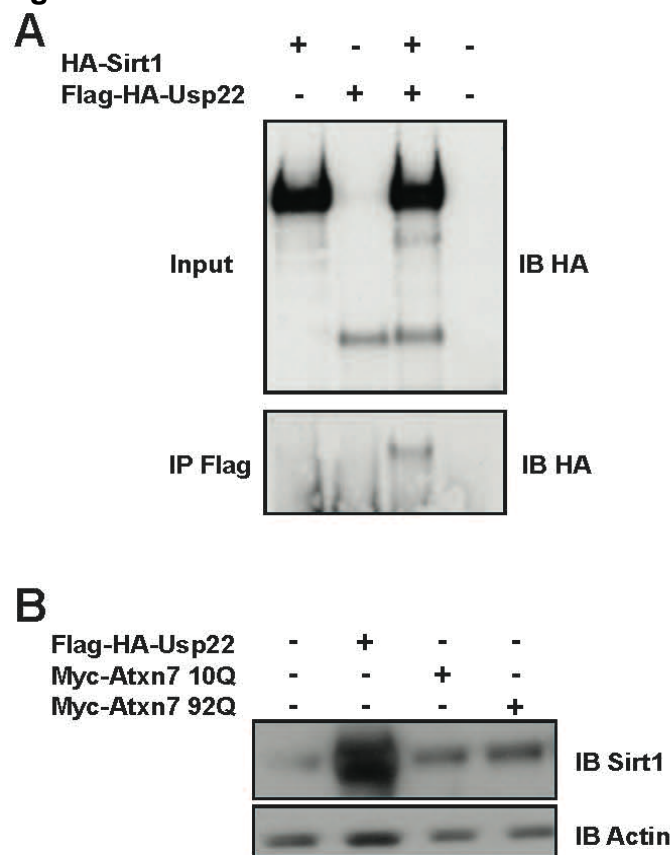
Figure 4.1 Usp22 interacts with and stabilizes Sirt1
A) We transiently transfected HEK293T cells with epitope tagged Sirt1 and Usp22, followed by coimmunoprecipitation of cell lysate with the HA probe. **B)** We probed for levels of Sirt1 protein from HEK293T cells transiently transfected with epitope tagged Usp22, Atxn7 10Q, or polyglutamine expanded Atxn7 92Q.   Experiments were replicated n=3, representative blots shown.

A

HA-Sirt1	-	-	+	+	+	-
Myc-ATXN7 10Q	+	-	-	+	-	-
Myc-ATXN7 92Q	-	+	-	-	+	-

Input   IB HA

Input   IB Myc

IP Myc   IB HA

B

	Input			IP Myc	
HA-Sirt1	+	-	-	+	+
Myc-ATXN7 10Q	-	+	-	+	-
Myc-ATXN7 92Q	-	-	+	-	+

117kDa   IB HA

171kDa
117kDa   IB Myc
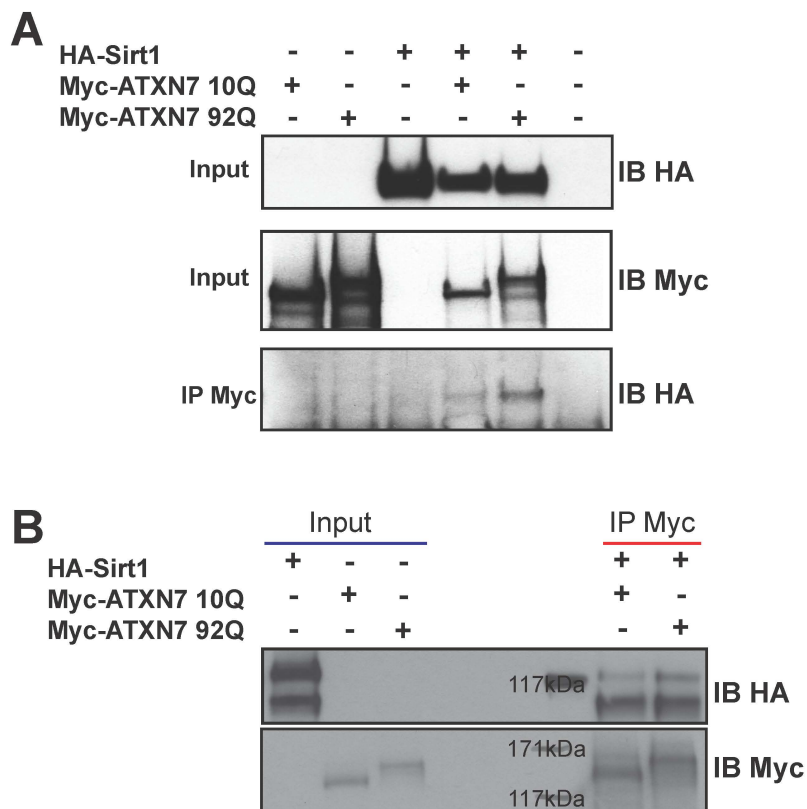
Figure 4.2 Atxn7 directly interacts with Sirt1
A) We transiently transfected HEK293T cells with epitope tagged Sirt1, Atxn7 10Q, or polyglutamine expanded Atxn7 92Q. We then performed coimmunoprecipitation on the cell lysates using an antibody against the Myc probe, and immunoblotted for the HA tag. **B)** Sirt1, Atxn7 10Q, and Atxn7 92Q were generated by IVT. The Sirt1 protein was split in half and mixed with either Atxn7 10Q or 92Q, and followed by coimmunoprecipitation with an antibody against the Myc probe. Experiment were replicated n=3, representative blots shown.
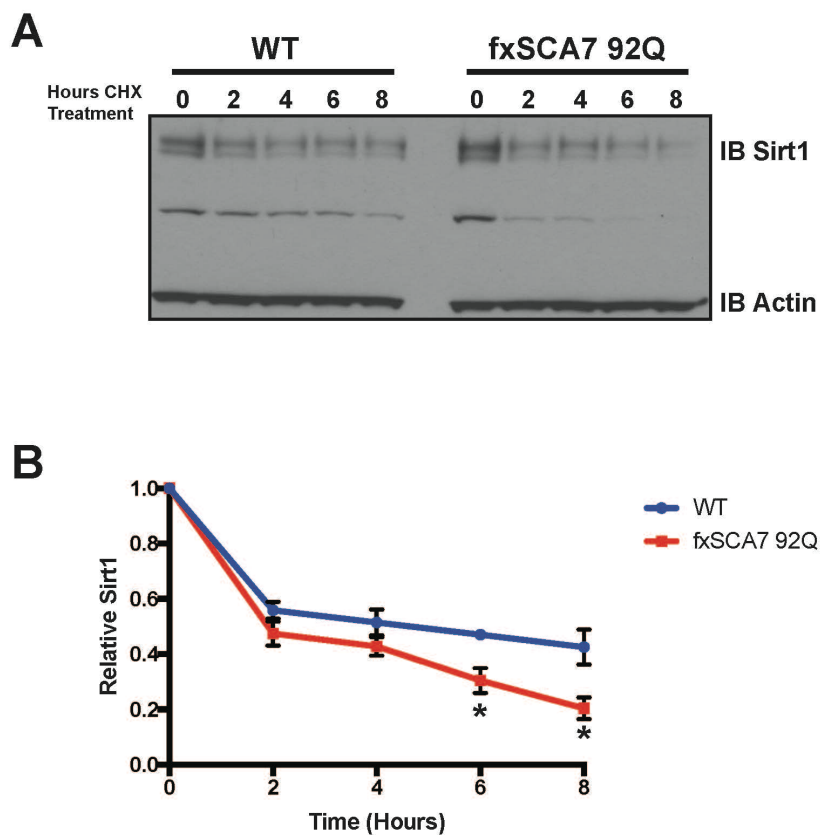
Figure 4.3 Sirt1 is degraded more rapidly in SCA7
A) Primary cerebellar granule neurons derived from fxSCA7 92Q mice and wild type littermates were treated with 5mM cyclohexamide for 0, 2, 4, 6, and 8 hours. Equivalent amounts of protein were loaded for all time points. B) Each blot represents one wild type and one fxSCA7 92Q individual. N=3 mice per genotype were treated, and blots were run in triplicate; two-tailed *t*-test was completed at each time point, *P <0.05, error bars = S.E.M.

Chapter 5:

Summary and Future Directions

Utilizing unbiased transcriptome based analysis, we have identified decreased expression of genes central to phosphatidyl-insoitol signaling and calcium homeostasis in the SCA7 cerebellum. We have described altered calcium handling in Purkinje cells and cerebellar granule neurons in our SCA7 mice, and verified these phenotypes in human neuronal cells differentiated from SCA7 patient iPSCs. Because of the link to these pathways in other spinocerebellar ataxias and the unique dependence of cerebellar coincidence detection on inositol triphosphate signaling, we hypothesize these changes contribute to the cerebellar specificity of SCA7.

Due to the decreased expression of several genes involved in other forms of ataxia, we used putative transcription factor binding site (TFBS) analysis to determine shared transcription factors among these genes and identify an upstream regulator of this pathway. We noted a highly significant enrichment of the PPAR response element (PPRE) and the hypoxia-inducible factor response element (HRE). These results led us to consider a role for Sirt1 in SCA7, as PGC-1α-PPARγ and HIF-1α bind these regulatory elements and are major targets of Sirt1. We determined Sirt1 activity is impaired in SCA7 based on reduced NAD^+, the necessary Sirt1 cofactor, in the cerebellum and dramatically decreased gene expression levels of NMNAT1, the nuclear NAD^+ salvage enzyme, in addition to cerebellar increases in PARP1 protein. This profound defect in NAD^+ metabolism led us to pursue a genetic rescue of SCA7 disease in two mouse models. Upon Sirt1 overexpression, we rescued motor function, cerebellar neurodegeneration, survival, transcription regulation,

neuronal calcium handling and electrophysiological function in two mouse models of SCA7 and in patient-derived cell lines. Rescue of SCA7 disease phenotypes by Sirt1 over-expression suggests that while overall NAD^+ levels are reduced, a substantial increase in nuclear Sirt1 may result in more rapid utilization of the nuclear NAD^+ pool, leading to shuttling of NAD^+ from the cytosol to the nucleus to support increased Sirt1 activity in neuroprotection.

Finally we explored the functional relationship between mammalian Sirt1 and Atxn7, an interaction previously characterized between the orthologous proteins in yeast. We showed these two proteins directly interact, and this interaction may be enhanced in the presence of polyQ-expanded Atxn7. We observed increased turnover of Sirt1 in SCA7 neurons, possibly due to changes in deubiquitination of Sirt1 by Usp22, a conclusion that requires additional experimentation to fully validate. Collectively these studies provide a direct role for Sirt1 in neuroprotection as a regulator of calcium homeostasis, and describe a novel Sirt1-Atxn7 interaction that may influence the modulation of transcription in response to metabolites. These findings are summarized graphically in **Figure 5.1**.

Are these changes in NAD^+ metabolism and Sirt1 activity unique to SCA7 due to the Sirt1-Atxn7 interaction, or a general mechanism of neurodegeneration? A mounting body of evidence supports depletion of NAD^+ and resulting Sirt1 activity loss in neurological disease[141], and simply exposing neuronal cells to prion proteins is enough to cause NAD^+ depletion that can be rescued by exogenous NAD^+ or nicotinamide (NAM)[180]. The activation of the

poly(ADP-ribose) polymerase (PARP) family of enzymes is generally considered the driver of this NAD^+ reduction in neurodegeneration, as PARP1 likely outcompetes Sirt1 for NAD^{+}[141]. Aberrant PARP1 activity has also been observed in ataxia-telegiectasia (AT), Cockayne syndrome (CS) and xermadoma pigmentosum group A (XPA)- a group of diseases that all present with ataxia, cerebellar atrophy, and peripheral neuropathy[181-184]. Each of these diseases displays a reduction in NAD^+ and Sirt1 activity that is rescued when PARP1 is inhibited pharmacologically[181-184]. Importantly common cellular abnormalities in these three diseases are driven by loss of NAD^+ through PARP1 hyperactivity and reduced activation of the Sirt1-PGC1α axis[181-184], a pathway also described in this study. Given the high prevalence of PGC-1α in cerebellum[150] and that PGC-1 α $^{-/-}$ mice exhibit severe motor phenotypes early in life (4wks of age)[151], perhaps cerebellar specificity of these diseases is explained by NAD^+ reduction decreasing Sirt1 activity and resulting downstream expression of inositol triphosphate signaling.

Another common theme in inherited cerebellar ataxias is the vulnerability of the cerebellum to DNA damage. Indeed, mutations in DNA repair proteins account for numerous inherited ataxias, including AT, AT-like disease, CS, XPA, ataxia with oculomotor apraxia types 1 and 2, and spinocerebellar ataxia with axonal neuropathy[185]. What is particularly intriguing about these disorders is that post-mitotic neurons of the cerebellum are especially prone to neurodegeneration, perhaps due the large metabolic needs of Purkinje cells increasing oxidative stress and making them highly susceptible to DNA

damage. Recent work has extended this line of investigation by identifying loss-of-function mutations in the gene for the DNA repair protein XRCC1 in a patient with cerebellar ataxia, ocular apraxia, and neuropathy, and has implicated PARP1 activation in cerebellar degeneration by documenting rescue of cerebellar neuron demise in XRCC1 CNS-null mice cross to a PARP1 null background[186].

While no role has yet been described for DNA damage in SCA7, recent work in mammalian cell lines has shown that the deubiquitinase module of STAGA- notably Atxn7, Usp22, and Eny2- is necessary for double stranded break repair (DDBR) upstream of the kinase ATM (Ataxia Telangiectasia Mutated)[187]. Given that we saw an increase in PARP1 expression in our SCA7 mice, we can hypothesize an upstream dysfunction in DNA damage response in SCA7. Interestingly, NAD^+ replenishment therapy reduced the severity of AT neuropathy, normalized neuromuscular function, delayed memory loss, and extended lifespan of AT mouse models via stimulation of DNA repair[182]. Given the importance of cerebellar changes in NAD^+ metabolism described in this work and the newly identified role of Atxn7 to DDBR, increased DNA damage in SCA7 pathogenesis and the potential relevance of the Sirt1-Atxn7 interaction should be the focus of future investigation (**Figure 5.2**).

In this study, we have uncovered a series of related defects that represent viable targets for rationale therapy development for SCA7 and related neurodegenerative disorders (summarized in **Figure 5.3**). As aberrant calcium handling is a shared mechanism amongst ataxias, many therapies have

targeted the calcium-activated potassium channels SK and BK. Because they regulate tonic firing of cerebellar Purkinje cells[101], activation of SK and BK channels with small molecules can rectify Purkinje cell firing abnormalities. SK channels in particular show promise as the drug riluzole, which simultaneously inhibits glutamate release and activates SK channels, has been shown to be clinically effective for symptomatic treatment of several etiologies of autosomal dominant SCA and Friedrich's ataxia[102,103].

Another attractive therapeutic strategy based on these studies is to boost the function of Sirt1. Many small molecule activators of Sirt1, termed STACs (sirtuin activating compounds) include natural (resveratrol) and synthetic compounds that work via a common allosteric binding mechanism to stimulate Sirt1 activity[188]. Unfortunately, STACs are extremely nonspecific and have widespread off-target effects, resulting in mixed outcomes when used as a disease therapy[188]. A more feasible approach may be to increase NAD^+ levels, which account for impaired Sirt1 function in SCA7. A variety of choices for NAD^+ repletion are available, including supplementation with vitamin B3 (nicotinamide), supplementation with NMN, a precursor of NAD^+ in the salvage pathway, and supplementation with nicotinamide riboside (NR), which enters the salvage pathway as NMN. Indeed, recent work indicates that NAD^+ repletion may have therapeutic application in the ataxia AT[182] in addition to other neuromuscular disorders and neurodegenerative diseases[154-157]. As niacin (nicotininamide/vitamin B3) is readily available and long been prescribed for

dyslipidemia[189-193], oral administration of this compound may prove an easy addition to existing SCA7 treatments.

Yet another potential neurotherapeutic target is PARP1, as inhibition has previously shown to increase NAD$^+$ levels accompanied by enhanced Sirt1 activity[145,146]. Clinical trials are underway utilizing chemical PARP1 inhibition to treat cancer[158], and should further inform us on their safety and efficacy as a therapeutic.

A final therapeutic alternative is targeted gene therapy using antisense oligonucleotides (ASOs). Single-stranded ASOs base pair with target mRNAs to form heteroduplexes, which are degraded by the endogenous RNase H pathway[194,195]. Non-allele specific ASO injections have decreased disease features in models of other polyglutamine disorders including Huntington's disease[196] , SCA2[197], and SBMA[198]. Indeed, unpublished work in our lab indicates this is a viable therapy for both cerebellar and retinal degeneration in SCA7.

As ASOs do not cross the blood-brain barrier delivery remains a limitation of this treatment approach, and the pathways defined by this work may thus prove a more promising therapeutic avenue for SCA7. As recent findings in the neurodegenerative disease field underscore the intriguing possibility that Sirt1-NAD$^+$ pathways are dysregulated in related disorders[159], these studies provide evidence for potential therapies targeting shared pathogenic processes with wide application to neurodegenerative disease. In light of the changing

demographics of the world population, there is a pressing need to expand such

efforts for age-related degenerative disorders.
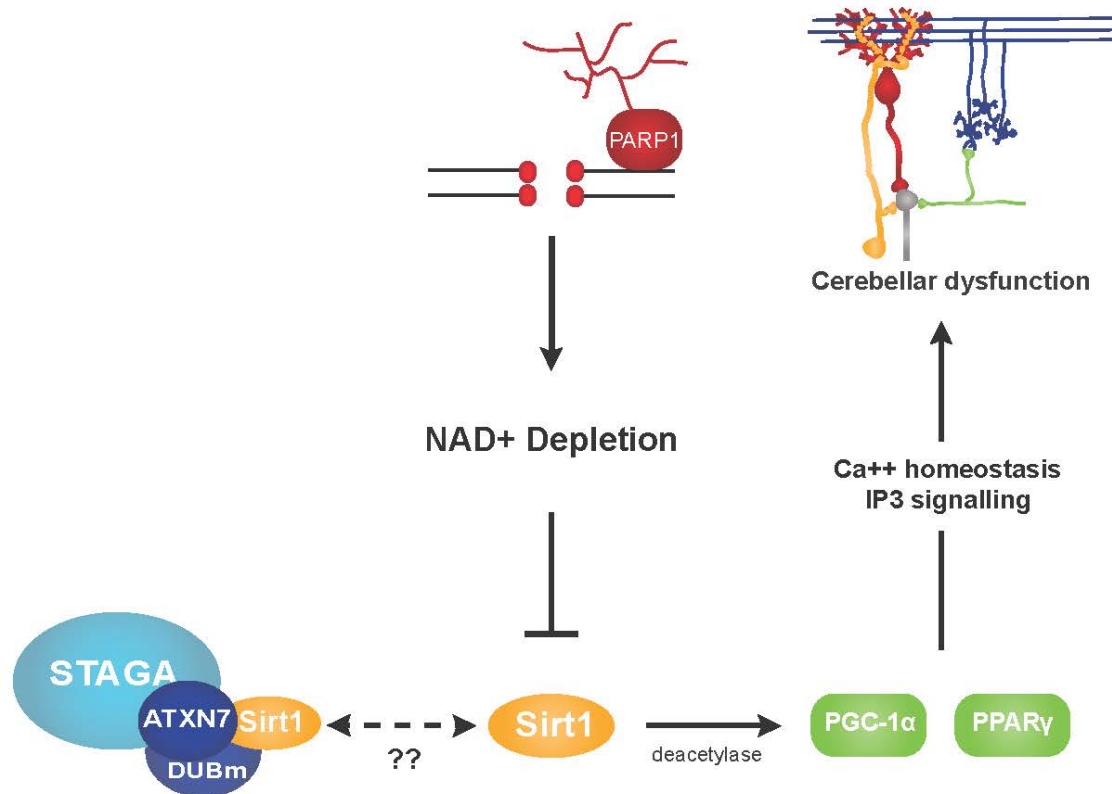
Figure 5.1 Summary of SCA7 molecular pathology described in this study
Increase in PARP1 protein and other changes in NAD$^+$ metabolism in the SCA7 cerebellum deplete the nuclear pool of NAD$^+$ and inhibit Sirt1 activity. This results in inhibition of Sirt1 deacetylase activity on the PPAR transcription factor proteins, namely PGC-1α and PPARγ, rendering them inactive. Dormancy of PPARs results in decreased expression of genes central to calcium homeostasis and inositol triphosphate signaling, resulting in altered calcium handling in neurons that contributes to the cerebellar dysfunction of SCA7. The full implications of the direct Sirt1-Atxn7 interaction on this molecular pathology yet remains unclear.
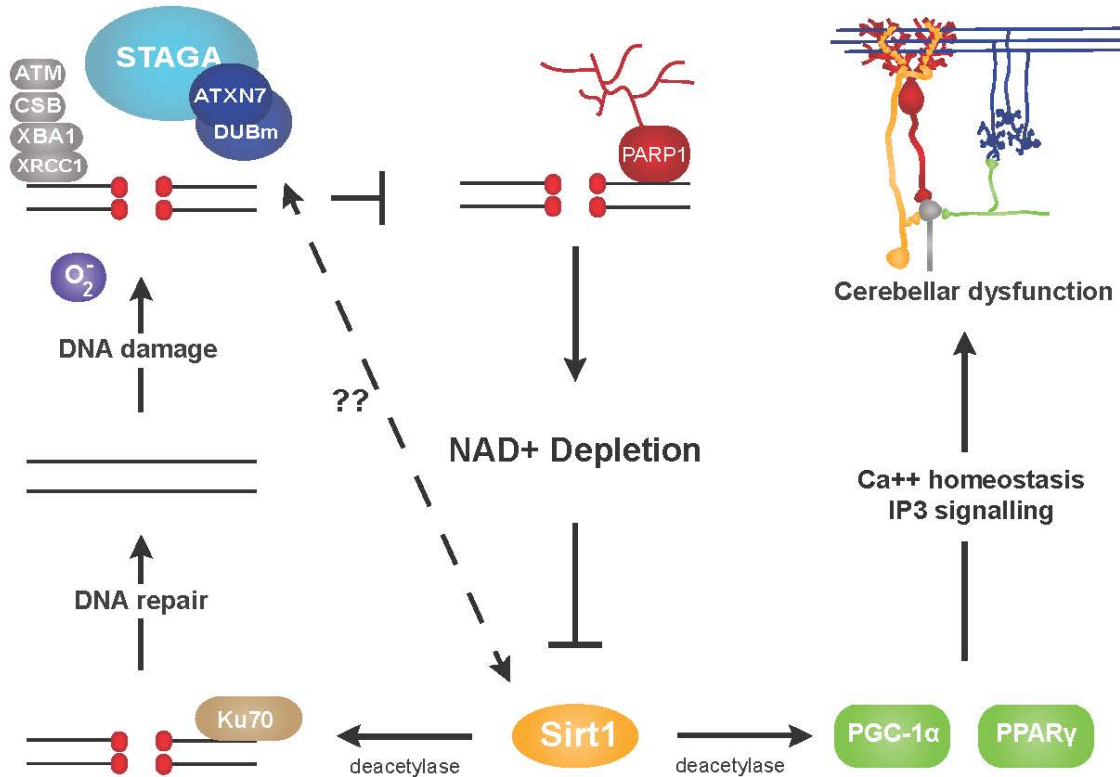
Figure 5.2 Implications of this work on pathways described in other cerebellar diseases
Mutations in DNA repair proteins account for numerous inherited ataxias. These include mutations in the proteins ATM, CSB, XBA1, and XRCC1. Recently the deubuiquitination module of STAGA and Atxn7 have also been shown to be necessary for early DNA damage response. When DNA is not repaired, excessive PARP1 activity depletes nuclear NAD$^+$ stores, inhibiting Sirt1 activity. Previous work describes a feedback mechanism as Sirt1 promotes DNA repair by deacetylation of the protein Ku70. Given the newly defined role of Atxn7 in DNA damage response and the findings of this dissertation, namely that reduction of NAD$^+$ results in altered Sirt1 activity that decreases calcium homeostasis and inositol triphosphate signaling, may thus apply to these other disorders of the cerebellum. The contribution of the direct physical interaction between Sirt1 and Atxn7 to this disease pathway is remains unclear.
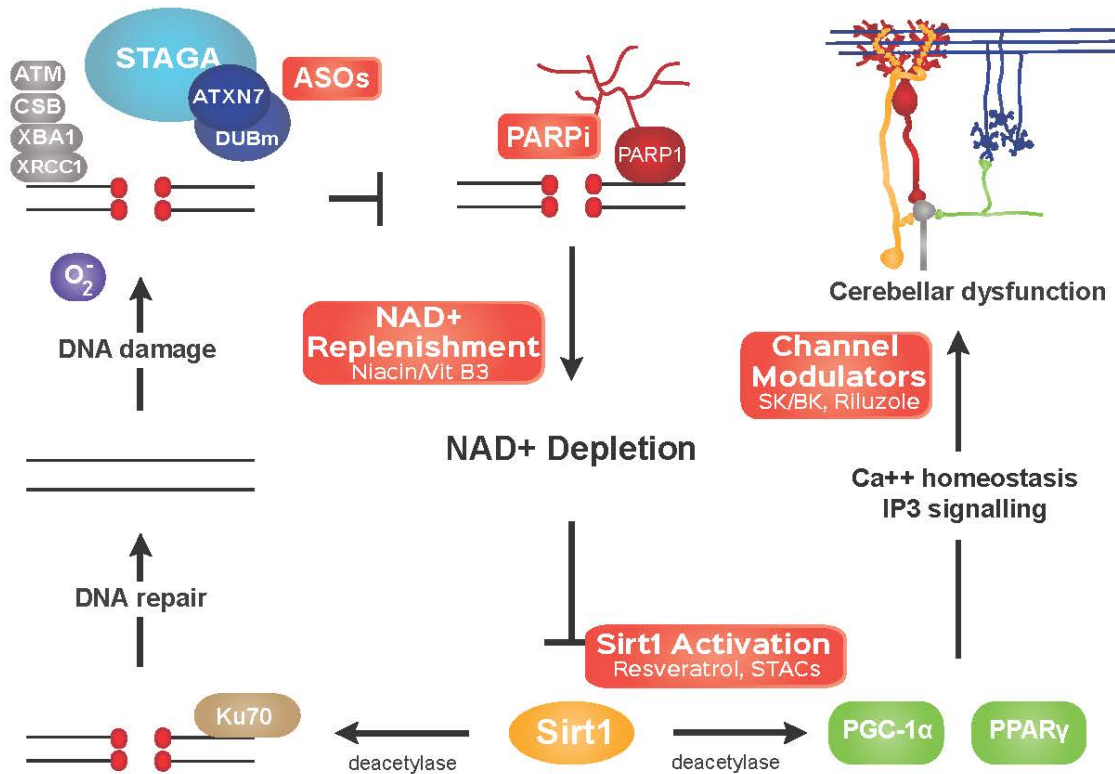
Figure 5.3 Potential therapeutic interventions for SCA7 and other related disorders
This work provides evidence for a variety of therapeutic interventions in SCA7 and related disorders. Based on our findings that SCA7 displays irregular calcium handling commonly described in other ataxias, modulators of calcium-activated potassium channels, such as riluzole, may regulate Purkinje cell firing in this disease. Sirt1 activation via natural and synthetic compounds could also drive transcription of the phosphatidyl-inositol pathway, as our Sirt1 over-expression studies showed increased Sirt1 delays SCA7 progression. NAD^+ replenishment, most easily achievable in humans with dietary supplementation of vitamin B3, may provide a readily-available therapeutic option to activate Sirt1. Based on our data in SCA7 patient-derived cells that NAD^+ replenishment rescues neuronal firing activity in disease, replenishment may thus be an applicable treatment for other ataxias. Chemical inhibition of PARP1 is another option to increase NAD^+ availability, and is currently in clinical trials to treat cancer. Finally, gene therapy targeting Atxn7 allele transcripts for degradation may prevent any of the cerebellar ataxias or DNA damage mechanisms from reducing NAD^+ by directly targeting the causative gene.

References

1. Abe, T., Tsuda, T., Yoshida, M., Wada, Y., Kano, T., Itoyama, Y. & Tamai, M. Macular degeneration associated with aberrant expansion of trinucleotide repeat of the SCA7 gene in 2 Japanese families. *Arch Ophthalmol* **118**, 1415-1421 (2000).

2. Bryer, A., Krause, A., Bill, P., Davids, V., Bryant, D., Butler, J., Heckmann, J., Ramesar, R. & Greenberg, J. The hereditary adult-onset ataxias in South Africa. *J Neurol Sci* **216**, 47-54 (2003).

3. Gu, W., Wang, Y., Liu, X., Zhou, B., Zhou, Y. & Wang, G. Molecular and clinical study of spinocerebellar ataxia type 7 in Chinese kindreds. *Archives of neurology* **57**, 1513-1518 (2000).

4. Jardim, L.B., Silveira, I., Pereira, M.L., Ferro, A., Alonso, I., do Ceu Moreira, M., Mendonca, P., Ferreirinha, F., Sequeiros, J. & Giugliani, R. A survey of spinocerebellar ataxia in South Brazil - 66 new cases with Machado-Joseph disease, SCA7, SCA8, or unidentified disease-causing mutations. *J Neurol* **248**, 870-876 (2001).

5. Johansson, J., Forsgren, L., Sandgren, O., Brice, A., Holmgren, G. & Holmberg, M. Expanded CAG repeats in Swedish spinocerebellar ataxia type 7 (SCA7) patients: effect of CAG repeat length on the clinical manifestation. *Hum Mol Genet* **7**, 171-176 (1998).

6. Storey, E., du Sart, D., Shaw, J.H., Lorentzos, P., Kelly, L., McKinley Gardner, R.J., Forrest, S.M., Biros, I. & Nicholson, G.A. Frequency of spinocerebellar ataxia types 1, 2, 3, 6, and 7 in Australian patients with spinocerebellar ataxia. *Am J Med Genet* **95**, 351-357 (2000).

7. Filla, A., Mariotti, C., Caruso, G., Coppola, G., Cocozza, S., Castaldo, I., Calabrese, O., Salvatore, E., De Michele, G., Riggio, M.C., Pareyson, D., Gellera, C. & Di Donato, S. Relative frequencies of CAG expansions in spinocerebellar ataxia and dentatorubropallidoluysian atrophy in 116 Italian families. *Eur Neurol* **44**, 31-36 (2000).

8. Trottier, Y., Lutz, Y., Stevanin, G., Imbert, G., Devys, D., Cancel, G., Saudou, F., Weber, C., David, G., Tora, L., Yves, A., Brice, A. & Jean-Louis, M. Polyglutamine expansion as a pathological epitope in

Huntington's disease and four dominant cerebellar ataxias. *Nature* **378**, 403-406. (1995).

9.   David, G., Abbas, N., Stevanin, G., Durr, A., Yvert, G., Cancel, G., Weber, C., Imbert, G., Saudou, F., Antoniou, E., Drabkin, H., Gemmill, R., Giunti, P., Benomar, A., Wood, N., Ruberg, M., Agid, Y., Mandel, J.L. & Brice, A. Cloning of the SCA7 gene reveals a highly unstable CAG repeat expansion. *Nat Genet* **17**, 65-70 (1997).

10.   David, G., Durr, A., Stevanin, G., Cancel, G., Abbas, N., Benomar, A., Belal, S., Lebre, A.S., Abada-Bendib, M., Grid, D., Holmberg, M., Yahyaoui, M., Hentati, F., Chkili, T., Agid, Y. & Brice, A. Molecular and clinical correlations in autosomal dominant cerebellar ataxia with progressive macular dystrophy (SCA7). *Human molecular genetics* **7**, 165-170 (1998).

11.   Giunti, P., Stevanin, G., Worth, P.F., David, G., Brice, A. & Wood, N.W. Molecular and clinical study of 18 families with ADCA type II: evidence for genetic heterogeneity and de novo mutation. *American journal of human genetics* **64**, 1594-1603 (1999).

12.   Martin, J.J., Van Regemorter, N., Krols, L., Brucher, J.M., de Barsy, T., Szliwowski, H., Evrard, P., Ceuterick, C., Tassignon, M.J. & Smet-Dieleman, H. On an autosomal dominant form of retinal-cerebellar degeneration: an autopsy study of five patients in one family. *Acta Neuropathol* **88**, 277-286 (1994).

13.   Michalik, A., Martin, J.J. & Van Broeckhoven, C. Spinocerebellar ataxia type 7 associated with pigmentary retinal dystrophy. *Eur J Hum Genet* **12**, 2-15 (2004).

14.   Martin, J., Van Regemorter, N., Del-Favero, J., Lofgren, A. & Van Broeckhoven, C. Spinocerebellar ataxia type 7 (SCA7) - correlations between phenotype and genotype in one large Belgian family. *J Neurol Sci* **168**, 37-46 (1999).

15.   Bang, O.Y., Lee, P.H., Kim, S.Y., Kim, H.J. & Huh, K. Pontine atrophy precedes cerebellar degeneration in spinocerebellar ataxia 7: MRI-based volumetric analysis. *J Neurol Neurosurg Psychiatry* **75**, 1452-1456 (2004).

16.   Holmberg, M., Duyckaerts, C., Durr, A., Cancel, G., Gourfinkel-An, I., Damier, P., Faucheux, B., Trottier, Y., Hirsch, E.C., Agid, Y. & Brice, A. Spinocerebellar ataxia type 7 (SCA7): a neurodegenerative disorder with neuronal intranuclear inclusions. *Hum Mol Genet* **7**, 913-918 (1998).

17.   Takahashi, J., Fujigasaki, H., Zander, C., El Hachimi, K.H., Stevanin, G., Durr, A., Lebre, A.S., Yvert, G., Trottier, Y., de The, H., Hauw, J.J., Duyckaerts, C. & Brice, A. Two populations of neuronal intranuclear inclusions in SCA7 differ in size and promyelocytic leukaemia protein content. *Brain* **125**, 1534-1543 (2002).

18.   Zoghbi, H.Y. & Orr, H.T. Glutamine repeats and neurodegeneration. *Annu Rev Neurosci* **23**, 217-247 (2000).

19.   Benton, C.S., de Silva, R., Rutledge, S.L., Bohlega, S., Ashizawa, T. & Zoghbi, H.Y. Molecular and clinical studies in SCA-7 define a broad clinical spectrum and the infantile phenotype. *Neurology* **51**, 1081-1086 (1998).

20.   Gouw, L.G., Castaneda, M.A., McKenna, C.K., Digre, K.B., Pulst, S.M., Perlman, S., Lee, M.S., Gomez, C., Fischbeck, K., Gagnon, D., Storey, E., Bird, T., Jeri, F.R. & Ptacek, L.J. Analysis of the dynamic mutation in the SCA7 gene shows marked parental effects on CAG repeat transmission. *Hum Mol Genet* **7**, 525-532 (1998).

21.   Whitney, A., Lim, M., Kanabar, D. & Lin, J.P. Massive SCA7 expansion detected in a 7-month-old male with hypotonia, cardiomegaly, and renal compromise. *Dev Med Child Neurol* **49**, 140-143 (2007).

22.   van de Warrenburg, B.P., Frenken, C.W., Ausems, M.G., Kleefstra, T., Sinke, R.J., Knoers, N.V. & Kremer, H.P. Striking anticipation in spinocerebellar ataxia type 7: the infantile phenotype. *J Neurol* **248**, 911-914 (2001).

23.   Ansorge, O., Giunti, P., Michalik, A., Van Broeckhoven, C., Harding, B., Wood, N. & Scaravilli, F. Ataxin-7 aggregation and ubiquitination in infantile SCA7 with 180 CAG repeats. *Ann Neurol* **56**, 448-452 (2004).

24.   Timmers, H.T. & Tora, L. SAGA unveiled. *Trends in biochemical sciences* **30**, 7-10 (2005).

25.   Helmlinger, D., Hardy, S., Sasorith, S., Klein, F., Robert, F., Weber, C., Miguet, L., Potier, N., Van-Dorsselaer, A., Wurtz, J.M., Mandel, J.L., Tora, L. & Devys, D. Ataxin-7 is a subunit of GCN5 histone acetyltransferase-containing complexes. *Hum Mol Genet* **13**, 1257-1265 (2004).

26.   Palhan, V.B., Chen, S., Peng, G.H., Tjernberg, A., Gamper, A.M., Fan, Y., Chait, B.T., La Spada, A.R. & Roeder, R.G. Polyglutamine-expanded ataxin-7 inhibits STAGA histone acetyltransferase activity to produce retinal degeneration. *Proc Natl Acad Sci U S A* **102**, 8472-8477 (2005).

27.	Blazek, E., Mittler, G. & Meisterernst, M. The mediator of RNA polymerase II. *Chromosoma* **113**, 399-408 (2005).

28.	Conaway, J.W., Florens, L., Sato, S., Tomomori-Sato, C., Parmely, T.J., Yao, T., Swanson, S.K., Banks, C.A., Washburn, M.P. & Conaway, R.C. The mammalian Mediator complex. *FEBS letters* **579**, 904-908 (2005).

29.	Samara, N.L. & Wolberger, C. A new chapter in the transcription SAGA. *Current opinion in structural biology* **21**, 767-774 (2011).

30.	Balasubramanian, R., Pray-Grant, M.G., Selleck, W., Grant, P.A. & Tan, S. Role of the Ada2 and Ada3 transcriptional coactivators in histone acetylation. *The Journal of biological chemistry* **277**, 7989-7995 (2002).

31.	Wyce, A., Xiao, T., Whelan, K.A., Kosman, C., Walter, W., Eick, D., Hughes, T.R., Krogan, N.J., Strahl, B.D. & Berger, S.L. H2B ubiquitylation acts as a barrier to Ctk1 nucleosomal recruitment prior to removal by Ubp8 within a SAGA-related complex. *Molecular cell* **27**, 275-288 (2007).

32.	McMahon, S.B., Wood, M.A. & Cole, M.D. The essential cofactor TRRAP recruits the histone acetyltransferase hGCN5 to c-Myc. *Molecular and cellular biology* **20**, 556-562 (2000).

33.	Gamper, A.M. & Roeder, R.G. Multivalent binding of p53 to the STAGA complex mediates coactivator recruitment after UV damage. *Molecular and cellular biology* **28**, 2517-2527 (2008).

34.	Liu, X., Vorontchikhina, M., Wang, Y.L., Faiola, F. & Martinez, E. STAGA recruits Mediator to the MYC oncoprotein to stimulate transcription and cell proliferation. *Molecular and cellular biology* **28**, 108-121 (2008).

35.	Liu, X., Tesfai, J., Evrard, Y.A., Dent, S.Y. & Martinez, E. c-Myc transformation domain recruits the human STAGA complex and requires TRRAP and GCN5 acetylase activity for transcription activation. *The Journal of biological chemistry* **278**, 20405-20412 (2003).

36.	Lang, S.E., McMahon, S.B., Cole, M.D. & Hearing, P. E2F transcriptional activation requires TRRAP and GCN5 cofactors. *The Journal of biological chemistry* **276**, 32627-32634 (2001).

37.	Helmlinger, D., Hardy, S., Abou-Sleymane, G., Eberlin, A., Bowman, A.B., Gansmuller, A., Picaud, S., Zoghbi, H.Y., Trottier, Y., Tora, L. & Devys, D. Glutamine-expanded ataxin-7 alters TFTC/STAGA recruitment and chromatin structure leading to photoreceptor dysfunction. *PLoS biology* **4**, e67 (2006).

38. Chen, S., Peng, G.H., Wang, X., Smith, A.C., Grote, S.K., Sopher, B.L. & La Spada, A.R. Interference of Crx-dependent transcription by ataxin-7 involves interaction between the glutamine regions and requires the ataxin-7 carboxy-terminal region for nuclear localization. *Hum Mol Genet* **13**, 53-67 (2004).

39. La Spada, A.R., Fu, Y., Sopher, B.L., Libby, R.T., Wang, X., Li, L.Y., Einum, D.D., Huang, J., Possin, D.E., Smith, A.C., Martinez, R.A., Koszdin, K.L., Treuting, P.M., Ware, C.B., Hurley, J.B., Ptacek, L.J. & Chen, S. Polyglutamine-expanded ataxin-7 antagonizes CRX function and induces cone-rod dystrophy in a mouse model of SCA7. *Neuron* **31**, 913-927. (2001).

40. Orr, H.T. & Zoghbi, H.Y. Trinucleotide repeat disorders. *Annu Rev Neurosci* **30**, 575-621 (2007).

41. Custer, S.K., Garden, G.A., Gill, N., Rueb, U., Libby, R.T., Schultz, C., Guyenet, S.J., Deller, T., Westrum, L.E., Sopher, B.L. & La Spada, A.R. Bergmann glia expression of polyglutamine-expanded ataxin-7 produces neurodegeneration by impairing glutamate transport. *Nat Neurosci* **9**, 1302-1311 (2006).

42. Furrer, S.A., Mohanachandran, M.S., Waldherr, S.M., Chang, C., Damian, V.A., Sopher, B.L., Garden, G.A. & La Spada, A.R. Spinocerebellar ataxia type 7 cerebellar disease requires the coordinated action of mutant ataxin-7 in neurons and glia, and displays non-cell-autonomous bergmann glia degeneration. *J Neurosci* **31**, 16269-16278 (2011).

43. Furrer, S.A., Waldherr, S.M., Mohanachandran, M.S., Baughn, T.D., Nguyen, K.T., Sopher, B.L., Damian, V.A., Garden, G.A. & La Spada, A.R. Reduction of mutant ataxin-7 expression restores motor function and prevents cerebellar synaptic reorganization in a conditional mouse model of SCA7. *Hum Mol Genet* (2012).

44. Yoo, S.Y., Pennesi, M.E., Weeber, E.J., Xu, B., Atkinson, R., Chen, S., Armstrong, D.L., Wu, S.M., Sweatt, J.D. & Zoghbi, H.Y. SCA7 knockin mice model human SCA7 and reveal gradual accumulation of mutant ataxin-7 in neurons and abnormalities in short-term plasticity. *Neuron* **37**, 383-401 (2003).

45. Takahashi, K. & Yamanaka, S. Induction of pluripotent stem cells from mouse embryonic and adult fibroblast cultures by defined factors. *Cell* **126**, 663-676 (2006).

46. Takahashi, K., Tanabe, K., Ohnuki, M., Narita, M., Ichisaka, T., Tomoda, K. & Yamanaka, S. Induction of pluripotent stem cells from adult human fibroblasts by defined factors. *Cell* **131**, 861-872 (2007).

47. Han, S.S., Williams, L.A. & Eggan, K.C. Constructing and deconstructing stem cell models of neurological disease. *Neuron* **70**, 626-644 (2011).

48. Stein, J.L., de la Torre-Ubieta, L., Tian, Y., Parikshak, N.N., Hernandez, I.A., Marchetto, M.C., Baker, D.K., Lu, D., Hinman, C.R., Lowe, J.K., Wexler, E.M., Muotri, A.R., Gage, F.H., Kosik, K.S. & Geschwind, D.H. A quantitative framework to evaluate modeling of cortical development by neural stem cells. *Neuron* **83**, 69-86 (2014).

49. Cortes, C.J., Miranda, H.C., Frankowski, H., Batlevi, Y., Young, J.E., Le, A., Ivanov, N., Sopher, B.L., Carromeu, C., Muotri, A.R., Garden, G.A. & La Spada, A.R. Polyglutamine-expanded androgen receptor interferes with TFEB to elicit autophagy defects in SBMA. *Nat Neurosci* **17**, 1180-1189 (2014).

50. Consortium, H.D.i. Induced pluripotent stem cells from patients with Huntington's disease show CAG-repeat-expansion-associated phenotypes. *Cell Stem Cell* **11**, 264-278 (2012).

51. Cooper, O., Seo, H., Andrabi, S., Guardia-Laguarta, C., Graziotto, J., Sundberg, M., McLean, J.R., Carrillo-Reid, L., Xie, Z., Osborn, T., Hargus, G., Deleidi, M., Lawson, T., Bogetofte, H., Perez-Torres, E., Clark, L., Moskowitz, C., Mazzulli, J., Chen, L., Volpicelli-Daley, L., Romero, N., Jiang, H., Uitti, R.J., Huang, Z., Opala, G., Scarffe, L.A., Dawson, V.L., Klein, C., Feng, J., Ross, O.A., Trojanowski, J.Q., Lee, V.M., Marder, K., Surmeier, D.J., Wszolek, Z.K., Przedborski, S., Krainc, D., Dawson, T.M. & Isacson, O. Pharmacological rescue of mitochondrial deficits in iPSC-derived neural cells from patients with familial Parkinson's disease. *Sci Transl Med* **4**, 141ra190 (2012).

52. Raman, I.M. & Bean, B.P. Ionic currents underlying spontaneous action potentials in isolated cerebellar Purkinje neurons. *J Neurosci* **19**, 1663-1674 (1999).

53. Egorova, P., Popugaeva, E. & Bezprozvanny, I. Disturbed calcium signaling in spinocerebellar ataxias and Alzheimer's disease. *Semin Cell Dev Biol* **40**, 127-133 (2015).

54. Mark, M.D., Schwitalla, J.C., Groemmke, M. & Herlitze, S. Keeping Our Calcium in Balance to Maintain Our Balance. *Biochem Biophys Res Commun* **483**, 1040-1050 (2017).

55. Schorge, S., van de Leemput, J., Singleton, A., Houlden, H. & Hardy, J. Human ataxias: a genetic dissection of inositol triphosphate receptor (ITPR1)-dependent signaling. *Trends Neurosci* **33**, 211-219 (2010).

56. Houtkooper, R.H., Pirinen, E. & Auwerx, J. Sirtuins as regulators of metabolism and healthspan. *Nat Rev Mol Cell Biol* **13**, 225-238 (2012).

57. Finkel, T., Deng, C.X. & Mostoslavsky, R. Recent progress in the biology and physiology of sirtuins. *Nature* **460**, 587-591 (2009).

58. Burnett, C., Valentini, S., Cabreiro, F., Goss, M., Somogyvari, M., Piper, M.D., Hoddinott, M., Sutphin, G.L., Leko, V., McElwee, J.J., Vazquez-Manrique, R.P., Orfila, A.M., Ackerman, D., Au, C., Vinti, G., Riesen, M., Howard, K., Neri, C., Bedalov, A., Kaeberlein, M., Soti, C., Partridge, L. & Gems, D. Absence of effects of Sir2 overexpression on lifespan in C. elegans and Drosophila. *Nature* **477**, 482-485 (2011).

59. Imai, S.I. & Guarente, L. It takes two to tango: NAD+ and sirtuins in aging/longevity control. *NPJ Aging Mech Dis* **2**, 16017 (2016).

60. Kanfi, Y., Naiman, S., Amir, G., Peshti, V., Zinman, G., Nahum, L., Bar-Joseph, Z. & Cohen, H.Y. The sirtuin SIRT6 regulates lifespan in male mice. *Nature* **483**, 218-221 (2012).

61. Satoh, A., Brace, C.S., Rensing, N., Cliften, P., Wozniak, D.F., Herzog, E.D., Yamada, K.A. & Imai, S. Sirt1 extends life span and delays aging in mice through the regulation of Nk2 homeobox 1 in the DMH and LH. *Cell Metab* **18**, 416-430 (2013).

62. Satoh, A., Imai, S.I. & Guarente, L. The brain, sirtuins, and ageing. *Nat Rev Neurosci* **18**, 362-374 (2017).

63. Duan, W., Guo, Z., Jiang, H., Ware, M., Li, X.J. & Mattson, M.P. Dietary restriction normalizes glucose metabolism and BDNF levels, slows disease progression, and increases survival in huntingtin mutant mice. *Proc Natl Acad Sci U S A* **100**, 2911-2916 (2003).

64. Halagappa, V.K., Guo, Z., Pearson, M., Matsuoka, Y., Cutler, R.G., Laferla, F.M. & Mattson, M.P. Intermittent fasting and caloric restriction ameliorate age-related behavioral deficits in the triple-transgenic mouse model of Alzheimer's disease. *Neurobiol Dis* **26**, 212-220 (2007).

65. Patel, N.V., Gordon, M.N., Connor, K.E., Good, R.A., Engelman, R.W., Mason, J., Morgan, D.G., Morgan, T.E. & Finch, C.E. Caloric restriction attenuates Abeta-deposition in Alzheimer transgenic models. *Neurobiol Aging* **26**, 995-1000 (2005).

66. Wang, J., Ho, L., Qin, W., Rocher, A.B., Seror, I., Humala, N., Maniar, K., Dolios, G., Wang, R., Hof, P.R. & Pasinetti, G.M. Caloric restriction attenuates beta-amyloid neuropathology in a mouse model of Alzheimer's disease. *Faseb J* **19**, 659-661 (2005).

67. Jeong, H., Cohen, D.E., Cui, L., Supinski, A., Savas, J.N., Mazzulli, J.R., Yates, J.R., 3rd, Bordone, L., Guarente, L. & Krainc, D. Sirt1 mediates neuroprotection from mutant huntingtin by activation of the TORC1 and CREB transcriptional pathway. *Nat Med* **18**, 159-165 (2012).

68. Jiang, M., Wang, J., Fu, J., Du, L., Jeong, H., West, T., Xiang, L., Peng, Q., Hou, Z., Cai, H., Seredenina, T., Arbez, N., Zhu, S., Sommers, K., Qian, J., Zhang, J., Mori, S., Yang, X.W., Tamashiro, K.L., Aja, S., Moran, T.H., Luthi-Carter, R., Martin, B., Maudsley, S., Mattson, M.P., Cichewicz, R.H., Ross, C.A., Holtzman, D.M., Krainc, D. & Duan, W. Neuroprotective role of Sirt1 in mammalian models of Huntington's disease through activation of multiple Sirt1 targets. *Nat Med* **18**, 153-158 (2012).

69. Donmez, G. & Outeiro, T.F. SIRT1 and SIRT2: emerging targets in neurodegeneration. *EMBO Mol Med* **5**, 344-352 (2013).

70. Stevanin, G., Durr, A. & Brice, A. Clinical and molecular advances in autosomal dominant cerebellar ataxias: from genotype to phenotype and physiopathology. *Eur J Hum Genet* **8**, 4-18 (2000).

71. Garden, G.A., Truant, R., Ellerby, L.M. & La Spada, A.R. "Spinocerebellar Ataxia Type 7: Clinical Features to Cellular Pathogenesis". *Genetic Instabilities and Hereditary Neurological Diseases*, Academic Press, San Diego, CA (2006).

72. Johansson, J., Forsgren, L., Sandgren, O., Brice, A., Holmgren, G. & Holmberg, M. Expanded CAG repeats in Swedish spinocerebellar ataxia type 7 (SCA7) patients: effect of CAG repeat length on the clinical manifestation. *Hum Mol Genet* **7**, 171-176 (1998).

73. Paulson, H.L., Bonini, N.M. & Roth, K.A. Polyglutamine disease and neuronal cell death. *Proc Natl Acad Sci U S A* **97**, 12957-12958 (2000).

74. La Spada, A.R., Wilson, E.M., Lubahn, D.B., Harding, A.E. & Fischbeck, K.H. Androgen receptor gene mutations in X-linked spinal and bulbar muscular atrophy. *Nature* **352**, 77-79 (1991).

75. La Spada, A.R. & Taylor, J.P. Polyglutamines placed into context. *Neuron* **38**, 681-684 (2003).

76. Helmlinger, D., Hardy, S., Abou-Sleymane, G., Eberlin, A., Bowman, A.B., Gansmuller, A., Picaud, S., Zoghbi, H.Y., Trottier, Y., Tora, L. & Devys, D. Glutamine-expanded ataxin-7 alters TFTC/STAGA recruitment and chromatin structure leading to photoreceptor dysfunction. *PLoS Biol* **4**, e67 (2006).

77. Yang, H., Liu, S., He, W.T., Zhao, J., Jiang, L.L. & Hu, H.Y. Aggregation of Polyglutamine-expanded Ataxin 7 Protein Specifically Sequesters Ubiquitin-specific Protease 22 and Deteriorates Its Deubiquitinating Function in the Spt-Ada-Gcn5-Acetyltransferase (SAGA) Complex. *J Biol Chem* **290**, 21996-22004 (2015).

78. Schols, L., Bauer, P., Schmidt, T., Schulte, T. & Riess, O. Autosomal dominant cerebellar ataxias: clinical features, genetics, and pathogenesis. *Lancet Neurol* **3**, 291-304 (2004).

79. Duenas, A.M., Goold, R. & Giunti, P. Molecular pathogenesis of spinocerebellar ataxias. *Brain* **129**, 1357-1370 (2006).

80. Bettencourt, C., Ryten, M., Forabosco, P., Schorge, S., Hersheson, J., Hardy, J., Houlden, H. & United Kingdom Brain Expression, C. Insights from cerebellar transcriptomic analysis into the pathogenesis of ataxia. *JAMA neurology* **71**, 831-839 (2014).

81. Carter, B.C. & Bean, B.P. Sodium entry during action potentials of mammalian neurons: incomplete inactivation and reduced metabolic efficiency in fast-spiking neurons. *Neuron* **64**, 898-909 (2009).

82. Huang da, W., Sherman, B.T. & Lempicki, R.A. Systematic and integrative analysis of large gene lists using DAVID bioinformatics resources. *Nat Protoc* **4**, 44-57 (2009).

83. Huang da, W., Sherman, B.T. & Lempicki, R.A. Bioinformatics enrichment tools: paths toward the comprehensive functional analysis of large gene lists. *Nucleic Acids Res* **37**, 1-13 (2009).

84. Kasumu, A. & Bezprozvanny, I. Deranged calcium signaling in Purkinje cells and pathogenesis in spinocerebellar ataxia 2 (SCA2) and other ataxias. *Cerebellum* **11**, 630-639 (2012).

85. Rogers, T.B., Inesi, G., Wade, R. & Lederer, W.J. Use of thapsigargin to study Ca2+ homeostasis in cardiac cells. *Biosci Rep* **15**, 341-349 (1995).

86. Hansen, S.T., Meera, P., Otis, T.S. & Pulst, S.M. Changes in Purkinje cell firing and gene expression precede behavioral pathology in a mouse model of SCA2. *Hum Mol Genet* **22**, 271-283 (2013).

87.   Dell'Orco, J.M., Wasserman, A.H., Chopra, R., Ingram, M.A., Hu, Y.S., Singh, V., Wulff, H., Opal, P., Orr, H.T. & Shakkottai, V.G. Neuronal Atrophy Early in Degenerative Ataxia Is a Compensatory Mechanism to Regulate Membrane Excitability. *J Neurosci* **35**, 11292-11307 (2015).

88.   Sausbier, M., Hu, H., Arntz, C., Feil, S., Kamm, S., Adelsberger, H., Sausbier, U., Sailer, C.A., Feil, R., Hofmann, F., Korth, M., Shipston, M.J., Knaus, H.G., Wolfer, D.P., Pedroarena, C.M., Storm, J.F. & Ruth, P. Cerebellar ataxia and Purkinje cell dysfunction caused by Ca2+-activated K+ channel deficiency. *Proc Natl Acad Sci U S A* **101**, 9474-9478 (2004).

89.   Hurlock, E.C., McMahon, A. & Joho, R.H. Purkinje-cell-restricted restoration of Kv3.3 function restores complex spikes and rescues motor coordination in Kcnc3 mutants. *J Neurosci* **28**, 4640-4648 (2008).

90.   Ly, R., Bouvier, G., Schonewille, M., Arabo, A., Rondi-Reig, L., Lena, C., Casado, M., De Zeeuw, C.I. & Feltz, A. T-type channel blockade impairs long-term potentiation at the parallel fiber-Purkinje cell synapse and cerebellar learning. *Proc Natl Acad Sci U S A* **110**, 20302-20307 (2013).

91.   Sekerkova, G., Kim, J.A., Nigro, M.J., Becker, E.B., Hartmann, J., Birnbaumer, L., Mugnaini, E. & Martina, M. Early onset of ataxia in moonwalker mice is accompanied by complete ablation of type II unipolar brush cells and Purkinje cell dysfunction. *J Neurosci* **33**, 19689-19694 (2013).

92.   Walter, J.T., Alvina, K., Womack, M.D., Chevez, C. & Khodakhah, K. Decreases in the precision of Purkinje cell pacemaking cause cerebellar dysfunction and ataxia. *Nat Neurosci* **9**, 389-397 (2006).

93.   Didonna, A. & Opal, P. Advances in Sequencing Technologies for Understanding Hereditary Ataxias: A Review. *JAMA neurology* **73**, 1485-1490 (2016).

94.   Jorntell, H. & Hansel, C. Synaptic memories upside down: bidirectional plasticity at cerebellar parallel fiber-Purkinje cell synapses. *Neuron* **52**, 227-238 (2006).

95.   Watanabe, M. Molecular mechanisms governing competitive synaptic wiring in cerebellar Purkinje cells. *Tohoku J Exp Med* **214**, 175-190 (2008).

96.   Bardo, S., Cavazzini, M.G. & Emptage, N. The role of the endoplasmic reticulum Ca2+ store in the plasticity of central neurons. *Trends Pharmacol Sci* **27**, 78-84 (2006).

97.   Nucifora, F.C., Jr., Li, S.H., Danoff, S., Ullrich, A. & Ross, C.A. Molecular cloning of a cDNA for the human inositol 1,4,5-trisphosphate receptor type 1, and the identification of a third alternatively spliced variant. *Brain Res Mol Brain Res* **32**, 291-296 (1995).

98.   Lin, X., Antalffy, B., Kang, D., Orr, H.T. & Zoghbi, H.Y. Polyglutamine expansion down-regulates specific neuronal genes before pathologic changes in SCA1. *Nat Neurosci* **3**, 157-163 (2000).

99.   Chen, X., Tang, T.S., Tu, H., Nelson, O., Pook, M., Hammer, R., Nukina, N. & Bezprozvanny, I. Deranged calcium signaling and neurodegeneration in spinocerebellar ataxia type 3. *J Neurosci* **28**, 12713-12724 (2008).

100.   Liu, J., Tang, T.S., Tu, H., Nelson, O., Herndon, E., Huynh, D.P., Pulst, S.M. & Bezprozvanny, I. Deranged calcium signaling and neurodegeneration in spinocerebellar ataxia type 2. *J Neurosci* **29**, 9148-9162 (2009).

101.   Womack, M.D. & Khodakhah, K. Somatic and dendritic small-conductance calcium-activated potassium channels regulate the output of cerebellar Purkinje neurons. *J Neurosci* **23**, 2600-2607 (2003).

102.   Ristori, G., Romano, S., Visconti, A., Cannoni, S., Spadaro, M., Frontali, M., Pontieri, F.E., Vanacore, N. & Salvetti, M. Riluzole in cerebellar ataxia: a randomized, double-blind, placebo-controlled pilot trial. *Neurology* **74**, 839-845 (2010).

103.   Romano, S., Coarelli, G., Marcotulli, C., Leonardi, L., Piccolo, F., Spadaro, M., Frontali, M., Ferraldeschi, M., Vulpiani, M.C., Ponzelli, F., Salvetti, M., Orzi, F., Petrucci, A., Vanacore, N., Casali, C. & Ristori, G. Riluzole in patients with hereditary cerebellar ataxia: a randomised, double-blind, placebo-controlled trial. *Lancet Neurol* **14**, 985-991 (2015).

104.   Trapnell, C., Pachter, L. & Salzberg, S.L. TopHat: discovering splice junctions with RNA-Seq. *Bioinformatics* **25**, 1105-1111 (2009).

105.   Trapnell, C., Williams, B.A., Pertea, G., Mortazavi, A., Kwan, G., van Baren, M.J., Salzberg, S.L., Wold, B.J. & Pachter, L. Transcript assembly and quantification by RNA-Seq reveals unannotated transcripts and isoform switching during cell differentiation. *Nat Biotechnol* **28**, 511-515 (2010).

106.   Sturn, A., Quackenbush, J. & Trajanoski, Z. Genesis: cluster analysis of microarray data. *Bioinformatics* **18**, 207-208 (2002).

107. Schmittgen, T.D. & Livak, K.J. Analyzing real-time PCR data by the comparative C(T) method. *Nat Protoc* **3**, 1101-1108 (2008).

108. Zagha, E., Lang, E.J. & Rudy, B. Kv3.3 channels at the Purkinje cell soma are necessary for generation of the classical complex spike waveform. *J Neurosci* **28**, 1291-1300 (2008).

109. Young, J.E., Gouw, L., Propp, S., Sopher, B.L., Taylor, J., Lin, A., Hermel, E., Logvinova, A., Chen, S.F., Chen, S., Bredesen, D.E., Truant, R., Ptacek, L.J., La Spada, A.R. & Ellerby, L.M. Proteolytic cleavage of ataxin-7 by caspase-7 modulates cellular toxicity and transcriptional dysregulation. *J Biol Chem* **282**, 30150-30160 (2007).

110. Zagha, E., Manita, S., Ross, W.N. & Rudy, B. Dendritic Kv3.3 potassium channels in cerebellar purkinje cells regulate generation and spatial dynamics of dendritic Ca2+ spikes. *J Neurophysiol* **103**, 3516-3525 (2010).

111. Haigis, M.C. & Sinclair, D.A. Mammalian sirtuins: biological insights and disease relevance. *Annual review of pathology* **5**, 253-295 (2010).

112. Feldman, J.L., Dittenhafer-Reed, K.E. & Denu, J.M. Sirtuin catalysis and regulation. *J Biol Chem* **287**, 42419-42427 (2012).

113. Satoh, A., Brace, C.S., Ben-Josef, G., West, T., Wozniak, D.F., Holtzman, D.M., Herzog, E.D. & Imai, S. SIRT1 promotes the central adaptive response to diet restriction through activation of the dorsomedial and lateral nuclei of the hypothalamus. *J Neurosci* **30**, 10220-10232 (2010).

114. Cho, S.H., Chen, J.A., Sayed, F., Ward, M.E., Gao, F., Nguyen, T.A., Krabbe, G., Sohn, P.D., Lo, I., Minami, S., Devidze, N., Zhou, Y., Coppola, G. & Gan, L. SIRT1 deficiency in microglia contributes to cognitive decline in aging and neurodegeneration via epigenetic regulation of IL-1beta. *J Neurosci* **35**, 807-818 (2015).

115. Qin, W., Yang, T., Ho, L., Zhao, Z., Wang, J., Chen, L., Zhao, W., Thiyagarajan, M., MacGrogan, D., Rodgers, J.T., Puigserver, P., Sadoshima, J., Deng, H., Pedrini, S., Gandy, S., Sauve, A.A. & Pasinetti, G.M. Neuronal SIRT1 activation as a novel mechanism underlying the prevention of Alzheimer disease amyloid neuropathology by calorie restriction. *J Biol Chem* **281**, 21745-21754 (2006).

116. Kim, D., Nguyen, M.D., Dobbin, M.M., Fischer, A., Sananbenesi, F., Rodgers, J.T., Delalle, I., Baur, J.A., Sui, G., Armour, S.M., Puigserver, P., Sinclair, D.A. & Tsai, L.H. SIRT1 deacetylase protects against

neurodegeneration in models for Alzheimer's disease and amyotrophic lateral sclerosis. *EMBO J* **26**, 3169-3179 (2007).

117. Min, S.W., Cho, S.H., Zhou, Y., Schroeder, S., Haroutunian, V., Seeley, W.W., Huang, E.J., Shen, Y., Masliah, E., Mukherjee, C., Meyers, D., Cole, P.A., Ott, M. & Gan, L. Acetylation of tau inhibits its degradation and contributes to tauopathy. *Neuron* **67**, 953-966 (2010).

118. Bonda, D.J., Lee, H.G., Camins, A., Pallas, M., Casadesus, G., Smith, M.A. & Zhu, X. The sirtuin pathway in ageing and Alzheimer disease: mechanistic and therapeutic considerations. *Lancet Neurol* **10**, 275-279 (2011).

119. Ferretta, A., Gaballo, A., Tanzarella, P., Piccoli, C., Capitanio, N., Nico, B., Annese, T., Di Paola, M., Dell'aquila, C., De Mari, M., Ferranini, E., Bonifati, V., Pacelli, C. & Cocco, T. Effect of resveratrol on mitochondrial function: implications in parkin-associated familiar Parkinson's disease. *Biochim Biophys Acta* **1842**, 902-915 (2014).

120. Guo, Y.J., Dong, S.Y., Cui, X.X., Feng, Y., Liu, T., Yin, M., Kuo, S.H., Tan, E.K., Zhao, W.J. & Wu, Y.C. Resveratrol alleviates MPTP-induced motor impairments and pathological changes by autophagic degradation of alpha-synuclein via SIRT1-deacetylated LC3. *Mol Nutr Food Res* **60**, 2161-2175 (2016).

121. Parker, J.A., Arango, M., Abderrahmane, S., Lambert, E., Tourette, C., Catoire, H. & Neri, C. Resveratrol rescues mutant polyglutamine cytotoxicity in nematode and mammalian neurons. *Nat Genet* **37**, 349-350 (2005).

122. Parker, J.A., Vazquez-Manrique, R.P., Tourette, C., Farina, F., Offner, N., Mukhopadhyay, A., Orfila, A.M., Darbois, A., Menet, S., Tissenbaum, H.A. & Neri, C. Integration of beta-catenin, sirtuin, and FOXO signaling protects from mutant huntingtin toxicity. *J Neurosci* **32**, 12630-12640 (2012).

123. Wareski, P., Vaarmann, A., Choubey, V., Safiulina, D., Liiv, J., Kuum, M. & Kaasik, A. PGC-1{alpha} and PGC-1{beta} regulate mitochondrial density in neurons. *J Biol Chem* **284**, 21379-21385 (2009).

124. Yanez, M., Galan, L., Matias-Guiu, J., Vela, A., Guerrero, A. & Garcia, A.G. CSF from amyotrophic lateral sclerosis patients produces glutamate independent death of rat motor brain cortical neurons: protection by resveratrol but not riluzole. *Brain Res* **1423**, 77-86 (2011).

125. Jeong, H., Cohen, D.E., Cui, L., Supinski, A., Savas, J.N., Mazzulli, J.R., Yates, J.R., 3rd, Bordone, L., Guarente, L. & Krainc, D. Sirt1 mediates neuroprotection from mutant huntingtin by activation of the TORC1 and CREB transcriptional pathway. *Nat Med* **18**, 159-165 (2011).

126. Jiang, M., Wang, J., Fu, J., Du, L., Jeong, H., West, T., Xiang, L., Peng, Q., Hou, Z., Cai, H., Seredenina, T., Arbez, N., Zhu, S., Sommers, K., Qian, J., Zhang, J., Mori, S., Yang, X.W., Tamashiro, K.L., Aja, S., Moran, T.H., Luthi-Carter, R., Martin, B., Maudsley, S., Mattson, M.P., Cichewicz, R.H., Ross, C.A., Holtzman, D.M., Krainc, D. & Duan, W. Neuroprotective role of Sirt1 in mammalian models of Huntington's disease through activation of multiple Sirt1 targets. *Nat Med* **18**, 153-158 (2011).

127. Tsunemi, T. & La Spada, A.R. PGC-1alpha at the intersection of bioenergetics regulation and neuron function: From Huntington's disease to Parkinson's disease and beyond. *Prog Neurobiol* **97**, 142-151 (2012).

128. La Spada, A.R. Finding a sirtuin truth in Huntington's disease. *Nat Med* **18**, 24-26 (2012).

129. Donmez, G., Arun, A., Chung, C.Y., McLean, P.J., Lindquist, S. & Guarente, L. SIRT1 protects against alpha-synuclein aggregation by activating molecular chaperones. *J Neurosci* **32**, 124-132 (2012).

130. Raynes, R., Leckey, B.D., Jr., Nguyen, K. & Westerheide, S.D. Heat shock and caloric restriction have a synergistic effect on the heat shock response in a sir2.1-dependent manner in Caenorhabditis elegans. *J Biol Chem* **287**, 29045-29053 (2012).

131. Westerheide, S.D., Anckar, J., Stevens, S.M., Jr., Sistonen, L. & Morimoto, R.I. Stress-inducible regulation of heat shock factor 1 by the deacetylase SIRT1. *Science* **323**, 1063-1066 (2009).

132. Chen, J., Zhou, Y., Mueller-Steiner, S., Chen, L.F., Kwon, H., Yi, S., Mucke, L. & Gan, L. SIRT1 protects against microglia-dependent amyloid-beta toxicity through inhibiting NF-kappaB signaling. *J Biol Chem* **280**, 40364-40374 (2005).

133. Longo, V.D. & Kennedy, B.K. Sirtuins in aging and age-related disease. *Cell* **126**, 257-268 (2006).

134. Herskovits, A.Z. & Guarente, L. Sirtuin deacetylases in neurodegenerative diseases of aging. *Cell Res* **23**, 746-758 (2013).

135. Ho Sui, S.J., Mortimer, J.R., Arenillas, D.J., Brumm, J., Walsh, C.J., Kennedy, B.P. & Wasserman, W.W. oPOSSUM: identification of over-represented transcription factor binding sites in co-expressed genes. *Nucleic Acids Res* **33**, 3154-3164 (2005).

136. Ho Sui, S.J., Fulton, D.L., Arenillas, D.J., Kwon, A.T. & Wasserman, W.W. oPOSSUM: integrated tools for analysis of regulatory motif over-representation. *Nucleic Acids Res* **35**, W245-252 (2007).

137. Kwon, A.T., Arenillas, D.J., Worsley Hunt, R. & Wasserman, W.W. oPOSSUM-3: advanced analysis of regulatory motif over-representation across genes or ChIP-Seq datasets. *G3* **2**, 987-1002 (2012).

138. Gatchel, J.R., Watase, K., Thaller, C., Carson, J.P., Jafar-Nejad, P., Shaw, C., Zu, T., Orr, H.T. & Zoghbi, H.Y. The insulin-like growth factor pathway is altered in spinocerebellar ataxia type 1 and type 7. *Proc Natl Acad Sci U S A* **105**, 1291-1296 (2008).

139. Rodgers, J.T., Lerin, C., Haas, W., Gygi, S.P., Spiegelman, B.M. & Puigserver, P. Nutrient control of glucose homeostasis through a complex of PGC-1alpha and SIRT1. *Nature* **434**, 113-118 (2005).

140. Joo, H.Y., Yun, M., Jeong, J., Park, E.R., Shin, H.J., Woo, S.R., Jung, J.K., Kim, Y.M., Park, J.J., Kim, J. & Lee, K.H. SIRT1 deacetylates and stabilizes hypoxia-inducible factor-1alpha (HIF-1alpha) via direct interactions during hypoxia. *Biochem Biophys Res Commun* **462**, 294-300 (2015).

141. Canto, C., Menzies, K.J. & Auwerx, J. NAD(+) Metabolism and the Control of Energy Homeostasis: A Balancing Act between Mitochondria and the Nucleus. *Cell Metab* **22**, 31-53 (2015).

142. Lau, C., Niere, M. & Ziegler, M. The NMN/NaMN adenylyltransferase (NMNAT) protein family. *Front Biosci (Landmark Ed)* **14**, 410-431 (2009).

143. Emanuelli, M., Carnevali, F., Saccucci, F., Pierella, F., Amici, A., Raffaelli, N. & Magni, G. Molecular cloning, chromosomal localization, tissue mRNA levels, bacterial expression, and enzymatic properties of human NMN adenylyltransferase. *J Biol Chem* **276**, 406-412 (2001).

144. Verdin, E. NAD(+) in aging, metabolism, and neurodegeneration. *Science* **350**, 1208-1213 (2015).

145. Bai, P., Cantó, C., Oudart, H., Brunyánszki, A., Cen, Y., Thomas, C., Yamamoto, H., Huber, A., Kiss, B., Houtkooper, Riekelt H., Schoonjans, K., Schreiber, V., Sauve, Anthony A., Menissier-de Murcia, J. & Auwerx,

J. PARP-1 Inhibition Increases Mitochondrial Metabolism through SIRT1 Activation. *Cell Metabolism* **13**, 461-468 (2011).

146. Pirinen, E., Cantó, C., Jo, Young S., Morato, L., Zhang, H., Menzies, Keir J., Williams, Evan G., Mouchiroud, L., Moullan, N., Hagberg, C., Li, W., Timmers, S., Imhof, R., Verbeek, J., Pujol, A., van Loon, B., Viscomi, C., Zeviani, M., Schrauwen, P., Sauve, Anthony A., Schoonjans, K. & Auwerx, J. Pharmacological Inhibition of Poly(ADP-Ribose) Polymerases Improves Fitness and Mitochondrial Function in Skeletal Muscle. *Cell Metabolism* **19**, 1034-1041 (2014).

147. Firestein, R., Blander, G., Michan, S., Oberdoerffer, P., Ogino, S., Campbell, J., Bhimavarapu, A., Luikenhuis, S., de Cabo, R., Fuchs, C., Hahn, W.C., Guarente, L.P. & Sinclair, D.A. The SIRT1 deacetylase suppresses intestinal tumorigenesis and colon cancer growth. *PLoS One* **3**, e2020 (2008).

148. Guyenet, S.J., Furrer, S.A., Damian, V.M., Baughan, T.D., La Spada, A.R. & Garden, G.A. A simple composite phenotype scoring system for evaluating mouse models of cerebellar ataxia. *J Vis Exp* (2010).

149. Canto, C., Houtkooper, R.H., Pirinen, E., Youn, D.Y., Oosterveer, M.H., Cen, Y., Fernandez-Marcos, P.J., Yamamoto, H., Andreux, P.A., Cettour-Rose, P., Gademann, K., Rinsch, C., Schoonjans, K., Sauve, A.A. & Auwerx, J. The NAD(+) precursor nicotinamide riboside enhances oxidative metabolism and protects against high-fat diet-induced obesity. *Cell Metab* **15**, 838-847 (2012).

150. Cowell, R.M., Blake, K.R. & Russell, J.W. Localization of the transcriptional coactivator PGC-1alpha to GABAergic neurons during maturation of the rat brain. *J Comp Neurol* **502**, 1-18 (2007).

151. Lucas, E.K., Dougherty, S.E., McMeekin, L.J., Trinh, A.T., Reid, C.S. & Cowell, R.M. Developmental alterations in motor coordination and medium spiny neuron markers in mice lacking pgc-1alpha. *PLoS One* **7**, e42878 (2012).

152. Ingram, M., Wozniak, E.A., Duvick, L., Yang, R., Bergmann, P., Carson, R., O'Callaghan, B., Zoghbi, H.Y., Henzler, C. & Orr, H.T. Cerebellar Transcriptome Profiles of ATXN1 Transgenic Mice Reveal SCA1 Disease Progression and Protection Pathways. *Neuron* **89**, 1194-1207 (2016).

153. Guarente, L. CELL METABOLISM. The resurgence of NAD(+). *Science* **352**, 1396-1397 (2016).

154. Ryu, D., Zhang, H., Ropelle, E.R., Sorrentino, V., Mazala, D.A., Mouchiroud, L., Marshall, P.L., Campbell, M.D., Ali, A.S., Knowels, G.M., Bellemin, S., Iyer, S.R., Wang, X., Gariani, K., Sauve, A.A., Canto, C., Conley, K.E., Walter, L., Lovering, R.M., Chin, E.R., Jasmin, B.J., Marcinek, D.J., Menzies, K.J. & Auwerx, J. NAD+ repletion improves muscle function in muscular dystrophy and counters global PARylation. *Sci Transl Med* **8**, 361ra139 (2016).

155. Williams, P.A., Harder, J.M., Foxworth, N.E., Cochran, K.E., Philip, V.M., Porciatti, V., Smithies, O. & John, S.W. Vitamin B3 modulates mitochondrial vulnerability and prevents glaucoma in aged mice. *Science* **355**, 756-760 (2017).

156. Long, A.N., Owens, K., Schlappal, A.E., Kristian, T., Fishman, P.S. & Schuh, R.A. Effect of nicotinamide mononucleotide on brain mitochondrial respiratory deficits in an Alzheimer's disease-relevant murine model. *BMC Neurol* **15**, 19 (2015).

157. Wang, X., Hu, X., Yang, Y., Takata, T. & Sakurai, T. Nicotinamide mononucleotide protects against beta-amyloid oligomer-induced cognitive impairment and neuronal death. *Brain Res* **1643**, 1-9 (2016).

158. Lin, K.Y. & Kraus, W.L. PARP Inhibitors for Cancer Therapy. *Cell* **169**, 183 (2017).

159. Hoch, N.C., Hanzlikova, H., Rulten, S.L., Tetreault, M., Komulainen, E., Ju, L., Hornyak, P., Zeng, Z., Gittens, W., Rey, S.A., Staras, K., Mancini, G.M., McKinnon, P.J., Wang, Z.Q., Wagner, J.D., Care4Rare Canada, C., Yoon, G. & Caldecott, K.W. XRCC1 mutation is associated with PARP1 hyperactivation and cerebellar ataxia. *Nature* **541**, 87-91 (2017).

160. Schneider, C.A., Rasband, W.S. & Eliceiri, K.W. NIH Image to ImageJ: 25 years of image analysis. *Nat Methods* **9**, 671-675 (2012).

161. Gariani, K., Menzies, K.J., Ryu, D., Wegner, C.J., Wang, X., Ropelle, E.R., Moullan, N., Zhang, H., Perino, A., Lemos, V., Kim, B., Park, Y.K., Piersigilli, A., Pham, T.X., Yang, Y., Ku, C.S., Koo, S.I., Fomitchova, A., Canto, C., Schoonjans, K., Sauve, A.A., Lee, J.Y. & Auwerx, J. Eliciting the mitochondrial unfolded protein response by nicotinamide adenine dinucleotide repletion reverses fatty liver disease in mice. *Hepatology* **63**, 1190-1204 (2016).

162. Yang, T. & Sauve, A.A. NAD metabolism and sirtuins: metabolic regulation of protein deacetylation in stress and toxicity. *AAPS J* **8**, E632-643 (2006).

163. Abramoff, M.D., Magalhaes, P.J., Ram, S.J. Image Processing with ImageJ. *Biophotonics International* **11**, 36-42 (2004).

164. Zhang, X.Y., Varthi, M., Sykes, S.M., Phillips, C., Warzecha, C., Zhu, W., Wyce, A., Thorne, A.W., Berger, S.L. & McMahon, S.B. The putative cancer stem cell marker USP22 is a subunit of the human SAGA complex required for activated transcription and cell-cycle progression. *Molecular cell* **29**, 102-111 (2008).

165. Zhao, Y., Lang, G., Ito, S., Bonnet, J., Metzger, E., Sawatsubashi, S., Suzuki, E., Le Guezennec, X., Stunnenberg, H.G., Krasnov, A., Georgieva, S.G., Schule, R., Takeyama, K., Kato, S., Tora, L. & Devys, D. A TFTC/STAGA module mediates histone H2A and H2B deubiquitination, coactivates nuclear receptors, and counteracts heterochromatin silencing. *Molecular cell* **29**, 92-101 (2008).

166. Lee, K.K., Sardiu, M.E., Swanson, S.K., Gilmore, J.M., Torok, M., Grant, P.A., Florens, L., Workman, J.L. & Washburn, M.P. Combinatorial depletion analysis to assemble the network architecture of the SAGA and ADA chromatin remodeling complexes. *Molecular systems biology* **7**, 503 (2011).

167. Samara, N.L., Datta, A.B., Berndsen, C.E., Zhang, X., Yao, T., Cohen, R.E. & Wolberger, C. Structural insights into the assembly and function of the SAGA deubiquitinating module. *Science* **328**, 1025-1029 (2010).

168. Kohler, A., Zimmerman, E., Schneider, M., Hurt, E. & Zheng, N. Structural basis for assembly and activation of the heterotetrameric SAGA histone H2B deubiquitinase module. *Cell* **141**, 606-617 (2010).

169. Lee, K.K., Swanson, S.K., Florens, L., Washburn, M.P. & Workman, J.L. Yeast Sgf73/Ataxin-7 serves to anchor the deubiquitination module into both SAGA and Slik(SALSA) HAT complexes. *Epigenetics & chromatin* **2**, 2 (2009).

170. Kohler, A., Schneider, M., Cabal, G.G., Nehrbass, U. & Hurt, E. Yeast Ataxin-7 links histone deubiquitination with gene gating and mRNA export. *Nat Cell Biol* **10**, 707-715 (2008).

171. McCormick, M.A., Mason, A.G., Guyenet, S.J., Dang, W., Garza, R.M., Ting, M.K., Moller, R.M., Berger, S.L., Kaeberlein, M., Pillus, L., La Spada, A.R. & Kennedy, B.K. The SAGA Histone Deubiquitinase Module Controls Yeast Replicative Lifespan via Sir2 Interaction. *Cell Reports* **8**, 477-486 (2014).

172. Lin, Z., Yang, H., Kong, Q., Li, J., Lee, S.M., Gao, B., Dong, H., Wei, J., Song, J., Zhang, D.D. & Fang, D. USP22 Antagonizes p53 Transcriptional Activation by Deubiquitinating Sirt1 to Suppress Cell Apoptosis and Is Required for Mouse Embryonic Development. *Mol Cell* (2012).

173. Armour, S.M., Bennett, E.J., Braun, C.R., Zhang, X.Y., McMahon, S.B., Gygi, S.P., Harper, J.W. & Sinclair, D.A. A high-confidence interaction map identifies SIRT1 as a mediator of acetylation of USP22 and the SAGA coactivator complex. *Molecular and cellular biology* **33**, 1487-1502 (2013).

174. Sowa, M.E., Bennett, E.J., Gygi, S.P. & Harper, J.W. Defining the human deubiquitinating enzyme interaction landscape. *Cell* **138**, 389-403 (2009).

175. Ennis, H.L. & Lubin, M. Cycloheximide: Aspects of Inhibition of Protein Synthesis in Mammalian Cells. *Science* **146**, 1474-1476 (1964).

176. Cai, L., Sutter, B.M., Li, B. & Tu, B.P. Acetyl-CoA induces cell growth and proliferation by promoting the acetylation of histones at growth genes. *Molecular cell* **42**, 426-437 (2011).

177. Mason, A.G., Garza, R.M., McCormick, M.A., Patel, B., Kennedy, B.K., Pillus, L. & La Spada, A.R. The replicative lifespan-extending deletion of SGF73 results in altered ribosomal gene expression in yeast. *Aging Cell* **16**, 785-796 (2017).

178. Huisinga, K.L. & Pugh, B.F. A genome-wide housekeeping role for TFIID and a highly regulated stress-related role for SAGA in Saccharomyces cerevisiae. *Mol Cell* **13**, 573-585 (2004).

179. Bonnet, J., Wang, C.Y., Baptista, T., Vincent, S.D., Hsiao, W.C., Stierle, M., Kao, C.F., Tora, L. & Devys, D. The SAGA coactivator complex acts on the whole transcribed genome and is required for RNA polymerase II transcription. *Genes Dev* **28**, 1999-2012 (2014).

180. Zhou, M., Ottenberg, G., Sferrazza, G.F., Hubbs, C., Fallahi, M., Rumbaugh, G., Brantley, A.F. & Lasmezas, C.I. Neuronal death induced by misfolded prion protein is due to NAD+ depletion and can be relieved in vitro and in vivo by NAD+ replenishment. *Brain* **138**, 992-1008 (2015).

181. Fang, E.F., Scheibye-Knudsen, M., Brace, L.E., Kassahun, H., SenGupta, T., Nilsen, H., Mitchell, J.R., Croteau, D.L. & Bohr, V.A. Defective mitophagy in XPA via PARP-1 hyperactivation and NAD(+)/SIRT1 reduction. *Cell* **157**, 882-896 (2014).

182. Fang, E.F., Kassahun, H., Croteau, D.L., Scheibye-Knudsen, M., Marosi, K., Lu, H., Shamanna, R.A., Kalyanasundaram, S., Bollineni, R.C., Wilson, M.A., Iser, W.B., Wollman, B.N., Morevati, M., Li, J., Kerr, J.S., Lu, Q., Waltz, T.B., Tian, J., Sinclair, D.A., Mattson, M.P., Nilsen, H. & Bohr, V.A. NAD+ Replenishment Improves Lifespan and Healthspan in Ataxia Telangiectasia Models via Mitophagy and DNA Repair. *Cell Metab* **24**, 566-581 (2016).

183. Scheibye-Knudsen, M., Mitchell, S.J., Fang, E.F., Iyama, T., Ward, T., Wang, J., Dunn, C.A., Singh, N., Veith, S., Hasan-Olive, M.M., Mangerich, A., Wilson, M.A., Mattson, M.P., Bergersen, L.H., Cogger, V.C., Warren, A., Le Couteur, D.G., Moaddel, R., Wilson, D.M., 3rd, Croteau, D.L., de Cabo, R. & Bohr, V.A. A high-fat diet and NAD(+) activate Sirt1 to rescue premature aging in cockayne syndrome. *Cell Metab* **20**, 840-855 (2014).

184. Guarente, L. Linking DNA damage, NAD(+)/SIRT1, and aging. *Cell Metab* **20**, 706-707 (2014).

185. Paulson, H.L. & Miller, V.M. Breaks in coordination: DNA repair in inherited ataxia. *Neuron* **46**, 845-848 (2005).

186. Lee, Y., Katyal, S., Li, Y., El-Khamisy, S.F., Russell, H.R., Caldecott, K.W. & McKinnon, P.J. The genesis of cerebellar interneurons and the prevention of neural DNA damage require XRCC1. *Nat Neurosci* **12**, 973-980 (2009).

187. Ramachandran, S., Haddad, D., Li, C., Le, M.X., Ling, A.K., So, C.C., Nepal, R.M., Gommerman, J.L., Yu, K., Ketela, T., Moffat, J. & Martin, A. The SAGA Deubiquitination Module Promotes DNA Repair and Class Switch Recombination through ATM and DNAPK-Mediated gammaH2AX Formation. *Cell Rep* **15**, 1554-1565 (2016).

188. Hubbard, B.P. & Sinclair, D.A. Small molecule SIRT1 activators for the treatment of aging and age-related diseases. *Trends Pharmacol Sci* **35**, 146-154 (2014).

189. Altschul, R., Hoffer, A. & Stephen, J.D. Influence of nicotinic acid on serum cholesterol in man. *Arch Biochem Biophys* **54**, 558-559 (1955).

190. Blankenhorn, D.H., Nessim, S.A., Johnson, R.L., Sanmarco, M.E., Azen, S.P. & Cashin-Hemphill, L. Beneficial effects of combined colestipol-niacin therapy on coronary atherosclerosis and coronary venous bypass grafts. *JAMA* **257**, 3233-3240 (1987).

191. Blankenhorn, D.H., Azen, S.P., Kramsch, D.M., Mack, W.J., Cashin-Hemphill, L., Hodis, H.N., DeBoer, L.W., Mahrer, P.R., Masteller, M.J., Vailas, L.I., Alaupovic, P., Hirsch, L.J. & Group, M.R. Coronary angiographic changes with lovastatin therapy. The Monitored Atherosclerosis Regression Study (MARS). *Ann Intern Med* **119**, 969-976 (1993).

192. Brown, B.G., Zhao, X.Q., Chait, A., Fisher, L.D., Cheung, M.C., Morse, J.S., Dowdy, A.A., Marino, E.K., Bolson, E.L., Alaupovic, P., Frohlich, J. & Albers, J.J. Simvastatin and niacin, antioxidant vitamins, or the combination for the prevention of coronary disease. *N Engl J Med* **345**, 1583-1592 (2001).

193. Canner, P.L., Berge, K.G., Wenger, N.K., Stamler, J., Friedman, L., Prineas, R.J. & Friedewald, W. Fifteen year mortality in Coronary Drug Project patients: long-term benefit with niacin. *J Am Coll Cardiol* **8**, 1245-1255 (1986).

194. Cerritelli, S.M. & Crouch, R.J. Ribonuclease H: the enzymes in eukaryotes. *The FEBS journal* **276**, 1494-1505 (2009).

195. Crooke, S.T. Molecular mechanisms of action of antisense drugs. *Biochim Biophys Acta* **1489**, 31-44 (1999).

196. Kordasiewicz, H.B., Stanek, L.M., Wancewicz, E.V., Mazur, C., McAlonis, M.M., Pytel, K.A., Artates, J.W., Weiss, A., Cheng, S.H., Shihabuddin, L.S., Hung, G., Bennett, C.F. & Cleveland, D.W. Sustained therapeutic reversal of Huntington's disease by transient repression of huntingtin synthesis. *Neuron* **74**, 1031-1044 (2012).

197. Becker, L.A., Huang, B., Bieri, G., Ma, R., Knowles, D.A., Jafar-Nejad, P., Messing, J., Kim, H.J., Soriano, A., Auburger, G., Pulst, S.M., Taylor, J.P., Rigo, F. & Gitler, A.D. Therapeutic reduction of ataxin-2 extends lifespan and reduces pathology in TDP-43 mice. *Nature* **544**, 367-371 (2017).

198. Lieberman, A., Yu, Z., Murray, S., Peralta, R., Low, A., Shuling, G., Yu, X.X., Cortes, C.J., Bennett, C.F., Monia, B.P., La Spada, A.R. & Hung, G. Peripheral androgen receptor gene suppression rescues disease in mouse models of spinal and bulbar muscular atrophy. *Cell Reports*, [submitted] (2014).